Use of recombinant self-associating proteins for altering cellular fate and behavior

Thesis by

Mark Tybalt Kozlowski

In Partial Fulfillment of the Requirements for

the degree of

Doctor of Philosophy

CALIFORNIA INSTITUTE OF TECHNOLOGY

Pasadena, California

2019

(Defended May 13, 2019)

Mark Tybalt Kozlowski
ORCID: 0000-0003-4714-8697

ACKNOWLEDGEMENTS

I would first like to thank my parents, who encouraged my early interest in science, who took pains to ensure I got an education, and who have supported me, pushed me, and above all believed in me when I didn't believe in myself.

This work would not have been possible without the personal and professional support of my friends, labmates, and colleagues at Caltech and City of Hope. I would like to thank my adviser, David Tirrell, for hiring me, for providing guidance and support, and for encouraging my personal and professional development. Thanks also to H. Teresa Ku, my mentor/co-adviser at City of Hope, for teaching me the techniques of mammalian cell culture and characterization. Both of my mentors have been exemplars of patience and compassion, and their insistence on meticulousness and rigor has made me a better scientist. I would also like to thank my thesis committee, Profs. Dennis Dougherty, Julia Kornfield, and Zhen-Gang Wang, for their help and suggestions, for their insistence on scientific rigor, and for making me a better scientist.

I have also relied on the help of many other faculty and staff at both Caltech and City of Hope, of whom I'd like to specifically acknowledge Andres Collazo, Mona Shahgholi, Hung-Ping (Ben) Shih, Jeff Park, Matt Thomson, and Fan Gao. Administration is an often-overlooked part of science, so I would be remiss to not thank the Tirrell Group administrative assistants Anne Hormann, Elizabeth Garcia, and Irina Meininger for making the lab run smoothly, and helping with scheduling. I also acknowledge all of my labmates, past and present, but particularly acknowledge Bradley Silverman, who is co-first author on one of my upcoming publications, and my other officemates Joshua Baccile, Katharine Fang, and Michael Srienc. None of this work would have been possible without hands-on training provided by seasoned members of both labs, for which I acknowledge Lawrence Dooling, who undertook my initial training at Caltech, and Jeanne LeBon, Grace Wu, Cecile Donohue, Janine Quijano, and Jacob Tremblay for helping train me at City of Hope, and for helping me with myriad miscellaneous tasks. Finally, I have had the chance to mentor three very talented undergraduate students, Desnor Chigumba, Luis Caldera Guzman, and Christopher Johnstone, who made key contributions to the research presented here, and whose careers I will follow with great interest. I would also like to acknowledge the American taxpayer, who funded my PhD in part through an NDSEG grant from the Department of Defense.

I would like to thank my undergraduate research advisers at the University of Pittsburgh, Nathaniel Rosi and Tao Li, for giving me the research bug and inspiring me to continue studies in chemistry. I would also like to thank my academic advisers Toby Chapman and George Bandik, who encouraged me to pursue graduate studies.

Outside of the lab, I was involved in two extracurricular activities that helped me maintain my sanity and good humor. Choral music and theater were an integral part of my time at Caltech, and for making them so thoroughly enjoyable, I thank Nancy Sulahian and William Schmidt of the Caltech Glee Club, Brian Brophy of TACIT, Cindy De Mesa of

Performing and Visual Arts, Todd Brun (who cast me in my first show), the cast and crew of *Faustus, PhD* (a play I wrote), and all of the other wonderful people I've had a chance to meet and work with over the last six years in these organizations.

Of course, the most important person I met in theater was my wife, Penelope, who like her namesake enjoys the fabric arts when I'm working strange hours. I'm not sure I can write an acknowledgement that captures everything she has done to help me finish this undertaking, but I hope it is sufficient to say, she is the light of my life, the joy of my days, and the dedicatee of this volume.

For Penelope

ABSTRACT

The behavior of mammalian and bacterial cells is governed by their surroundings, and the interactions of cells with their nearest neighbors. In this work, I will demonstrate how self-associating proteins such as leucine zippers or SpyTag and SpyCatcher can be used either in hydrogels for cell culture, or to drive the aggregation of cells into artificial, engineered communities. I further demonstrate how these self-associating protein-based materials can either alter the fate of cultured cells, or directly change cellular behavior through the activation of a quorum sensing circuit.

In the first chapter, I discuss protein-based methods for making different types of organoids. Organoids are groups of cells derived from stem or progenitor cells that form a multicellular structure consisting of different cell types. These organoids are currently of interest as disease model systems, pharmaceutical test platforms, and replacement tissues. However, most studies of organoids to date have derived them from Matrigel-based cultures. While versatile and inexpensive, Matrigel is undefined, suffers from batch-to-batch variability, and its xenogeneic nature means that organoids derived from Matrigel are unlikely to be approved for clinical use. In Chapter 1, I review current state-of-the-art materials developed as alternatives to Matrigel, such as naturally-derived extracellular matrices, synthetic hydrogels, and recombinant proteins serving as artificial extracellular matrices. I consider the advantages and disadvantages of each method, as well as speculate on possible future directions for the field.

Of these alternatives to Matrigel, recombinant protein-based artificial extracellular matrices have the advantage of being easy to engineer, as genetic encoding of the material allows precise control over molecular weight and functionality. Development of these types of materials has long been a focus of work in our laboratory, and in Chapter 2, I discuss the development of two protein-based hydrogels expressed in *Escherichia coli,* which are based on a previously-reported PEP hydrogel. These new “PEXEP-type” hydrogels are physically cross-linked by leucine zippers derived from rat cartilage oligomeric matrix protein (COMPcc), incorporate chemical cues from fibronectin and collagen IV, and were

used for pancreatic cell culture in defined medium. When comparing this defined, protein-based medium to methylcellulose-Matrigel, we find that the growth of endocrine cells is promoted, as opposed to the ductal cells found in methylcellulose-Matrigel culture. We further find a difference in colony types observed based on whether the fibronectin or collagen IV cue is present. More interestingly, the protein-based culture material promotes the growth of endocrine progenitor cells, which may be useful for further studying the formation of the Islets of Langerhans. Finally, we observe that sorted populations of murine cells cultured in our protein hydrogels have a lower rate of colony formation, and this reduction in the number of colonies is not observed in methylcellulose-Matrigel culture. We believe that this might be evidence for a paracrine effect that promotes cell growth, particularly the growth of putative endocrine colonies, though further experiments are required to confirm this effect.

In Chapter 2, I demonstrate how a self-associating protein can be used to change the fate of a cell culture, and give rise to multicellular colonies. However, for the purpose of constructing bioreactors, microbial fuel cells, or systems for environmental remediation, it may be advantageous to design tissue-like systems *de novo,* making multifunctional communities of bacteria that function as artificial tissues. In Chapter 3, I will discuss the construction of a synthetic microbial community of *E. coli* cells, whose quorum sensing response is governed by aggregation of the cells. This aggregation in turn is driven by the expression of surface-displayed self-associating proteins, and I will discuss methods developed to control the size, reversibility, and morphology of these aggregates. As the behavior of these aggregates is dependent on cell-cell communication facilitated by proximity, these consortia represent early examples of synthetically-designed artificial tissues that can be governed by engineered cell-cell signaling.

PUBLISHED CONTENT AND CONTRIBUTIONS

No previously-published information is present in this thesis.

The work presented in Chapter 1 is a review article currently being prepared in collaboration with H. Teresa Ku at City of Hope.

The work presented in Chapter 2 was primarily conducted and entirely written by the author. ESI data was collected by Dr. Mona Shahgholi of the Caltech CCE mass spectrometry facility. The flow cytometry data presented was collected by the Analytical Cytometry Core at City of Hope.

The work presented in Chapter 3 was a collaboration between the author and Bradley R. Silverman. MTK and BRS contributed equally to the work, and are co-first authors on its impending publication. MTK is responsible for Figures 2, 3, and 5-7. BRS is responsible for Figures 1 and 4, and quantitative image analysis.

TABLE OF CONTENTS

Chapter I

ORGANOID CULTURE IN NON-MATRIGEL MATERIALS

INTRODUCTION

Organoids are groups of cells derived from stem and progenitor cells that form structures similar to organs in function, spatial organization, and cellular diversity (1). Organoids recapitulate important organ function *in vitro* while remaining a convenient size. They also lack interfering cell types such as epithelial, vascular, or nervous tissue. For these reasons, organoids are used to study the development of entire organs (2), as disease model systems for cancers (3), neural disorders (4), diabetes and autism (5), as pharmaceutical testing platforms (6), as model systems for CRISPR-CAS9-mediated treatment of genetic diseases (7), and as replacement organs for transplant (8, 9). By obtaining either adult or induced pluripotent stem cells from patients with a given disease, it is in theory possible to recapitulate their specific organs in miniature, leading ultimately to personalized medicine (10). The wide range of clinical applications of organoids is the subject of a recent review by Drost and Clevers (11), and these promising tissues are subject to intensive study in medicine and studies of cellular development.

A great diversity of organoids have been cultured in the milieu of Matrigel, a material derived from the secretion of Engelbreth-Holm-Swarm mouse sarcoma cells and used for a wide variety of cell culture studies (12). An important property of Matrigel is that at high concentrations Matrigel is semisolid, thereby permitting organoid growth in a 3-dimensional space. In the organoid culture system first reported, Clevers and co-workers grew human intestinal Lgr5+ cells in high concentrations of Matrigel supplemented with growth factors WNT, Noggin, R-spondin and EGF (13). This culture system has been widely adapted to form organoids from other organs such as the colon, stomach, and liver (14-18). Related methods have been used to construct simulated versions of the inner ear (19), and pancreas (20-23). The wide number of organoid types that can be made using

Matrigel-based culture methods has been excellently reviewed elsewhere (24, 25), and is outside the scope of the present work.

Despite its versatility and relatively low cost, Matrigel is an extremely complex medium, with a proteomic profile determining that it consists of over 1800 unique proteins (26). The undefined nature of Matrigel makes it difficult to determine exactly which factors are responsible for the creation of a given organoid, and in many stem cell culture contexts, the lot-to-lot variation of Matrigel is observed to affect ultimate cellular fate (27, 28). In fact, standardization and reproducibility of organoid culture is one of the foremost concerns in the field at present, and this is impossible to realize as long as an undefined medium remains at the center of organoid creation (29, 30). Its undefined nature aside, the xenogeneic origin of Matrigel precludes its use in making organoids for clinical applications (31, 32). Injections of human embryonic stem cells in the presence of Matrigel in an *in vivo* system are also linked to a higher incidence of formation of cancer cells such as teratomas (33-35). Matrigel also may not contain all ECM proteins necessary for proper organoid formation. For example, it has been observed that gut organoids cultured in Matrigel lack villi-type structures, and this has been attributed to an insufficient concentration of laminin 511 (36, 37). Finally, it has become increasingly obvious that the mechanical properties of a 3D cell culture medium such as stiffness or viscoelasticity (38), can have a large effect on cell (39), tissue (40), organoid (41), and organ development (42, 43).

A critical limitation of a Matrigel-based culture is that the mechanical properties of Matrigel can only be changed by altering the concentration, chemical composition, or morphology of the material, making it difficult to conduct properly-controlled experiments where the variables of elastic modulus and chemical concentration are isolated (44-46). Worse, the mechanical properties of Matrigel are heterogeneous within an individual gel, with certain patches of a gel found to have an elastic modulus several times higher than the average elastic modulus of the overall medium, in a manner not easily controlled by the

experimenter (47, 48). It is therefore possible that mechanical differences in an individual Matrigel culture have an effect that is not well understood, or even detected.

While organoids clearly have great potential, there is a need to develop alternate culture materials and methods that do not rely on Matrigel. These defined culture media will enable a more systematic study of the effects of mechanical and chemical properties on the development and behavior of organoids, and permit their use in clinical transplantation studies. In this review, we will discuss recently-developed alternatives to Matrigel for culture of stem cells and organoids *in vitro*, and suggest areas where further research is needed.

ORGANOID CULTURE IN NATURAL DECELLULARIZED ECM

Organ development occurs in the complex chemical and mechanical environment of the extracellular matrix, which provides signaling cues, serves as an adhesive substrate, and sequesters growth factors to create complex microenvironments that allow organs to become spatially organized (49). In order to accurately recapitulate the composition and structure of native ECM in organ development, as well as retain native vascularization, some organoids have been grown in decellularized ECM from human or animal donors. Methods for decellularization of ECM typically involve the perfusion of various detergents such as sodium dodecyl sulfate (SDS) through donor tissues under the pressure of a peristaltic pump. The methods used are dependent on target tissue and not readily generalizable: the various methods to decellularize tissues have been reviewed elsewhere (50). Some of these tissues can be derived from human donors, while others are derived from xenogeneic materials in order to obviate the need for human donors. If the xenogeneic materials are properly prepared, they do not cause a serious immune response (51), and similar decellularized ECM scaffolds are FDA approved for numerous clinical applications such as heart valve replacement, facial reconstruction, and osteopathic implants (49, 52).

The approach of decellularization has been extensively used in the domain of liver reconstruction, as there is a shortage of liver donors. As an alternative, cells can be seeded

into liver ECM obtained either by using decellularized livers that are otherwise unsuitable for transplantation, or by removing a portion of a patient's damaged liver (surgical resection), decellularizing it, and using the ECM as a cellular scaffold. As early as 2004, Lin and co-workers reported liver tissue decellularization to support growth and maintenance of rat hepatocytes; however, this method relied on mechanical disruption of resectioned tissue, leading to loss of organ architecture and vascular networks (53). In contrast, Baptista and co-workers perfused Triton X-100 and ammonium hydroxide through a ferret hepatic vascular network to remove the cells. This method preserves the underlying ECM and vasculature while retaining most of the glycosaminoglycans, collagen, and elastin. The decellularized material could then be colonized by human fetal liver and endothelial cells to make a functioning organoid (54). Pinzani and co-workers removed cells from a human liver deemed unsuitable for transplantation by perfusion, finding that the perfusion process entirely removed the native cells, yet maintained the composition and microstructure of the liver ECM. They also found that the decellularized human liver sections did not cause an immune reaction when transplanted into C57BL/6J immunocompetent mice, and that hepatic cell lines, HepG2, LX2 and Sk-Hep-1, re-colonized, and proliferated within the decellularized matrix (55). Further optimization of the decellularization protocol in rat tissue, by adding EDTA to the detergent solution, allows for a more compact decellularized ECM and more complete removal of cells (56). A limitation of this latter study by Pinzani and co-workers is that it was not conducted with undifferentiated stem cells to see what effect the protocol may have on differentiation. An alternate approach involves decellularizing the liver matrix, lyophilizing, grinding the liver into a fine powder, and then using this powder to form a gel or coating to support differentiation, forming a liver extracellular matrix gel or LEMgel. Cho and co-workers used this approach with rat liver ECM, which promoted the differentiation of human adipose-derived stem cells into functional hepatocytes (57). More recently, Saheli and co-workers used liver-derived ECM hydrogel to culture hepatocarcinoma cells with mesenchymal stem cells and umbilical cord stem cells, leading to liver-like organoids that have greater hepatocyte function than a comparable collagen I culture (58).

Decellularized matrices have also been used for the growth of human intestinal organoids (HIOs), though each decellularization protocol is unique, and must be conducted in a way that preserves vital growth factors or chemical cues on the surface of the material. However, merely having the appropriate ECM present is no guarantee of successful directed differentiation. Finkbeiner and co-workers found that the chemical cues provided by decellularized porcine intestinal ECM were insufficient to direct differentiation of human embryonic stem cells towards an endodermal or intestinal fate, even when this matrix was able to support seeded HIOs that had been made separately on a Matrigel-based matrix (59). Indeed, in a number of cases, merely having the nominally correct ECM present was insufficient to drive pluripotent cell differentiation: the cells have to be differentiated into the correct progenitor population first (60). In contrast, Shojaie and co-workers were able to grow mouse embryonic stem cells into complex lung organoids on decellularized rat lung without intervening differentiation to progenitor cells. The ability to make these organoids was dependent on the retention of heparin sulfate proteoglycans on the surface of the decellularized scaffold, which suggests that in some cases the maintenance of proteoglycan cues is critical in directing differentiation (61).

Similar methods have been proposed for kidney (62, 63), heart (64, 65), lung (66), and pancreatic (67, 68) tissues, with each tissue displaying unique challenges depending on organ type, as well as organ provenance. For example, the human pancreas has a higher lipid content than those of mouse or other animal models, meaning that decellularizing human organs requires different, specific conditions (68). Of particular interest to the pancreatic researchers is a technique developed by Chaimov and co-workers, who used decellularized porcine pancreas as a scaffold. Both human mesenchymal stem cells (hMSC) and adult human liver cells (AHLC) had pancreatic transcription factors Pax4, Pdx1 and MafA transduced into them by adenovirus in order to either bias the hMSCs towards a pancreatic lineage, or to reprogram the AHLCs into pancreatic cells. Seeding the cells in decellularized porcine pancreas was found to have no effect on C-peptide secretion of hMSCs, but AHLCs transduced while grown in the matrix did show enhanced C-peptide secretion. The authors then attempted to encapsulate these transduced cells in

decellularized ECM as a method of treating diabetic mice. The authors first encapsulated the cells in alginate to immobilize the cells. Decellularized ECM was then added and allowed to solidify around the alginate core. After the ECM had solidified, the alginate was removed by washing with HEPES-sodium citrate solution. The authors found that the decellularized ECM material did not trigger an allergic reaction in immunocompetent mice, that the encapsulated cells remained viable, and that the encapsulated cells differentiated to insulin-producing beta cells. Encapsulating the cells within decellularized ECM enhanced the secretion of C-peptide relative to encapsulation in alginate. The encapsulated cells were able to improve glycemic control in diabetic mice over a period of approximately 7 days (69).

Distinct from the use of decellularized ECM, there has been a fair amount of organoid culture conducted within commercially-available naturally-derived proteins, such as cellMatrix^{tm} products, which consist of collagen derived from porcine tendon or skin, or bovine lens capsules (70). Collagen I has been used to make colorectal tumor model organoids in 3D culture (71), and as coatings for 2D cultures of intestinal crypts (72), or pancreatic carcinomas (73). Aside from collagen, collagen vitrigel (74), vitronectin, and fibronectin have also been used as a support for organoid and mammalian cell culture. The primary method for culture of organoids in a collagen I matrix is the so-called Tokyo Medical and Dental University (TMDU) method, which was first developed by Nakamura and co-workers for intestinal-enteroid culture (75). Murine intact intestinal crypts and isolated single Lgr5+ progenitor cells are embedded in Collagen I with hepatocyte growth factor, bovine serum albumin (BSA) and Rspo1, EGF and Noggin growth factors resulting in an organoid that was able to repair damaged mouse intestinal epithelia upon transplantation. In contrast, the Ootani method uses a Collagen I gel where small and large intestinal cells are kept suspended at an air-liquid interface, which enables improved oxygenation of the organoid and therefore allows maintenance of viable murine organoids in culture for up to 350 days (76). Variants of the TMDU method have been used elsewhere in murine models where the organoid was then successfully implanted subcutaneously (77) in a long-term (one month) culture of human intestinal epithelium

(78), and in modelling tissue remodeling after damage to the epithelium (79). Variants of the Ootani method have been used in modelling the immune microenvironment of epithelial tumors (80), and resistance of colorectal tumors to anticancer drugs (81).

Two factors that have been shown to affect the differentiation of progenitor cells into organoids in collagen-based matrices are the source of seeded cells, and the spacial arrangement of collagen types around the cells. Shinomura and co-workers reported that the choice between using the Ootani method and the TMDU method should be governed by the source of cells used to make the intestinal organoid. The authors found that more consistent results for the culture of rat organoids were obtained when homogenized tissue of the entire colon is grown at the air-liquid interface (the Ootani method), whereas attempting to grow organoids using seeded isolated intestinal crypts is more effectively done in 3D culture using the TMDU method (82).

Aside from judicious selection of cell type, the chemical makeup of the collagen or derived protein is also relevant. Cell fate is intimately tied to the attachment of the appropriate cell surface integrins to biochemical cues in the extracellular matrix (83). Collagen I has a higher affinity for $\alpha_2\beta_1$ integrin, whereas collagen IV prefers binding to $\alpha_1\beta_1$ integrin (84). Both the collagens in the ECM and the integrins are spatially organized. Collagen IV, for instance, tends to occur exclusively in basement membranes, unlike other collagen types (84). Integrins are likewise spatially organized on the cell surface: for example, in intestinal organoids, β4 integrins arrange themselves on the basal side of the cells (85), and the anchoring of β1 integrins on the basal layer is also required for proper apical-basal polarization (86, 87). Proper cell polarization, and engagement of the correct integrins, is vital to maintaining the identity and function of the cells in the organoid and in the body. In an attempt to simulate the spacial homogeneity of the intestine in an *in vitro* environment, Tong and co-workers cultured Lgr5+ cells that were sandwiched between a collagen IV-coated substrate and a collagen I gel overlay in what was termed a “Bolstering Lgr5 Transformational Sandwich” or “BLT sandwich.” Ultimately, this culture system favored the proliferation of Lgr5+ cells that remained undifferentiated (88). Similar

findings about matrix heterogeneity were reported by Wang and co-workers, who found that hepatic differentiation of mesenchymal stem cells is enhanced by using a PEG gel functionalized with both collagen I and fibronectin, as opposed to gels functionalized with only collagen I (89).

Decellularized ECM and naturally-derived protein methods have the advantage of quickly recapitulating organ function, as all the chemical cues required for the formation of a spatially-defined organ are already present. This minimizes the need for additional chemical modification of the ECM. Decellularized ECM in particular already has clearly defined basal and apical surfaces, and this can be simulated in naturally-derived protein culture by using culture methods such as the BLT sandwich. Collagen-based culture materials also have the advantage of already being FDA approved for a wide variety of applications (90), meaning that organoid culture methods using naturally-derived protein matrices can be rapidly translated to clinical application.

There are, however, several disadvantages to using decellularized ECM. First, the amount of these materials that are available for study is ultimately limited by the availability of donor animals or humans. Availability is further constrained by the fact that the health of a donor can influence the outcomes of cell seeding. For example, emphysematic or fibrotic lung tissue has hardened and undergone alterations in the architecture of the tissue. These alterations can lead to cells failing to survive beyond one week of culture (91), or shifts in the expression levels of particular growth factors (92). Similarly, myocardial infarct is known to trigger remodeling events that stiffen the ECM and change its chemical composition. When mesenchymal stem cells are seeded on infarcted tissue, the phenotype of the cells shifts, with higher secretion levels of prosurvival and immunomodulatory growth factors (93). While some of these disease states appear to enhance the survival of seeded cells, the effects of diseased tissue should not be discounted. Even if the donor tissue is known to be healthy, there remains the problem of lot-to-lot variability. Second, the physical properties of this decellularized ECM cannot be precisely controlled or designed, limiting the scope of experiments that can be conducted with these types of

materials. The material is also chemically undefined, meaning that the vital factors driving differentiation might remain unknown, unless serendipitously discovered. As noted above, using too harsh decellularization can strip surface proteoglycans necessary to successful organoid formation (61). A related difficulty is that not all decellularization protocols are equally effective at removing cells or other immunogenic particles, which leads to varying host immune responses, and in some cases the failure of implants in clinical trials (94). Finally, the need for pre-differentiation of pluripotent or induced-pluripotent stem cells into organ-specific progenitor cells means that a differentiation step is often necessary for the decellularized matrix approach to work, and this step not only adds complexity, but is typically conducted in Matrigel.

As methods for generating large quantities of porcine or bovine collagen on an industrial scale at biomedical grades are well-established, collagen-driven culture methods are not limited by the availability of appropriate donor tissue. However, these methods still suffer from a lack of precise chemical definition, and some collagen-based culture methods rely on feeder cells (89), which introduce further undefined components into the culture conditions. Furthermore, it is difficult to modify the mechanical properties of these culture systems independent of altering chemical concentration. To more effectively elucidate the effect of mechanical properties on organoid development, it may be necessary to resort to synthetic hydrogels functionalized with cell-binding cues.

ORGANOID CULTURE IN SYNTHETIC HYDROGELS

The elimination of mechanically and chemically undefined fractions from organoid culture has recently been the focus of a number of research efforts. These efforts have primarily focused on culturing organoids in hyaluronic acid-type materials, or synthetic polymers such as polyethylene glycol (PEG), poly-L-lactic acid (PLLA) or polylactic(co-glycolic) acid (PLGA). Synthetic hydrogels are particularly attractive as there are many methods to control their mechanical properties, mesh size, and functionality. By the inclusion of matrix metalloprotease (MMP) recognition sites, it is also possible to tune the erosion rate of the material, which is known to have consequences in cellular and organoid development (95).

Expanding the number of materials in which organoids can be cultured allows researchers precise control of the size and shape of the organoid culture, and enables use of methods such as electrospinning (96), photopatterning (97, 98), spraying of microspheres (99), inkjet and 3D printing (100), or use of microfluidic channels (101), to precisely control the shape and size of the organoid culture. Synthetic hydrogels can also be made responsive to external stimulus, such as in a recent report of a chemically-reversible hydrogel (102). It is also possible to alter the mechanical and physical properties of these hydrogels for ease of experimental use such as a thermoplastic hyaluronic acid-based hydrogel that solidifies at 37 degrees and which will re-liquify upon cooling, enabling recovery of viable organoids from culture without resorting to enzymatic digestion of the matrix (103). Light-sensitive polyvinyl alcohol (PVA) matrices have also recently been developed for cell culture, allowing an unprecedented degree of control over the precise spacing of incorporated biochemical cues, and local control over the material environment (104). The ability to exert excellent local control of the chemical and mechanical properties of specific locations of the material is particularly exciting, as it allows researchers to duplicate the heterogeneous stiffness and composition found in organs. This heterogeneity is important to study, as it has implications for organ disease states (105, 106). A light-crosslinkable system allows for this heterogeneity to be effectively duplicated *in vitro*, and more precise reconstruction of diseased organs where tissue hardening has occurred, such as in liver fibrosis and cirrhosis (107, 108).

Synthetic polymer-based culture also allows the evaluation of conditions for organoid formation using high-throughput methods (109-111). Synthetic hydrogels such as PEG can be functionalized with a dizzying array of biologically-active moieties that permit the growth and spread of a wide variety of different cell types (112-117), and it is possible to precisely control the concentration and spacing of these cues (118-121). Therefore, using synthetic hydrogels allows for the independent optimization of various factors involved in organoid creation, allowing researchers to more easily separate the variables of organoid formation. A dramatic demonstration of the utility of a PEG-based culture strategy in this respect was provided by Ranga and co-workers, who developed a high-throughput method

that allowed them to analyze 1,000 different variations of matrix elastic modulus, cell-binding peptide, and susceptibility of the matrix to degradation by matrix metalloprotease (MMP) for their effects on embryonic stem cell fate at nanoliter scales (122). These efforts culminated in a PEG-based hydrogel system with recombinant peptides for growth of a neural tube-type organoid, where it was found that a laminin-functionalized PEG leads to a more homogenous population of neurites in terms of size and morphology, and a higher degree of apical-basal polarity, than cells grown in Matrigel. Patterning of cells was also influenced by overall matrix stiffness, with intermediate elastic moduli of 2-4 kPa found to be optimum for apical-basal patterning. Patterning was also dependent on how quickly the PEG matrix was digested by cell-secreted MMP, with more-sensitive scaffolds found to support less patterning, and matrix stiffness was also found to affect patterns of cell proliferation and apoptosis (123).

The ability to make precisely-structured, latticed assemblies of PEG with defined pore size was recently used by Ng and co-workers in the creation of functional liver organoids derived from induced pluripotent stem cells in a colloidal crystal of PEG functionalized by collagen I, fibronectin, or laminin-521 (124, 125). They found that attachment of the iPSCs was dependent on the functionalization, with collagen I and laminin-521 leading to cellular attachment, and cells failing to attach to assemblies functionalized by fibronectin. This builds on previous work, where basic liver function could be recapitulated by such a PEG-based scaffold (126). Similarly, the group of Kloxin and co-workers synthesized a photocrosslinked PEG-based gel that contained a variety of different chemical cues binding to different integrins in iPSCs, finding that encapsulation in these materials could drive different ultimate organoid fates (127). Hepatic organoids have also been grown on non PEG-based scaffolds, such as functionalized polyurethane surfaces (128, 129), or a hyaluronic acid matrix (130).

Synthetic hydrogels allow precise control of the mechanical properties of culture medium

Aside from the ability to precisely control the chemical cues facing cells in organoid culture, synthetic hydrogels also allow for the precise control of mechanical properties,

which have been shown to have consequences in cellular survival, proliferation, and ultimate fate. Lee and co-workers recently developed a hybrid biodegradable biomaterial for growth of liver organoids consisting of PEG-diacrylate (PEGdA) crosslinked by hyaluronic acid functionalized by degradable peptides, on which they cultured HepaRG hepatic progenitor cells as well as a co-culture of HepaRG with EC-SV40 immortalized cells, and fibroblasts (131). The materials were synthesized at various initial elasticities, ranging from 2 kPa to 20 kPa. The authors observed that HepaRG cells encapsulated by themselves on the softest medium did not survive, but the co-culture showed the ability to differentiate into both hepatic and biliary cells, and through first a decrease, then a dramatic increase in elastic modulus, along with evidence of collagen deposition, observed ECM remodeling. On a slightly stiffer culture medium, both individual cells and co-culture demonstrated this behavior. The authors also observed that the resulting organoids responded to pharmacological challenge, and that medium that was too stiff, or too soft, led to diminished organoid function.

The group of Lutholf and co-workers recently reported a well-defined, synthetic matrix for intestinal organoid culture from Lgr5+ progenitor cells derived from the intestinal crypt, which represents a major step towards more defined cultures of organoids. Their material consisted of a PEG gel functionalized with either an arginine-glycine-aspartic acid (RGD) peptide, or a laminin-111-derived peptide (132). Interestingly, the group found that higher matrix stiffnesses used with RGD-type materials tended to promote the survival and proliferation of undifferentiated stem cells, whereas the use of a softer matrix, and a laminin sequence, resulted in the formation of differentiated, functional organoids. It was also observed that the cell types were different in the defined PEG medium compared to a Matrigel culture, with the PEG medium both failing to support a population of Paneth cells, and suppressing cell proliferation more generally. General methods for the synthesis of these gels are presented in a subsequent methods paper that provides an excellent starting point for those interested in pursuing further studies in this field (133). In similar work by Grandi and co-workers, an oxidized polyvinyl alcohol (OxPVA), which was functionalized with decellularized intestinal wall, was used to treat short bowel syndrome, representing a

hybrid method that combines the chemical cues of native tissues with the mechanical tuneability of a synthetic polymer (134). The Grandi study demonstrates that organoids made in synthetic polymers have the potential for clinical application.

Similarly, the Garcia group used a 4-arm PEG maleimide to encapsulate and culture Matrigel-derived human intestinal organoids (HIOs), and found that viability of intestinal organoids was hampered if the density of PEG was too high, and the matrix was consequently too stiff. They also found that an RGD-containing or AG73 (CGGRKRLQVQLSIRT)- functionalized PEG material promoted organoid viability better than laminin-derived IKVAV or Type I collagen-derived GFOGER peptides (135, 136). Intriguingly, the Garcia group also found that when PEG was crosslinked in a manner that did not permit matrix degradation (i.e., crosslinking with DTT), organoid viability at 7 days was poor. When repeating the experiment with single cells in order to grow HIOs in their matrix, they likewise found that density of PEG was a key factor determining organoid growth and viability. Finally, and most dramatically, the authors demonstrated that these HIOs could be encapsulated *in situ* in a mouse model, and that the injection of these organoids promoted the healing of mucosal wounds in the mouse due to a successful engraftment of that organoid. While this encapsulation strategy was conducted with organoids that had previously been derived from Matrigel, it serves as further evidence that PEG-based materials need to be soft, and capable of degradation and remodeling, if they are to support intestinal organoid growth.

Synthetic polymer-based culture methods allows the construction of organoids otherwise difficult to obtain

The ability to precisely tailor the properties of synthetic hydrogels, and make them reproducibly, also makes them of interest for use in organoids that are difficult to grow reproducibly and consistently. Neural organoids, while extremely promising, have been known to have difficulties with reproducibility brought on by batch effects (137). Neural organoids were also grown on a PEG-based gel by the group of Murphy and co-workers, in order to develop a model system to assess neural toxicity of various chemicals in a

developing brain (138). By introducing neural, vascular, and microglia/macrophage cells in three sequential stages, the authors were able to construct organoids that were more representative of a complete neuronal model than ones previously published. Similarly, O'Brien and co-workers developed a method for culturing cerebral organoids comopoased of multiple cell types in a defined medium consisting of a blend of hyaluronan and chitosan (termed CellMate3D) in Essential 8 medium. Neural differentiation was directed by the use of retrovirus or Sendai virus. These organoids were developed as a model for adrenoleukodystrophy, and the group observed numerous cell types within the organoid (139). A similar method was used to create a line of neural organoids from stem cells derived from Down Syndrome patients (140). The group of Segura and co-workers developed a method by which hyaluronic acid hydrogels could be functionalized with a variety of cell binding peptides, finding that an exact concentration of the laminin mimetic IKVAV peptide led to the best survival of the organoid (141).

The strength of the synthetic polymer in the culture of organoids is illustrated by a recent paper by Qi and co-workers that used electrospun polylactic(co-glycolic) acid (PLGA) polymers to match the stiffness and permeability of the blood-brain barrier. The constructed barrier was found to be selectively permeable, displaying limited permeability of the anti-tumor drugs paclitaxel and bortezomib, and low permeability of sodium fluorescein. This work is both relevant and exciting, as the function of the blood-brain barrier is not only determined by what cells are present, but also by the tissue's stiffness, permeability to small molecules and shape. The blood-brain barrier organoid was constructed by doping human induced pluripotent stem cells (hiPSC) onto the PLGA matrix. The authors hope that this organoid may be used to study drug delivery across the blood-brain barrier, or to study processes such as addiction (96).

Other organoids, such as pancreatic organoids, have also proved difficult to obtain without resorting to Matrigel-based culture. To our knowledge, the first report of the use of a synthetic hydrogel in the creation of pancreatic organoids was a recent report of human pancreatic progenitors seeded in amikacin hydrate crosslinked with Poly(ethyleneglycol)

diglycidyl ether (PEGDE), also known as Amikagel (142). The group of Candiello and co-workers derived the human pancreatic progenitors from human embryonic stem cells using two previously reported protocols (143, 144). The progenitor cells were seeded in Amikagel synthesized at different elastic moduli.. Notably, no chemical signaling peptide was incorporated into the Amikagel. The authors found that a stiffer gel with a higher crosslinker content drove the progenitor cells to aggregate together, which led to an increased differentiation and maturation into beta-like cells. Compared to the cells grown in Matrigel, the beta-like cells grown in Amikagel produced higher levels of beta-cell functional markers PDX1 and NKX6.1, and were more responsive to glucose challenge. Addition of HUVEC (human umbilical vein endothelial) cells to progenitor cells grown on Amikagel led to even better responses to glucose challenge, suggesting the contribution of endothelial cells is important for more complete differentiation and maturation to beta cells. This article challenges the conventional wisdom that a cell binding moiety is required for effective organoid formation, and if the results hold, represents a potentially new paradigm in organoid formation, where the material's chemical properties do not contribute to the growth and differentiation of cells. A challenge to this approach is the need to control the size of the aggregates, and ensuring long-term viability of the resulting organoids: the authors observed that the aggregates were viable at 5 days, but made no determination of viability at later time points. We note that the size of the smallest cell aggregates reported by Candiello and co-workers was approximately 200 microns, yet the typical human islet has a diameter of approximately 130 microns (145). Larger aggregations of islets have been known to form necrotic centers because of a lack of nutrient diffusion, and the ideal size of an islet is approximately 100-150 microns in diameter (146). Precise control of the aggregate is essential if this method is to find broader application, particularly in transplantation, where viability must be maintained over a long period of time.

A major advantage of synthetic polymers for organoid culture is that they are well-defined mechanically and chemically, making it possible to tease out the effects of mechanical changes on cellular fate, as well as the effect, or necessity, of certain co-cultured cells (131, 147). Additionally, many of the materials developed, such as hyaluronic acid, PEG, and

PLGA, have already been approved by the FDA for use in human therapeutics. Thus, the organoids grown in these materials will face fewer hurdles in being approved for clinical use. Murphy and co-workers recently assessed over 1200 different synthetic polymer formulations for toxicity, vascularization of cell tissue, and the ability to support formation of endothelial cell networks (148). While not directly related to the growth of organoids, the evaluated polymer formulations may provide a valuable starting point for organoid researchers, particularly those concerned with vascularization of the organoids post-implantation.

The disadvantages of synthetic hydrogels are several. First, with the apparent exception of Amikagel, synthetic hydrogels require the deliberate incorporation of biochemical cues. In the absence of the biochemical cues, cells do not attach, which leads to anoikis, or programmed cell death (149), and failure of organoids formation (132). The biochemical cues also must be properly spaced, because improper spacing can also lead to cell death (150). For these reasons, it may be advantageous to engineer recombinant protein gels, where the chemical cues can be added with exact definition, the chemical and mechanical properties of the gel can be altered independently, and degradation rate can be tuned by inclusion of appropriate recognition sites for degradative enzymes such as MMP.

ORGANOID CULTURE IN RECOMBINANT PROTEIN MATRICES

Our group has long worked with programmable, genetically-encoded protein-based materials, which we believe may prove an attractive family of materials for the culture of organoids. Materials made of recombinant proteins display narrow polydispersity, are able to be tuned for stiffness and chemical functionality independent of each other (151, 152), can have their viscoelastic properties easily modified (153), and can be programmed to degrade and remodel at different rates via the inclusion of protease-specific recognition sites (154), or by changing the means by which these proteins are cross-linked (155). Protein-based hydrogels can also incorporate novel functionalities via site-specific incorporation of non-canonical amino acids (156, 157), be made thermally dynamic through the use of elastin-like domains (158, 159), and can be readily tailored to a variety

of biomedical contexts (160, 161). This programmability and ready modifiability makes protein-based hydrogels attractive materials for organoid culture.

The Heilshorn group has previously demonstrated the encapsulation of stem cells in a collagen matrix crosslinked with tetrakis(hydroxymethyl)phosphonium chloride (162). Recently, this group used a recombinant collagen I matrix with a genetically-encoded RGD cell binding sequence to culture an adult intestinal organoid, crosslinking the collagen strains with varying concentrations of tetrakis(hydroxymethyl)phosphonium chloride. They found that a high concentration of RGD binding peptide, as well as a softer matrix or faster degradation rate, enhanced formation of the organoid (163). The same group also found that matrix degradation and remodeling was essential to the maintenance of neural cell stemness, and that this degradability was readily tunable by modifications to the collagen backbone (164).

Recombinant laminin matricies, such as those based off of the commercially-available Laminin 521 and Laminin 111, have also been used in the development of organoids. Cameron and co-workers used a mixture of cell-therapy grade laminin 521 and laminin 111 to differentiate human embryonic stem cells preferentially to functional and mature hepatocytes (165). Similarly, laminin 511 and 521 have also been used in combination for selective differentiation into hepatocytes (166). In contrast, laminin 411 and laminin 511 in combination are found to promote cholangiocyte differentiation instead (167). The effect of laminin 521 in particular is highly dependent upon culture conditions such as the presence of feeder cells. Rohn and co-workers, using a polystyrene surface coated with laminin 521, found that the presence of the α5 chain of laminin suppressed differentiation and instead promoted a quiescent mesenchymal stem cell type in rat liver culture (168). Similarly, Albalushi and co-workers found that pluripotent human embryonic stem cells grown on laminin 521 maintained their pluripotency when grown in conjunction with feeder cells (169), with Tryggvasson reporting similar results in both laminin 511(170) and laminin 521 (171). The interactions of various laminin types with cells is therefore complex, and was the subject of a recent review (149).

Peptide-based hydrogels have also recently found a use in organoid culture. Zhang and co-workers used self-assembling peptide called RADA-16 for the culture of differentiated neuronal organoids in an Alzheimer's disease model, wherein neural organoids were treated with amyloid-β, finding that the effects of the amyloid protein were dependent on whether organoid culture was conducted in 2D (where no substantial degradation of function was found) or 3D culture in peptide-supported matrix, which showed substantially lower levels of pPAK and Drebrin expression upon addition of amyloid (172). The difference in findings between 2D and 3D cultures in neuronal disease states is well-known, and is the subject of a recent review (173).

Protein-based materials have several disadvantages. First, and most obviously, not all proteins can be expressed in good yield, and successful expression is no guarantee of successful refolding or functionality. Certain recombinant proteins and self-assembling peptides have also been shown to be immunogenic (174, 175), immunogenic if aggregated (176), or are known to act as immune system adjuvants (177, 178). Merely ensuring that the recombinant protein comes from a human germline is insufficient to guarantee a lack of immune response (179), meaning that non-human proteins may also be immunogenic in ways that are difficult to predict. This may have an effect on organoid culture, particularly those (such as one that might model tuberculosis infection) that might contain an immune component. Care must therefore be taken to avoid introducing immunogenic epitopes, and preventing an immune response may require empirical optimization. Closely related to this issue is that proteins for clinical use would have to be expressed in mammalian expression systems such as Chinese Hamster Ovary (CHO), or in yeasts such as *Pichia pastoris*, to preclude the presence of bacterial endotoxin.

OUTLOOK

While there are a broad number of Matrigel-free techniques that have been developed, they have been used in a somewhat narrow range of target tissues. Expanding the number of organoid types that can be cultured using non-Matrigel methods will go a long way towards growing acceptance of these alternate culture techniques, as well as allow more organoids

to be made without the presence of xenogeneic material. The ideal material for organoid culture should be chemically and mechanically defined, so that changes in the chemical and mechanical properties of the culture material can be easily and independently correlated to a change in organoid growth, development, or morphology. This material should also be easy to functionalize with biologically-relevant cell binding proteins or peptides in order to promote cell attachment and growth. Finally, the ideal material should mimic the dynamic nature of the ECM, meaning that it is easily programmable in terms of erosion rate, viscoelasticity, and susceptibility to degradation by enzymes secreted by cultured cells. Because of these requirements, it is likely that either synthetic materials such as PEG gels, or programmable recombinant proteins, represent fruitful areas of future research.

Pancreatic organoids might be the next tissue type on which to focus efforts to create organoids in Matrigel-free material: transplantation of islets of Langerhans is a promising treatment for Type 1 diabetes (180, 181), but its wider adaptation is limited by the limited availability of suitable cadaveric donor islets (182). Deriving functional islets of Langerhans from stem cells is therefore an attractive option to ensure that there are enough islets available for transplantation. Current uses of pancreatic organoids include models for cancers and other diseases (73, 183-185). Would-be creators of pancreatic organoids using Matrigel-free techniques could take inspiration from methods that have proven successful in the development of hepatic organoids, as the liver and pancreas develop from the same population of endodermal progenitors (186), and there has been great success in the reprogramming of adult liver cells to pancreatic cells (187). Using the methods discussed above, we anticipate a gradual shifting away from the predominant use of Matrigel in organoid culture. In the following chapter, we will detail our efforts at making programmable protein-based hydrogel materials for the purpose of culturing pancreatic cells.

REFERENCES FOR CHAPTER 1

1. Lancaster MA & Knoblich JA (2014) Organogenesis in a dish: Modeling development and disease using organoid technologies. *Science* 345(6194):10.
2. Grapin-Botton A (2016) Three-dimensional pancreas organogenesis models. *Diabetes Obes. Metab.* 18:33-40.
3. Boj SF, *et al.* (2015) Organoid Models of Human and Mouse Ductal Pancreatic Cancer. *Cell* 160(1-2):324-338.
4. Qian XY, Nguyen HN, Jacob F, Song HJ, & Ming GL (2017) Using brain organoids to understand Zika virus-induced microcephaly. *Development* 144(6):952-957.
5. Choi H, Song J, Park G, & Kim J (2017) Modeling of Autism Using Organoid Technology. *Mol. Neurobiol.* 54(10):7789-7795.
6. van de Wetering M, *et al.* (2015) Prospective Derivation of a Living Organoid Biobank of Colorectal Cancer Patients. *Cell* 161(4):933-945.
7. Schwank G, *et al.* (2013) Functional Repair of CFTR by CRISPR/Cas9 in Intestinal Stem Cell Organoids of Cystic Fibrosis Patients. *Cell Stem Cell* 13(6):653-658.
8. Takebe T, *et al.* (2013) Vascularized and functional human liver from an iPSC-derived organ bud transplant. *Nature* 499(7459):481-+.
9. Takebe T, *et al.* (2014) Generation of a vascularized and functional human liver from an iPSC-derived organ bud transplant. *Nat. Protoc.* 9(2):396-409.
10. Dekkers JF, *et al.* (2016) Characterizing responses to CFTR-modulating drugs using rectal organoids derived from subjects with cystic fibrosis. *Sci. Transl. Med.* 8(344):12.
11. Drost J & Clevers H (2017) Translational applications of adult stem cell-derived organoids. *Development* 144(6):968-975.
12. Kleinman HK & Martin GR (2005) Matrigel: Basement membrane matrix with biological activity. *Semin. Cancer Biol.* 15(5):378-386.
13. Sato T, *et al.* (2009) Single Lgr5 stem cells build crypt-villus structures *in vitro* without a mesenchymal niche. *Nature* 459(7244):262-U147.
14. Sato T, *et al.* (2011) Long-term Expansion of Epithelial Organoids From Human Colon, Adenoma, Adenocarcinoma, and Barrett's Epithelium. *Gastroenterology* 141(5):1762-1772.
15. Stange DE, *et al.* (2013) Differentiated Troy(+) Chief Cells Act as Reserve Stem Cells to Generate All Lineages of the Stomach Epithelium. *Cell* 155(2):357-368.
16. Barker N, *et al.* (2010) Lgr5(+ve) Stem Cells Drive Self-Renewal in the Stomach and Build Long-Lived Gastric Units *In Vitro*. *Cell Stem Cell* 6(1):25-36.
17. Dekkers JF, *et al.* (2013) A functional CFTR assay using primary cystic fibrosis intestinal organoids. *Nat. Med.* 19(7):939-+.
18. Huch M, *et al.* (2013) *In vitro* expansion of single Lgr5(+) liver stem cells induced by Wnt-driven regeneration. *Nature* 494(7436):247-250.
19. Nie J, Koehler KR, & Hashino E (2017) Directed Differentiation of Mouse Embryonic Stem Cells Into Inner Ear Sensory Epithelia in 3D Culture. *Methods in molecular biology* 1597:67-83.
20. Tiriac H, *et al.* (2018) Organoid Profiling Identifies Common Responders to Chemotherapy in Pancreatic Cancer. *Cancer Discov.* 8(9):1112-1129.
21. Tsai S, *et al.* (2018) Development of primary human pancreatic cancer organoids, matched stromal and immune cells and 3D tumor microenvironment models. *BMC Cancer* 18:13.

22. Seino T, *et al.* (2018) Human Pancreatic Tumor Organoids Reveal Loss of Stem Cell Niche Factor Dependence during Disease Progression. *Cell Stem Cell* 22(3):454-+.
23. Wang WW, Jin S, & Ye KM (2017) Development of Islet Organoids from H9 Human Embryonic Stem Cells in Biomimetic 3D Scaffolds. *Stem Cells Dev.* 26(6):394-404.
24. Fatehullah A, Tan SH, & Barker N (2016) Organoids as an *in vitro* model of human development and disease. *Nat. Cell Biol.* 18(3):246-254.
25. Yiangou L, Ross ADB, Goh KJ, & Vallier L (2018) Human Pluripotent Stem Cell-Derived Endoderm for Modeling Development and Clinical Applications. *Cell Stem Cell* 22(4):485-499.
26. Hughes CS, Postovit LM, & Lajoie GA (2010) Matrigel: A complex protein mixture required for optimal growth of cell culture. *Proteomics* 10(9):1886-1890.
27. Goldstein AS, *et al.* (2011) Purification and direct transformation of epithelial progenitor cells from primary human prostate. *Nat. Protoc.* 6(5):656-667.
28. Vukicevic S, *et al.* (1992) IDENTIFICATION OF MULTIPLE ACTIVE GROWTH-FACTORS IN BASEMENT-MEMBRANE MATRIGEL SUGGESTS CAUTION IN INTERPRETATION OF CELLULAR-ACTIVITY RELATED TO EXTRACELLULAR-MATRIX COMPONENTS. *Exp. Cell Res.* 202(1):1-8.
29. Spence JR (2018) Taming the Wild West of Organoids, Enteroids, and Mini-Guts. *Cell. Mol. Gastroenterol. Hepatol.* 5(2):159-160.
30. Huch M, Knoblich JA, Lutolf MP, & Martinez-Arias A (2017) The hope and the hype of organoid research. *Development* 144(6):938-941.
31. Unger C, Skottman H, Blomberg P, Dilber MS, & Hovatta O (2008) Good manufacturing practice and clinical-grade human embryonic stem cell lines. *Hum. Mol. Genet.* 17:R48-R53.
32. Ludwig TE, *et al.* (2006) Derivation of human embryonic stem cells in defined conditions. *Nat. Biotechnol.* 24(2):185-187.
33. Prokhorova TA, *et al.* (2009) Teratoma Formation by Human Embryonic Stem Cells Is Site Dependent and Enhanced by the Presence of Matrigel. *Stem Cells Dev.* 18(1):47-54.
34. Hentze H, *et al.* (2009) Teratoma formation by human embryonic stem cells: Evaluation of essential parameters for future safety studies. *Stem Cell Res.* 2(3):198-210.
35. Vaillant F, Lindeman GJ, & Visvader JE (2011) Jekyll or Hyde: does Matrigel provide a more or less physiological environment in mammary repopulating assays? *Breast Cancer Res.* 13(3):4.
36. Mahoney ZX, Stappenbeck TS, & Miner JH (2008) Laminin alpha 5 influences the architecture of the mouse small intestine mucosa. *J. Cell Sci.* 121(15):2493-2502.
37. Gjorevski N, Ranga A, & Lutolf MP (2014) Bioengineering approaches to guide stem cell-based organogenesis. *Development* 141(9):1794-1804.
38. Chaudhuri O (2017) Viscoelastic hydrogels for 3D cell culture. *Biomaterials science* 5(8):1480-1490.
39. Engler AJ, Sen S, Sweeney HL, & Discher DE (2006) Matrix elasticity directs stem cell lineage specification. *Cell* 126(4):677-689.
40. Nelson CM & Gleghorn JP (2012) Sculpting Organs: Mechanical Regulation of Tissue Development. *Annual Review of Biomedical Engineering, Vol 14,* Annual Review of Biomedical Engineering, ed Yarmush ML (Annual Reviews, Palo Alto), Vol 14, pp 129-154.
41. Dahl-Jensen S & Grapin-Botton A (2017) The physics of organoids: a biophysical approach to understanding organogenesis. *Development* 144(6):946-951.
42. Murphy WL, McDevitt TC, & Engler AJ (2014) Materials as stem cell regulators. *Nature materials* 13(6):547-557.

43. Vining KH & Mooney DJ (2017) Mechanical forces direct stem cell behaviour in development and regeneration. *Nat. Rev. Mol. Cell Biol.* 18(12):728-742.
44. Slater KP, J; Nandivada, H. (Tuning the Elastic Moduli of Corning® Matrigel® and Collagen I 3D Matrices by Varying the Protein Concentration: Application Note. ed Sciences CIL.
45. Nemir S & West JL (2010) Synthetic Materials in the Study of Cell Response to Substrate Rigidity. *Ann. Biomed. Eng.* 38(1):2-20.
46. Miroshnikova YA, *et al.* (2011) Engineering strategies to recapitulate epithelial morphogenesis within synthetic three-dimensional extracellular matrix with tunable mechanical properties. *Phys. Biol.* 8(2):13.
47. Soofi SS, Last JA, Liliensiek SJ, Nealey PF, & Murphy CJ (2009) The elastic modulus of Matrigel (TM) as determined by atomic force microscopy. *J. Struct. Biol.* 167(3):216-219.
48. Reed J, Walczak WJ, Petzold ON, & Gimzewski JK (2009) In situ mechanical interferometry of matrigel films. *Langmuir* 25(1):36-39.
49. Hussey GSD, J.L.; Badylak, S.F. (2018) Extracellular matrix- based materials for regenerative medicine. *Nature Reviews Materials* 3:159-173.
50. Keane TJ, Swinehart IT, & Badylak SF (2015) Methods of tissue decellularization used for preparation of biologic scaffolds and *in vivo* relevance. *Methods* 84:25-34.
51. Allman AJ, *et al.* (2001) Xenogeneic extracellular matrix grafts elicit a Th2-restricted immune response. *Transplantation* 71(11):1631-1640.
52. Parmaksiz M, Dogan A, Odabas S, Elcin AE, & Elcin YM (2016) Clinical applications of decellularized extracellular matrices for tissue engineering and regenerative medicine. *Biomed. Mater.* 11(2):14.
53. Lin P, Chan WCW, Badylak SF, & Bhatia SN (2004) Assessing porcine liver-derived biomatrix for hepatic tissue engineering. *Tissue Eng.* 10(7-8):1046-1053.
54. Baptista PM, *et al.* (2011) The Use of Whole Organ Decellularization for the Generation of a Vascularized Liver Organoid. *Hepatology* 53(2):604-617.
55. Mazza G, *et al.* (2015) Decellularized human liver as a natural 3D-scaffold for liver bioengineering and transplantation. *Sci Rep* 5:15.
56. Maghsoudlou P, *et al.* (2016) Optimization of Liver Decellularization Maintains Extracellular Matrix Micro-Architecture and Composition Predisposing to Effective Cell Seeding. *PLoS One* 11(5):19.
57. Lee JS, *et al.* (2014) Liver Extracellular Matrix Providing Dual Functions of Two-Dimensional Substrate Coating and Three-Dimensional Injectable Hydrogel Platform for Liver Tissue Engineering. *Biomacromolecules* 15(1):206-218.
58. Saheli M, *et al.* (2018) Three-dimensional liver-derived extracellular matrix hydrogel promotes liver organoids function. *J Cell Biochem* 119(6):4320-4333.
59. Finkbeiner SR, *et al.* (2015) Generation of tissue-engineered small intestine using embryonic stem cell-derived human intestinal organoids. *Biol. Open* 4(11):1462-1472.
60. Sambi M, *et al.* (2017) Acellular Mouse Kidney ECM can be Used as a Three-Dimensional Substrate to Test the Differentiation Potential of Embryonic Stem Cell Derived Renal Progenitors. *Stem Cell Rev. Rep.* 13(4):513-531.
61. Shojaie S, *et al.* (2015) Acellular Lung Scaffolds Direct Differentiation of Endoderm to Functional Airway Epithelial Cells: Requirement of Matrix-Bound HS Proteoglycans. *Stem Cell Rep.* 4(3):419-430.
62. Orlando G, *et al.* (2013) Discarded human kidneys as a source of ECM scaffold for kidney regeneration technologies. *Biomaterials* 34(24):5915-5925.

63. Batchelder CA, Martinez ML, & Tarantal AF (2015) Natural Scaffolds for Renal Differentiation of Human Embryonic Stem Cells for Kidney Tissue Engineering. *PLoS One* 10(12):18.
64. Guyette JP, *et al.* (2014) Perfusion decellularization of whole organs. *Nat. Protoc.* 9(6):1451-1468.
65. Hong X, *et al.* (2018) Skeletal Extracellular Matrix Supports Cardiac Differentiation of Embryonic Stem Cells: a Potential Scaffold for Engineered Cardiac Tissue. *Cell. Physiol. Biochem.* 45(1):319-331.
66. Gilpin SE, *et al.* (2014) Perfusion decellularization of human and porcine lungs: Bringing the matrix to clinical scale. *J. Heart Lung Transplant.* 33(3):298-308.
67. Elebring E, Kuna VK, Kvarnstrom N, & Sumitran-Holgersson S (2017) Cold-perfusion decellularization of whole-organ porcine pancreas supports human fetal pancreatic cell attachment and expression of endocrine and exocrine markers. *J. Tissue Eng.* 8:10.
68. Sackett SD, *et al.* (2018) Extracellular matrix scaffold and hydrogel derived from decellularized and delipidized human pancreas. *Sci Rep* 8:16.
69. Chaimov D, *et al.* (2017) Innovative encapsulation platform based on pancreatic extracellular matrix achieve substantial insulin delivery. *Journal of controlled release : official journal of the Controlled Release Society* 257:91-101.
70. Nitta Gelatin N (2019) Biomedical Gelatin & Collagen. (Nitta Gelatin, NA).
71. Devarasetty M, Skardal A, Cowdrick K, Marini F, & Soker S (2017) Bioengineered Submucosal Organoids for *In Vitro* Modeling of Colorectal Cancer. *Tissue Eng. Part A* 23(19-20):1026-1041.
72. Scott A, *et al.* (2016) Long-term renewable human intestinal epithelial stem cells as monolayers: A potential for clinical use. *Journal of Pediatric Surgery* 51(6):995-1000.
73. Kim J, *et al.* (2013) An iPSC Line from Human Pancreatic Ductal Adenocarcinoma Undergoes Early to Invasive Stages of Pancreatic Cancer Progression. *Cell Reports* 3(6):2088-2099.
74. Takezawa T, Ozaki K, Nitani A, Takabayashi C, & Shimo-Oka T (2004) Collagen vitrigel: A novel scaffold that can facilitate a three-dimensional culture for reconstructing organoids. *Cell Transplant.* 13(4):463-473.
75. Yui SR, *et al.* (2012) Functional engraftment of colon epithelium expanded *in vitro* from a single adult Lgr5(+) stem cell. *Nat. Med.* 18(4):618-623.
76. Ootani A, *et al.* (2009) Sustained *in vitro* intestinal epithelial culture within a Wnt-dependent stem cell niche. *Nat. Med.* 15(6):1-U140.
77. Jabaji Z, *et al.* (2013) Use of Collagen Gel as an Alternative Extracellular Matrix for the *In Vitro* and *In Vivo* Growth of Murine Small Intestinal Epithelium. *Tissue Eng. Part C-Methods* 19(12):961-969.
78. Jabaji Z, *et al.* (2014) Type I Collagen as an Extracellular Matrix for the *In Vitro* Growth of Human Small Intestinal Epithelium. *PLoS One* 9(9):9.
79. Yui S, *et al.* (2018) YAP/TAZ-Dependent Reprogramming of Colonic Epithelium Links ECM Remodeling to Tissue Regeneration. *Cell Stem Cell* 22(1):35-+.
80. Neal JT, *et al.* (2018) Organoid Modeling of the Tumor Immune Microenvironment. *Cell* 175(7):1972-+.
81. Usui T, *et al.* (2018) Hedgehog Signals Mediate Anti-Cancer Drug Resistance in Three-Dimensional Primary Colorectal Cancer Organoid Culture. *Int. J. Mol. Sci.* 19(4):12.
82. Isshiki H, *et al.* (2017) Establishment of a refined culture method for rat colon organoids. *Biochem. Biophys. Res. Commun.* 489(3):305-311.
83. Streuli CH (2009) Integrins and cell-fate determination. *J. Cell Sci.* 122(2):171.

84. Khoshnoodi J, Pedchenko V, & Hudson BG (2008) Mammalian collagen IV. *Microscopy research and technique* 71(5):357-370.
85. Fatehullah A, Appleton PL, & Nathke IS (2013) Cell and tissue polarity in the intestinal tract during tumourigenesis: cells still know the right way up, but tissue organization is lost. *Philosophical transactions of the Royal Society of London. Series B, Biological sciences* 368(1629):20130014.
86. Lee JL & Streuli CH (2014) Integrins and epithelial cell polarity. *J. Cell Sci.* 127(Pt 15):3217-3225.
87. Myllymäki SM, Teräväinen TP, & Manninen A (2011) Two Distinct Integrin-Mediated Mechanisms Contribute to Apical Lumen Formation in Epithelial Cells. *PLoS One* 6(5):e19453.
88. Tong ZX, *et al.* (2018) Towards a defined ECM and small molecule based monolayer culture system for the expansion of mouse and human intestinal stem cells. *Biomaterials* 154:60-73.
89. Wang Y, *et al.* (2016) Extracellular Matrix Functionalization and Huh-7.5 Cell Coculture Promote the Hepatic Differentiation of Human Adipose-Derived Mesenchymal Stem Cells in a 3D ICC Hydrogel Scaffold. *ACS Biomater. Sci. Eng.* 2(12):2255-2265.
90. Matarasso SL (2006) The use of injectable collagens for aesthetic rejuvenation. *Semin. Cutan. Med. Surg.* 25(3):151-157.
91. Wagner DE, *et al.* (2014) Comparative decellularization and recellularization of normal versus emphysematous human lungs. *Biomaterials* 35(10):3281-3297.
92. Booth AJ, *et al.* (2012) Acellular Normal and Fibrotic Human Lung Matrices as a Culture System for *In Vitro* Investigation. *Am. J. Respir. Crit. Care Med.* 186(9):866-876.
93. Sullivan KE, Quinn KP, Tang KM, Georgakoudi I, & Black LD (2014) Extracellular matrix remodeling following myocardial infarction influences the therapeutic potential of mesenchymal stem cells. *Stem Cell Res. Ther.* 5:15.
94. Keane TJ, Londono R, Turner NJ, & Badylak SF (2012) Consequences of ineffective decellularization of biologic scaffolds on the host response. *Biomaterials* 33(6):1771-1781.
95. Sternlicht MD & Werb Z (2001) How matrix metalloproteinases regulate cell behavior. *Annu. Rev. Cell Dev. Biol.* 17:463-516.
96. Qi DJ, *et al.* (2018) Establishment of a Human iPSC- and Nanofiber-Based Microphysiological Blood-Brain Barrier System. *ACS Appl. Mater. Interfaces* 10(26):21825-21835.
97. Kloxin AM, Kasko AM, Salinas CN, & Anseth KS (2009) Photodegradable Hydrogels for Dynamic Tuning of Physical and Chemical Properties. *Science* 324(5923):59-63.
98. Guvendiren M & Burdick JA (2012) Stiffening hydrogels to probe short- and long-term cellular responses to dynamic mechanics. *Nat. Commun.* 3:9.
99. Qayyum AS, *et al.* (2017) Design of electrohydrodynamic sprayed polyethylene glycol hydrogel microspheres for cell encapsulation. *Biofabrication* 9(2):16.
100. Skardal A, *et al.* (2016) Bioprinting Cellularized Constructs Using a Tissue-specific Hydrogel Bioink. *J. Vis. Exp.* (110):8.
101. Tabata Y & Lutolf MP (2017) Multiscale microenvironmental perturbation of pluripotent stem cell fate and self-organization. *Sci Rep* 7:11.
102. Lambert CR, Nijsure D, Huynh V, & Wylie RG (2018) Hydrogels with reversible chemical environments for *in vitro* cell culture. *Biomed. Mater.* 13(4):11.
103. Ekerdt BL, *et al.* (2018) Thermoreversible Hyaluronic Acid-PNIPAAm Hydrogel Systems for 3D Stem Cell Culture. *Adv. Healthc. Mater.* 7(12):12.

104. Qin XH, Wang XP, Rottmar M, Nelson BJ, & Maniura-Weber K (2018) Near-Infrared Light-Sensitive Polyvinyl Alcohol Hydrogel Photoresist for Spatiotemporal Control of Cell-Instructive 3D Microenvironments. *Adv. Mater.* 30(10):7.
105. Malandrino A, Mak M, Kamm RD, & Moeendarbary E (2018) Complex mechanics of the heterogeneous extracellular matrix in cancer. *Extreme Mech. Lett.* 21:25-34.
106. Zhu JR, Liang L, Jiao Y, Liu LY, & Allianc US-CPS-O (2015) Enhanced Invasion of Metastatic Cancer Cells via Extracellular Matrix Interface. *PLoS One* 10(2):17.
107. Schuppan D & Afdhal NH (2008) Liver cirrhosis. *Lancet (London, England)* 371(9615):838-851.
108. Sun S, Song Z, Cotler SJ, & Cho M (2014) Biomechanics and functionality of hepatocytes in liver cirrhosis. *Journal of Biomechanics* 47(9):2205-2210.
109. Ranga A & Lutolf MP (2012) High-throughput approaches for the analysis of extrinsic regulators of stem cell fate. *Curr. Opin. Cell Biol.* 24(2):236-244.
110. Gobaa S, *et al.* (2011) Artificial niche microarrays for probing single stem cell fate in high throughput. *Nat. Methods* 8(11):949-955.
111. Anderson DG, Levenberg S, & Langer R (2004) Nanoliter-scale synthesis of arrayed biomaterials and application to human embryonic stem cells. *Nat. Biotechnol.* 22(7):863-866.
112. Lutolf MP & Hubbell JA (2005) Synthetic biomaterials as instructive extracellular microenvironments for morphogenesis in tissue engineering. *Nat. Biotechnol.* 23(1):47-55.
113. Nguyen KT & West JL (2002) Photopolymerizable hydrogels for tissue engineering applications. *Biomaterials* 23(22):4307-4314.
114. Saha K, Pollock JF, Schaffer DV, & Healy KE (2007) Designing synthetic materials to control stem cell phenotype. *Curr. Opin. Chem. Biol.* 11(4):381-387.
115. Tibbitt MW & Anseth KS (2012) Dynamic Microenvironments: The Fourth Dimension. *Sci. Transl. Med.* 4(160):4.
116. Lutolf MP & Hubbell JA (2003) Synthesis and physicochemical characterization of end-linked poly(ethylene glycol)-co-peptide hydrogels formed by Michael-type addition. *Biomacromolecules* 4(3):713-722.
117. Lutolf MR, *et al.* (2003) Repair of bone defects using synthetic mimetics of collagenous extracellular matrices. *Nat. Biotechnol.* 21(5):513-518.
118. Wylie RG, *et al.* (2011) Spatially controlled simultaneous patterning of multiple growth factors in three-dimensional hydrogels. *Nature materials* 10(10):799-806.
119. DeForest CA & Anseth KS (2012) Photoreversible Patterning of Biomolecules within Click-Based Hydrogels. *Angew. Chem.-Int. Edit.* 51(8):1816-1819.
120. Mosiewicz KA, *et al.* (2013) In situ cell manipulation through enzymatic hydrogel photopatterning. *Nature materials* 12(11):1071-1077.
121. DeForest CA & Tirrell DA (2015) A photoreversible protein-patterning approach for guiding stem cell fate in three-dimensional gels. *Nature materials* 14(5):523-531.
122. Ranga A, *et al.* (2014) 3D niche microarrays for systems-level analyses of cell fate. *Nat. Commun.* 5:10.
123. Ranga A, *et al.* (2016) Neural tube morphogenesis in synthetic 3D microenvironments. *Proc. Natl. Acad. Sci. U. S. A.* 113(44):E6831-E6839.
124. Ng SS, *et al.* (2018) Human iPS derived progenitors bioengineered into liver organoids using an inverted colloidal crystal poly (ethylene glycol) scaffold. *Biomaterials* 182:299-311.

125. Shirahama H, *et al.* (2016) Fabrication of Inverted Colloidal Crystal Poly(ethylene glycol) Scaffold: A Three-dimensional Cell Culture Platform for Liver Tissue Engineering. *J. Vis. Exp.* (114):12.
126. Ng SS, *et al.* (2017) Long-term culture of human liver tissue with advanced hepatic functions. *JCI Insight* 2(11):11.
127. Ovadia EM, Colby DW, & Kloxin AM (2018) Designing well-defined photopolymerized synthetic matrices for three-dimensional culture and differentiation of induced pluripotent stem cells. *Biomaterials science* 6(6):1358-1370.
128. Villarin BL, *et al.* (2015) Polymer Supported Directed Differentiation Reveals a Unique Gene Signature Predicting Stable Hepatocyte Performance. *Adv. Healthc. Mater.* 4(12):1820-1825.
129. Lucendo-Villarin B, *et al.* (2014) Stabilizing Hepatocellular Phenotype Using Optimized Synthetic Surfaces. *J. Vis. Exp.* (91):10.
130. Yan JX, Wang Y, & Wang YF (2018) Stem-cell Derived Functional Mouse Hepatic Organoids in Hyaluronan Hydrogels. *Prog. Biochem. Biophys.* 45(5):567-574.
131. Lee HJ, *et al.* (2017) Elasticity-based development of functionally enhanced multicellular 3D liver encapsulated in hybrid hydrogel. *Acta Biomater.* 64:67-79.
132. Gjorevski N, *et al.* (2016) Designer matrices for intestinal stem cell and organoid culture. *Nature* 539(7630):560-+.
133. Gjorevski N & Lutolf MP (2017) Synthesis and characterization of well-defined hydrogel matrices and their application to intestinal stem cell and organoid culture. *Nat. Protoc.* 12(11):2263-2274.
134. Grandi F, *et al.* (2018) Composite Scaffolds Based on Intestinal Extracellular Matrices and Oxidized Polyvinyl Alcohol: A Preliminary Study for a New Regenerative Approach in Short Bowel Syndrome. *Biomed Res. Int.*:13.
135. Cruz-Acuna R, *et al.* (2017) Synthetic hydrogels for human intestinal organoid generation and colonic wound repair. *Nat. Cell Biol.* 19(11):1326-+.
136. Cruz-Acuna R, *et al.* (2018) PEG-4MAL hydrogels for human organoid generation, culture, and *in vivo* delivery. *Nat. Protoc.* 13(9):2102-2119.
137. Di Lullo E & Kriegstein AR (2017) The use of brain organoids to investigate neural development and disease. *Nature Reviews Neuroscience* 18:573.
138. Schwartz MP, *et al.* (2015) Human pluripotent stem cell-derived neural constructs for predicting neural toxicity. *Proc. Natl. Acad. Sci. U. S. A.* 112(40):12516-12521.
139. Lindborg BA, *et al.* (2016) Rapid Induction of Cerebral Organoids From Human Induced Pluripotent Stem Cells Using a Chemically Defined Hydrogel and Defined Cell Culture Medium. *Stem Cells Transl. Med.* 5(7):970-979.
140. Wu SH, Xu RJ, Duan B, & Jiang P (2017) Three-dimensional hyaluronic acid hydrogel-based models for *in vitro* human iPSC-derived NPC culture and differentiation. *J. Mat. Chem. B* 5(21):3870-3878.
141. Lam J, Carmichael ST, Lowry WE, & Segura T (2015) Hydrogel Design of Experiments Methodology to Optimize Hydrogel for iPSC-NPC Culture. *Adv. Healthc. Mater.* 4(4):534-539.
142. Candiello J, *et al.* (2018) 3D heterogeneous islet organoid generation from human embryonic stem cells using a novel engineered hydrogel platform. *Biomaterials* 177:27-39.
143. Pagliuca Felicia W, *et al.* (2014) Generation of Functional Human Pancreatic Beta Cells *In Vitro*. *Cell* 159(2):428-439.

144. Jaramillo M, Mathew S, Mamiya H, Goh SK, & Banerjee I (2014) Endothelial Cells Mediate Islet-Specific Maturation of Human Embryonic Stem Cell-Derived Pancreatic Progenitor Cells. *Tissue Eng. Part A* 21(1-2):14-25.
145. Rorsman P & Braun M (2013) Regulation of Insulin Secretion in Human Pancreatic Islets. *Annual Review of Physiology, Vol 75*, Annual Review of Physiology, ed Julius D (Annual Reviews, Palo Alto), Vol 75, pp 155-179.
146. Hilderink J, *et al.* (2015) Controlled aggregation of primary human pancreatic islet cells leads to glucose-responsive pseudoislets comparable to native islets. *Journal of cellular and molecular medicine* 19(8):1836-1846.
147. Li CY, *et al.* (2014) Micropatterned Cell-Cell Interactions Enable Functional Encapsulation of Primary Hepatocytes in Hydrogel Microtissues. *Tissue Eng. Part A* 20(15-16):2200-2212.
148. Nguyen EH, *et al.* (2017) Versatile synthetic alternatives to Matrigel for vascular toxicity screening and stem cell expansion. *Nat. Biomed. Eng* 1(7):14.
149. Hagbard L, *et al.* (2018) Developing defined substrates for stem cell culture and differentiation. *Philos. Trans. R. Soc. B-Biol. Sci.* 373(1750):9.
150. Hof KS & Bastings MMC (2017) Programmable Control in Extracellular Matrix-mimicking Polymer Hydrogels. *Chimia* 71(6):342-348.
151. Madl CM, Katz LM, & Heilshorn SC (2016) Bio-Orthogonally Crosslinked, Engineered Protein Hydrogels with Tunable Mechanics and Biochemistry for Cell Encapsulation. *Adv. Funct. Mater.* 26(21):3612-3620.
152. Liu X, *et al.* (2018) Versatile Engineered Protein Hydrogels Enabling Decoupled Mechanical and Biochemical Tuning for Cell Adhesion and Neurite Growth. *ACS Applied Nano Materials* 1(4):1579-1585.
153. Dooling LJ & Tirrell DA (2016) Engineering the Dynamic Properties of Protein Networks through Sequence Variation. *ACS Central Sci.* 2(11):812-819.
154. Galler KM, Aulisa L, Regan KR, D'Souza RN, & Hartgerink JD (2010) Self-assembling multidomain peptide hydrogels: designed susceptibility to enzymatic cleavage allows enhanced cell migration and spreading. *J Am Chem Soc* 132(9):3217-3223.
155. Shen W, Zhang KC, Kornfield JA, & Tirrell DA (2006) Tuning the erosion rate of artificial protein hydrogels through control of network topology. *Nature materials* 5(2):153-158.
156. Link AJ, Mock ML, & Tirrell DA (2003) Non-canonical amino acids in protein engineering. *Curr. Opin. Biotechnol.* 14(6):603-609.
157. Connor RE & Tirrell DA (2007) Non-Canonical Amino Acids in Protein Polymer Design. *Polymer Reviews* 47(1):9-28.
158. Li NK, Quiroz FG, Hall CK, Chilkoti A, & Yingling YG (2014) Molecular Description of the LCST Behavior of an Elastin-Like Polypeptide. *Biomacromolecules* 15(10):3522-3530.
159. MacEwan SR & Chilkoti A (2010) Elastin-Like Polypeptides: Biomedical Applications of Tunable Biopolymers. *Biopolymers* 94(1):60-77.
160. Langer R & Tirrell DA (2004) Designing materials for biology and medicine. *Nature* 428(6982):487-492.
161. Fong E & Tirrell DA (2010) Collective Cell Migration on Artificial Extracellular Matrix Proteins Containing Full-Length Fibronectin Domains. *Adv. Mater.* 22(46):5271-5275.
162. Chung C, Lampe KJ, & Heilshorn SC (2012) Tetrakis(hydroxymethyl) phosphonium chloride as a covalent cross-linking agent for cell encapsulation within protein-based hydrogels. *Biomacromolecules* 13(12):3912-3916.

163. DiMarco RL, Dewi RE, Bernal G, Kuoc C, & Heilshorn SC (2015) Protein-engineered scaffolds for *in vitro* 3D culture of primary adult intestinal organoids. *Biomaterials science* 3(10):1376-1385.
164. Madl CM, *et al.* (2017) Maintenance of neural progenitor cell stemness in 3D hydrogels requires matrix remodelling. *Nature materials* 16(12):1233-+.
165. Cameron K, *et al.* (2015) Recombinant Laminins Drive the Differentiation and Self-Organization of hESC-Derived Hepatocytes. *Stem Cell Rep.* 5(6):1250-1262.
166. Kanninen LK, *et al.* (2016) Laminin-511 and laminin-521-based matrices for efficient hepatic specification of human pluripotent stem cells. *Biomaterials* 103:86-100.
167. Takayama K, *et al.* (2016) Laminin 411 and 511 promote the cholangiocyte differentiation of human induced pluripotent stem cells. *Biochem. Biophys. Res. Commun.* 474(1):91-96.
168. Rohn F, *et al.* (2018) Laminin-521 promotes quiescence in isolated stellate cells from rat liver. *Biomaterials* 180:36-51.
169. Albalushi H, *et al.* (2018) Laminin 521 Stabilizes the Pluripotency Expression Pattern of Human Embryonic Stem Cells Initially Derived on Feeder Cells. *Stem Cells Int.*:9.
170. Domogatskaya A, Rodin S, Boutaud A, & Tryggvason K (2008) Laminin-511 but Not-332,-111, or-411 Enables Mouse Embryonic Stem Cell Self-Renewal *In Vitro*. *Stem Cells* 26(11):2800-2809.
171. Rodin S, Antonsson L, Hovatta O, & Tryggvason K (2014) Monolayer culturing and cloning of human pluripotent stem cells on laminin-521-based matrices under xeno-free and chemically defined conditions. *Nat. Protoc.* 9(10):2354-2368.
172. Zhang DW, *et al.* (2014) A 3D Alzheimer's disease culture model and the induction of P21-activated kinase mediated sensing in iPSC derived neurons. *Biomaterials* 35(5):1420-1428.
173. Centeno EGZ, Cimarosti H, & Bithell A (2018) 2D versus 3D human induced pluripotent stem cell-derived cultures for neurodegenerative disease modelling. *Mol. Neurodegener.* 13:15.
174. Vigneswaran Y, *et al.* (2016) This paper is the winner of an SFB Award in the Hospital Intern, Residency category: Peptide biomaterials raising adaptive immune responses in wound healing contexts. *Journal of biomedical materials research. Part A* 104(8):1853-1862.
175. Collier JH, Rudra JS, Gasiorowski JZ, & Jung JP (2010) Multi-component extracellular matrices based on peptide self-assembly. *Chem. Soc. Rev.* 39(9):3413-3424.
176. Rosenberg AS (2006) Effects of protein aggregates: an immunologic perspective. *The AAPS journal* 8(3):E501-507.
177. Rudra JS, Tian YF, Jung JP, & Collier JH (2010) A self-assembling peptide acting as an immune adjuvant. *Proc Natl Acad Sci U S A* 107(2):622-627.
178. Rudra JS, *et al.* (2012) Modulating adaptive immune responses to peptide self-assemblies. *ACS Nano* 6(2):1557-1564.
179. Baker MP, Reynolds HM, Lumicisi B, & Bryson CJ (2010) Immunogenicity of protein therapeutics: The key causes, consequences and challenges. *Self/nonself* 1(4):314-322.
180. Shapiro AMJ, *et al.* (2000) Islet transplantation in seven patients with type 1 diabetes mellitus using a glucocorticoid-free immunosuppressive regimen. *N. Engl. J. Med.* 343(4):230-238.
181. Shapiro AMJ, Pokrywczynska M, & Ricordi C (2017) Clinical pancreatic islet transplantation. *Nat. Rev. Endocrinol.* 13(5):268-277.
182. Shapiro AMJ (2011) Strategies toward single-donor islets of Langerhans transplantation. *Curr. Opin. Organ Transpl.* 16(6):627-631.

183. Tsai S, *et al.* (2018) Development of primary human pancreatic cancer organoids, matched stromal and immune cells and 3D tumor microenvironment models. *BMC Cancer* 18(1):335-335.
184. Baker LA, Tiriac H, Clevers H, & Tuveson DA (2016) Modeling Pancreatic Cancer with Organoids. *Trends in Cancer* 2(4):176-190.
185. Moreira L, *et al.* (2017) Pancreas 3D Organoids: Current and Future Aspects as a Research Platform for Personalized Medicine in Pancreatic Cancer. *Cell. Mol. Gastroenterol. Hepatol.* 5(3):289-298.
186. Zaret KS (2008) Genetic programming of liver and pancreas progenitors: lessons for stem-cell differentiation. *Nat. Rev. Genet.* 9(5):329-340.
187. Cerdá-Esteban N, *et al.* (2017) Stepwise reprogramming of liver cells to a pancreas progenitor state by the transcriptional regulator Tgif2. *Nat. Commun.* 8:14127-14127.

Chapter II

A NOVEL METHOD FOR CULTURE OF PANCREATIC CELLS IN A DEFINED, PROTEIN-BASED MEDIUM

INTRODUCTION

Type 1 diabetes is an autoimmune disorder that results in the destruction of a patient's beta cells, which prevents endogenous regulation of blood glucose levels. This condition affects approximately 0.5% of the adult population in the United States (1), and can lead to serious complications such as coronary artery disease, retinopathy, and diabetic nephropathy resulting in kidney failure (2). Currently, Type 1 diabetes is treated by a combination of injections of exogenous insulin, and careful regulation of diet and lifestyle. Although life-saving, insulin injection does not completely prevent glucose excursion, which can lead to long-term complications (3). A promising alternative therapy is the transplantation of cadaveric human islets, which has been used effectively in approximately 1500 patients since the first report of a successful allogenic transplant in the year 2000 (4, 5). However, the demand for transplants will outstrip supply, as multiple donors are frequently required for each recipient (6), and repeated transplantations into a single recipient over time may be required due to progressive graft failure caused by allo- and autoimmunity (7). In order to meet the demand for transplantable islets, numerous researchers have sought to culture beta cells from pluripotent stem cells.

In order to drive stem cells towards a beta cell lineage, it is important to consider the developmental origins of beta cells. In mammals, the pancreas begins as a bud of cells that stems from the tuboidal gut lumen. The cells in this stem proliferate, and differentiate in three distinct events. First is the trunk-tip differentiation, where branches emerge from a central ductal axis. At the tips of these branches, differentiation proceeds to acinar cells, responsible for production of digestive enzymes, whereas ductal progenitor cells remain on the trunk. In the second event, some ductal progenitors differentiate into mature ductal cells, while others delaminate from the trunk and form endocrine progenitor cells. These

endocrine progenitors then undergo fivefold differentiation into the cells that compose the Islets of Langerhans, namely α cells (which produce glucagon, to increase blood glucose), β cells (which produce insulin, to stimulate uptake of glucose by somatic cells), γ cells (which produce pancreatic polypeptide, to regulate pancreatic secretions), Δ cells (which produce somatostatin, to inhibit glucagon and insulin secretion) and ε cells (which produce ghrelin, to regulate appetite) (8).

Several groups have reported the production of functional beta cells from multi-potent or pluripotent stem cells, in some cases resulting in islets that are capable of treating Type I diabetes in mice (9-11). However, these methods rely on the use of Matrigel, a medium composed of the secretion of Engelbreth-Holm-Swarm mouse sarcoma cells enriched for extracellular matrix (ECM). Despite its low cost, Matrigel is an undefined and extremely complex medium, with one proteomic profile determining that it consists of over 1800 unique proteins (12). The undefined nature of Matrigel makes it difficult to determine exactly which factors are responsible for the differentiation of a stem cell to a particular lineage. Matrigel also suffers from lot-to-lot variation, and in many stem cell culture contexts, this has been observed to affect ultimate cellular fate (13, 14). Its undefined nature aside, the xenogeneic origin of Matrigel precludes its use in clinical applications (15, 16). Injections of human embryonic stem cells in the presence of Matrigel in an *in vivo* system are also linked to a higher incidence of formation of cancer cells such as teratomas (17-19).

The present work aimed to eliminate the use of Matrigel in pancreatic cell culture, more thoroughly understand the processes governing beta cell development and differentiation, and bias pancreatic cell growth in favor of the beta cell lineage. To do so, we developed a new method for culture of pancreatic cells using a novel, defined medium based on recombinant, tunable protein hydrogels. Our group has extensively explored protein-based hydrogels which are formed by the physical interactions of leucine zippers (20, 21). In particular, we developed a class of protein-based hydrogel material known as PEP-type materials, consisting of two leucine zippers derived from rat Cartilage Oligomeric Matrix

Protein (P) separated by an elastin-like polypeptide (ELP) consisting of repeating units of the protein sequence VPGXG, where X can be any amino acid other than proline (22). PEP-type materials have been well-characterized in terms of its mechanical properties and strand exchange dynamics (23, 24), and their material properties are easily modified by introduction of point mutations in the COMPcc coils (25), or the addition of fatty acids to tailor coil relaxation properties (26). This makes PEP-type materials versatile and customizable, and materials of this type have already been used in mammalian cell culture (26).

The present work also builds on previous experiments conducted in the Ku and Tirrell laboratories which showed that addition of an ELP containing a 19-amino acid peptide sequence derived from laminin (laminin-19mer) to methylcellulose-Matrigel culture (27, 28) resulted in colonies of mixed endocrine-acinar lineage. In order to eliminate Matrigel from the culture, and thereby make a more defined cell culture medium, we hypothesized that we could incorporate cell binding motifs such as the laminin 19-mer sequence, an RGD sequence, or a collagen IV mimetic in a PEP-like material.

Herein we present the results of pancreatic cell culture in PEP-type materials containing either an RGD peptide (referred to either as PEREP or RGD), or a putative collagen IV binding motif previously reported by Fong and co-workers (referred to either as PEFEP or COL) (29). Compared to a Matrigel-methylcellulose culture, which favors colonies of ductal cells, we find that these PEP-type materials favor cells of an endocrine lineage when using an unsorted initial population of cells. RGD and COL also favor cells that demonstrate higher expression levels of Neurgenin3, which is a marker for endocrine progenitor cells. Furthermore, when the cells are sorted into separate populations and cultured in our protein-based materials, we observe fewer colonies than when the cells are not sorted. This effect is not observed when the sorted populations are grown in methylcellulose-Matrigel. We suspect that this difference in colony-forming efficiency may be due to paracrine signaling between individual populations which is removed by cell sorting, and that this paracrine signaling promotes colony formation, and favors the growth

of a colony morphology associated with endocrine cells. The present work thereby shows a new method for pancreatic cell culture, and if the putative paracrine effect is confirmed, may also illustrate the importance of using defined media to find effects of cell-cell communication on growth and differentiation.

MATERIALS AND METHODS

Protein Expression and Purification

The proteins PEREP-I58A (RGD) and PEFEP-I58A (COL) were expressed in *E. coli* and purified in a manner designed to reduce contamination with endotoxin. All antibiotics were obtained from BioPioneer Inc. (San Diego, CA), dissolved at 1000X working concentration, and sterile filtered. DNA constructs of both protein types were cloned in *E. coli* strain DH10B using recursive ligation into a pQE80-L plasmid (Qiagen, Hilden, Germany) as described in Figure 1. Colony selection was conducted on LB medium plates supplemented with 100 mg/L carbenicillin. The vectorpLJD1, containing the leucine zipper P on a pQE80-L backbone, was digested with XhoI and HindIII (New England Biolabs, Ipswich, MA). This digested vector was then ligated together with an insert consisting the elastin-like polypeptide E6 ($[(VPGAG)_2VPGEG(VPGAG)_2]_6$), and which was digested out of plasmid pLJD2 (pQE80-L backbone) using SalI and HindIII. As SalI and XhoI leave complementary sticky ends, ligation of this vector and this insert leads to a new vector, pMTK-PE. This vector was digested with XhoI and HindIII, allowing for the insertion of the appropriate peptide sequence, RGD or COL. Colonies were propagated overnight in LB medium supplemented with 100mg/L carbenicillin. By repeating this process several times, we are able to make the full RGD and COL constructs, which are presented in the supporting information in table ST1. Plasmids were isolated using a Qiagen QiaSpin DNA miniprep kit according to manufacturer's instructions, and sequences were confirmed by Laragen Inc. (Culver City, CA).

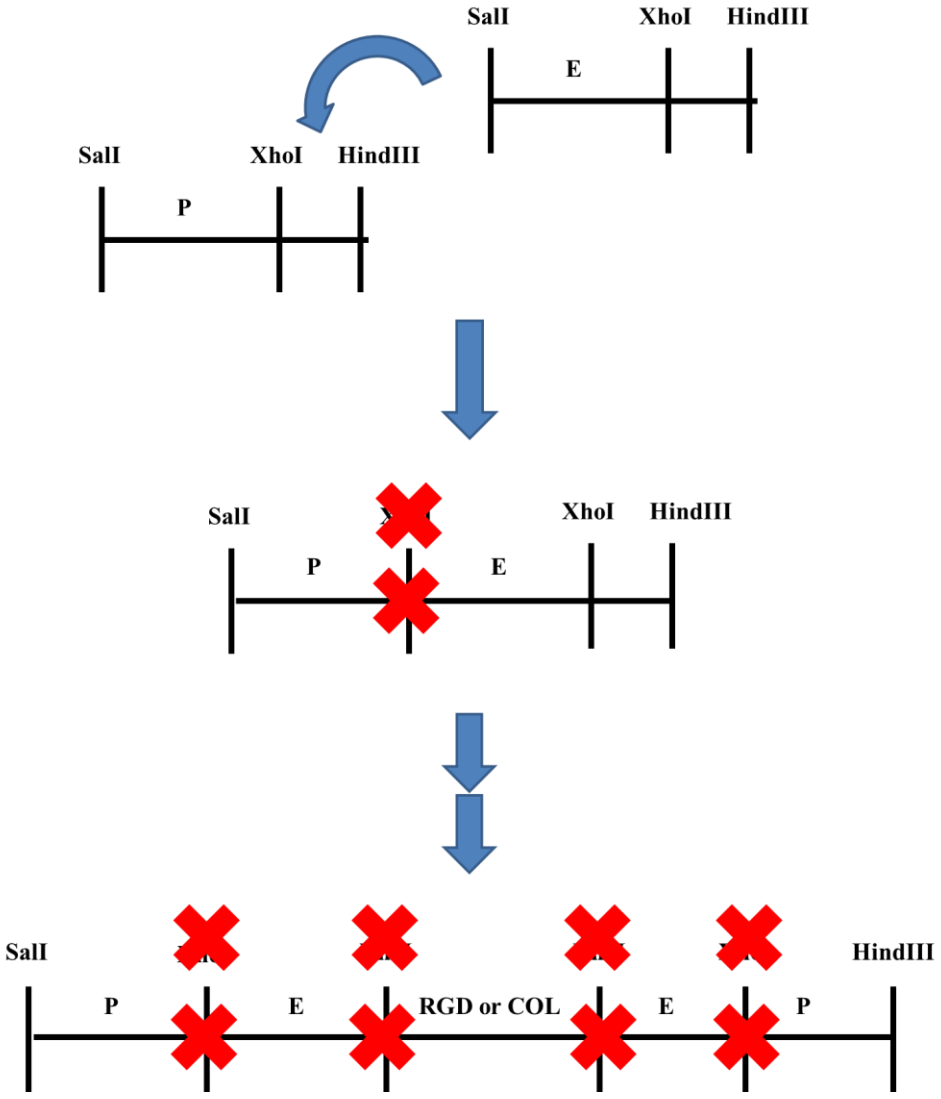

Figure 1: Cloning strategy for obtaining PEREP and PECOLEP

Our cloning strategy uses the fact that the sticky ends of SalI and XhoI are complementary, but that both sites are destroyed when these complementary ends are ligated together. The vector, P on a pQE80L backbone, is digested with XhoI and HindIII, whereas the insert, E6, is digested with SalI and HindIII (first image). The sticky ends are then ligated together, resulting in the formation of construct PE, and the destruction of the previous XhoI site C-terminal to P (second image). Through three more sequential digestions and ligations, the entire construct (PEREP or PEFEP) is made, with destroyed restriction sites marked "X".

After sequence verification, the plasmids were transformed into *E. coli* strain BL21 by electroporation, and selected for using LB plates supplemented with carbenicillin (100 mg/L). Individual colonies were grown to stationary phase in LB medium supplemented with ampicillin (100 mg/L) by overnight incubation at 37 C. This starter culture was used to inoculate Terrific Broth (TB) medium likewise supplemented with ampicillin, at an inoculation ratio of 50:1. The TB medium was then incubated at 37 C until the culture reached an optical density (OD) of between 0.6 and 0.8. Expression of the protein was induced by the addition of isopropyl β-D-1-thiogalactopyranoside (IPTG) to a final working concentration of 1mM. Expression was continued for 4 H and cells were pelleted by centrifugation at 8000 g for 8 min. The pellet was resuspended in Buffer B (8 M urea, 100 mM NaH_2PO_4, 10 mM Tris base, 10 mM imidazole, adjusted to pH 8 with NaOH) at a ratio of 4 mL of buffer per 1 g of wet bacterial pellet. This suspension was then frozen at -80 C overnight, re-thawed, and the bacteria were lysed by sonication in a Q500 probe sonicator (Qsonica, Newtown, CT). The bacterial lysate was clarified by centrifugation at 50,000 g for 1 H.

The resulting clarified supernatant was adjusted to pH 8.0 by the addition of 6 M sodium hydroxide, then nickel-nitrilotriacetic acid (Ni-NTA, Fisher Scientific, Tustin, CA) resin was added at a ratio of approximately 1mL of settled resin to 10 mL of clarified supernatant. The mixture was stirred at room temperature for 1 H, then passed through a chromatography column. The Ni-NTA resin was washed first with 10 column-volumes of cold Buffer B, then with 50 column volumes of cold Buffer B supplemented with 0.1% Triton X-144 (Sigma-Aldrich). Next, the resin was washed with 10 column volumes of Buffer C (10 mM Tris base, 10 mM imidazole, pH 8), then, alternating 10 column volume washes of 60% isopropanol/Buffer C and Buffer C. Alternate washing with Bufer C and 60% isopropanol/Buffer C was repeated to give 2-3 washes with the 60% isopropanol solution. After a final wash with Buffer C, the resin was washed with 10 column volumes of Buffer D (8 M urea, 100 mM Tris, pH 8). The resin was then eluted using 3 column volumes of Buffer D supplemented with 250 mM imidazole. The flow-through fraction and elution fraction of both proteins were then run on a NuPAGE 4-12% Bis-Tris protein gel

(ThermoFisher) after denaturation in SDS buffer, and stained with Coomassie InstantBlue (Expedeon, San Diego, CA).

For refolding, the elution fraction was dialyzed against deionized water at 4C for 48 H at a ratio of approximately 50 parts water to 1 part elution fraction, using a dialysis membrane with a molecular weight cutoff of 12-14 kDa (Spectrum Laboratories, Rancho Dominguez, CA). The water was changed three times each day. After dialysis, the elution fraction was sterile-filtered in a tissue culture hood through a 0.2 μm syringe filter into a sterile conical tube. The conical tube was then flash-frozen in liquid nitrogen, and lyophilized for 2-3 days. The yield of protein obtained by this method is approximately 100 mg/L of rich medium.

The amount of endotoxin present in the sample was tested using an Invivogen HEK-Blue Endotoxin Standard kit (Invivogen, San Diego, CA), and found to be between 3-10 endotoxin units/mg. The molecular weight of the protein was confirmed using electrospray ionization-time of flight (ESI-TOF) mass spectrometry on an LCT Premier XE electrospray TOF mass spectrometer (Waters, Milford, MA).

Rheology

Rheological studies were conducted on a TA Scientific ARES rheometer with TA Orchestrator software. We used a plate-and-cone geometry with a diameter of 25 mm, cone angle of 0.0396 radians, and a gap of 0.0483 mm (Rheometric Scientific). The geometry acted against a Peltier plate, which was heated to a temperature of 37 C. A thin ring of paraffin oil (JT Baker) was used around the geometry to prevent evaporation. A strain sweep was first conducted to establish the linear viscoelastic region of the material, at a frequency of 10 rad/s. Based on these results, frequency sweeps were conducted at a strain rate of 1%.

Isolation of the mouse pancreas

8 day old C57BL/6 mice were obtained through a breeding program at City of Hope. The mice were euthanized in accordance with a protocol approved by the Institutional Animal Care and Use Committee of City of Hope (IACUC protocol 11017). The pancreata of the mice were removed into petri dishes kept on ice, containing approximately 20 mL Phosphate Buffered Saline (PBS) solution supplemented with penicillin/streptomycin at a working concentration of 100 units/mL penicillin and 100 μg/mL streptomycin (Gibco, Grand Island, NY). The PBS was also supplemented with bovine serum albumin (BSA, Sigma) at a working concentration of 0.1%. The spleen and fat surrounding the pancreas were removed with tweezers under a dissecting microscope. The pancreata were washed twice in fresh PBS, and placed in a 1.7 mL Eppendorf tube. The pancreata were thoroughly minced using scissors. Cold PBS/BSA/PS (1 mL) was added, supplemented by 2 units of bovine pancreatic DNAseI (EMD Millipore, Temecula, CA) and 2 mg Collagenase B (Sigma-Aldrich, Milwaukee, WI). The pancreata were then pipetted up and down several times to disrupt the tissue, and incubated in a water bath at 37 C for 15 min with additional pipetting every 5 min. The cell suspension was placed in 25mL cold PBS/BSA/PS/DNAse, and centrifuged at 800 g for 5 min. The supernatant was removed, and the cells were resuspended in 1mL of PBS/BSA/PS/DNAse. The cell suspension was filtered sequentially through a 100 μm and 40 μm mesh filter, and once again centrifuged. The cells were finally resuspended in approximately 500 μL of PBS/BSA/PS/DNAse, stained with 0.02% Trypan Blue, and manually counted on a cytometer chip.

Cell Sorting

In order to sort cells into Ngn3+ and Ngn3- populations, we used the mouse strain B6.129S-*Neurog3*$^{tm1(EGFP)Khk}$/Mmucd (Ngn-GFP), which substitutes GFP for a copy of Neurogenin3 on the 10th chromosome of the mice, as detailed by Kaestner and co-workers (30). Mice were bred in mating trios between heterozygous females and homozygous males, or between heterozygous males and homozygous females. 3-day old pups were genotyped by Transnetyx (Cordova, TN) and heterozygous mice were used for staining and

sorting. Homozygous wild-type mice were used as a negative control to establish flow cytometry gating. The pancreata of these mice were dissociated as previously described.

The dissociated cells were then blocked for 10 min using LEAF purified anti-mouse CD16/32 rat IgG2a, λ antibody solution (BioLegend, San Diego, CA) at a concentration of 10 µL per 1mL at 4C. We then separated the cells into 150 µL aliquots representing the following controls for setting gates: 1) Unstained, wild-type, 2) Unstained, Ngn-GFP, 3) CD133-biotin positive control, 4) CD133-biotin isotype control and 5) the sample. The appropriate antibodies were added at concentration of 10 µL/mL. The cells were incubated for 20 min with pipette mixing every 5 min. Following this, the cells were pelleted and washed with cold PBS+BSA+PS+DNaseI. Then, Streptavidin-APC (BioLegend) was added at a concentration of 10 µL/mL to the CD133 controls and the sample. The tubes were then incubated for 15 min in the dark with mixing, then washed twice with PBS/BSA/PS/DNAseI. The samples were resuspended in 1 mL of PBS/BSA/PS/DNAseI, passed through a 60 µm mesh filter for sorting, and stained at a 1:10,000 ratio (v/v) with 4', 6-diamidino-2-phenylindole (DAPI, ThermoFisher). The cells were sorted on an Aria III instrument in the City of Hope analytical cell-sorting core. Sorting was conducted into DMEM-f12 supplemented with 16% filtered FCS 216. Recovered cells were plated at a density of either 2500 cells/100µL of medium, or 10,000 cells/100µL of medium.

Plating cells

Our plating medium consisted of either 1% Methylcellulose+1% Matrigel (Corning), or a 2% solution of proteins RGD or COL in Dulbecco's Modified Eagle Medium/Nutrient Mixture F-12 (DMEM/F12) containing L-glutamine and 15 mM HEPES (Corning, Manassas, VA). Proteins were dissolved in DMEM at slightly above working concentration, and allowed to dissolve overnight at 4 C. The addition of 2-factor growth medium and additional DMEM brought the final working concentration of the proteins to 2%. The defined 2-factor growth medium is the same as previously used by Wedeken and co-workers (31). The growth medium was made as a master mix at 9X concentration. 100 µL of master mix consisted of 90 µL KnockOut Serum Replacement (KSR, ThermoFisher

Scientific), 9 μL of 1M nicotinamide and 0.9 μL recombinant epidermal growth factor (EGF). The master mix was added to the dissolved protein or methylcellulose-Matrigel at a ratio of 11.1 μL of master mix per 100 μL of plating medium.

To the complete plating mix were added 10,000 cells per 100 uL of medium. This inoculated medium was then plated on flat-bottomed 96-well uncoated plates (ThermoFisher). Sterile distilled water (150 μL) was added to the wells at the edge of the plate to prevent evaporation. Control conditions consisted of a 1% methylcellulose and 1% Matrigel medium in DMEM/F-12 with the same 2-factor growth medium. The plate was then incubated at 37 C in a 5% CO_2 atmosphere in a stationary, humidified, mammalian cell incubator.

Colony count microscopy and whole-mount immunostaining

Colonies were observed and counted using an Olympus CKX31 optical microscope at 10X magnification, and a mechanical tabulator. For immunostaining, samples were fixed overnight at 4C in 4% paraformaldehyde (PFA) in PBS, by directly adding the PFA into the culture wells. The samples were then pooled, centrifuged at 400g for 15 min to pellet, and the supernatant removed. The samples were then washed in PBS, with three changes of wash buffer, and left on a rocking table overnight at 4C. The PBS was then removed and replaced with blocking buffer, and allowed to block overnight. Primary antibodies were then added, consisting of guinea pig anti-Ngn3 at a ratio of 1:500 (the Ngn3 antibody was a generous gift of the lab of Maike Sander, UC San Diego) (32), goat anti-chromogranin A at a ratio of 1:500 (Santa Cruz Bio, Santa Cruz, CA) and rat anti-EpCAM at a ratio of 1:100 (Development Studies Hybridoma Bank DSHB, Iowa City, IA). The primary antibody was allowed to stain the sample overnight, and was then removed by 3 washes of PBS supplemented by 0.15% Tween-20 (PBST), followed by a fourth overnight wash in PBST. Donkey secondary antibodies were then added, which consisted of Cy3 anti-guinea pig at a ratio of 1:2000, AlexaFluor 488 anti-rat at a ratio of 1:1000, and Cy5 anti-goat at a ratio of 1:500. All secondary antibodies were obtained from Jackson ImmunoResearch Laboratories (West Grove, PA). The sample was also stained with DAPI at a ratio of

1:2000. The secondary antibodies were applied overnight at 4C, washed three times, then washed for 3 days at 4C in PBST with rocking and daily changes of wash buffer. The cells were then imaged using an AxioObserver Z1 microscope with an ApoTome attachment (Carl Zeiss Inc., Oberkochen, Germany) at 20x magnification, with the averaging of three ApoTome images presented.

Single-colony RT-qPCR

Colonies of interest in the culture medium were photographed using an Olympus CKX41 optical microscope with a Luminera Infinity2 camera attachment. Individual colonies were selected using a pipette tip. The colonies were placed in a PCR pre-amplification mixture consisting of 5.0 μL of 2x reaction mix, 2.5 μL of Taqman probe mix, 0.2 μL of SuperScript III enzyme, and 1.3 μL TE buffer. The colonies were then subjected to PCR on a Veriti 96-well thermal cycler (Applied Biosystems, Foster City, CA) using the following cycles: 15 min at 55 C, then 22 cycles alternating between 95 C for 15 seconds and 65 C for 4 min, before being lowered to a temperature of 4 C. The pre-amplified samples were frozen at -20 C until used. The thawed samples were evaluated using a Fluidigm Biomark 48.48 IFC microfluidic RT-qPCR chip (South San Francisco, CA) according to the manufacturer's instructions. In brief, the samples were diluted to a volume of 45 μL using TE buffer. 2.7 μL of diluted sample was added to 3.3 μL of a master mix consisting of 3.0 μL Universal PCR Master Mix and 0.3 μL 20xGE Sample Loading Reagent. Separately, 3 μL of individual primers were mixed with 3 μL 2xGE Assay Loading Reagent. 5 μL of sample, and 5 μL of primer, were loaded into the appropriate well on the Fluidigm chip. The primer list is provided in the supporting information, Table ST3. The chip was then run on a Biomark real-time RT-qPCR instrument, and data was analyzed using Fluidigm software, followed by analysis in Microsoft Excel.

RESULTS AND DISCUSSION

Protein expression and purification

Proteins RGD and COL were obtained in yields of approximately 100 mg/L of rich medium after purification. The expected masses for RGD and COL were 41,202 Da and 40,700 Da based on their sequences (see supporting information table ST1). The purification resulted in clean protein samples, as seen in the Coomassie gel presented in Figure 2. In order to confirm protein masses, ESI-TOF was carried out, which found masses of 41,176 Da and 40,666 Da respectively, both within 0.1% of the expected masses (see Figures 3 and 4).

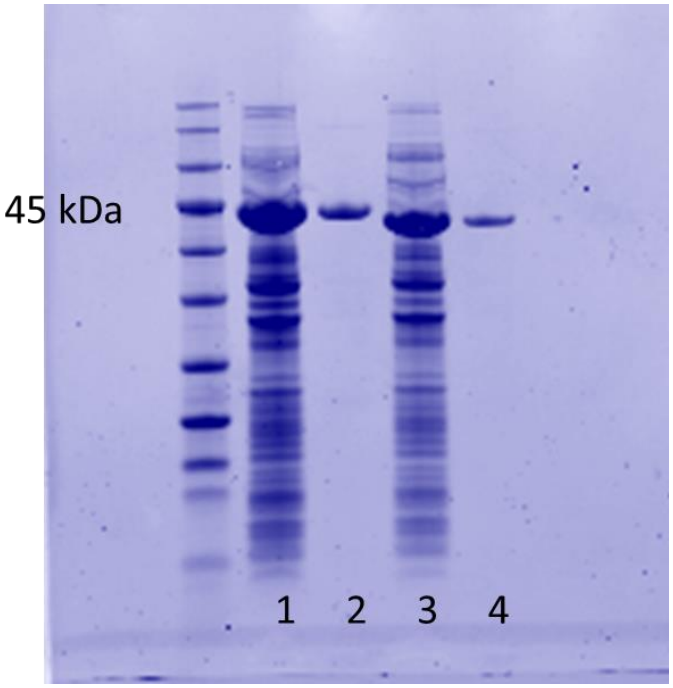

Figure 2: Coomassie gel of RGD and COL.

The column flow-through of RGD is in lane 1, the final elution of RGD is in lane 2, the column flow-through of COL is in lane 3, and the final elution of COL is in lane 3. Both proteins express and purify well, with the elution fraction showing no other observable proteins. The observed masses of approximately 45 kDa are heavier than the expected masses of approximately 41 kDa for both proteins. However, these ELP proteins have a large number of

glutamic acid residues, which are negatively charged when run on the gel. Our group has consistently found that highly negatively-charged artificial proteins consistently run slowly on PAGE gels, and we suspect this reflects reduced binding of SDS to the protein.

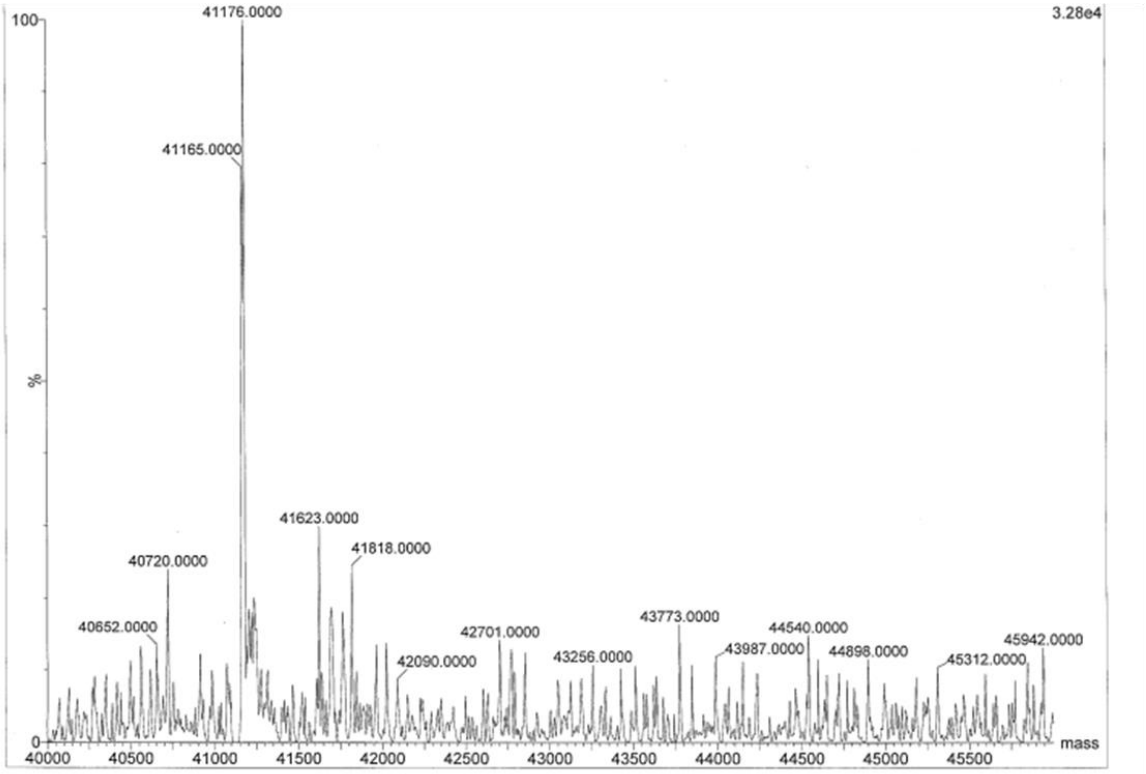

Figure3: RGD protein ESI trace
The ESI spectrum of protein PEREP (RGD) is presented above. The primary peak of 41165 Da is within 0.1% of the expected protein mass, which is 41,202 Da.

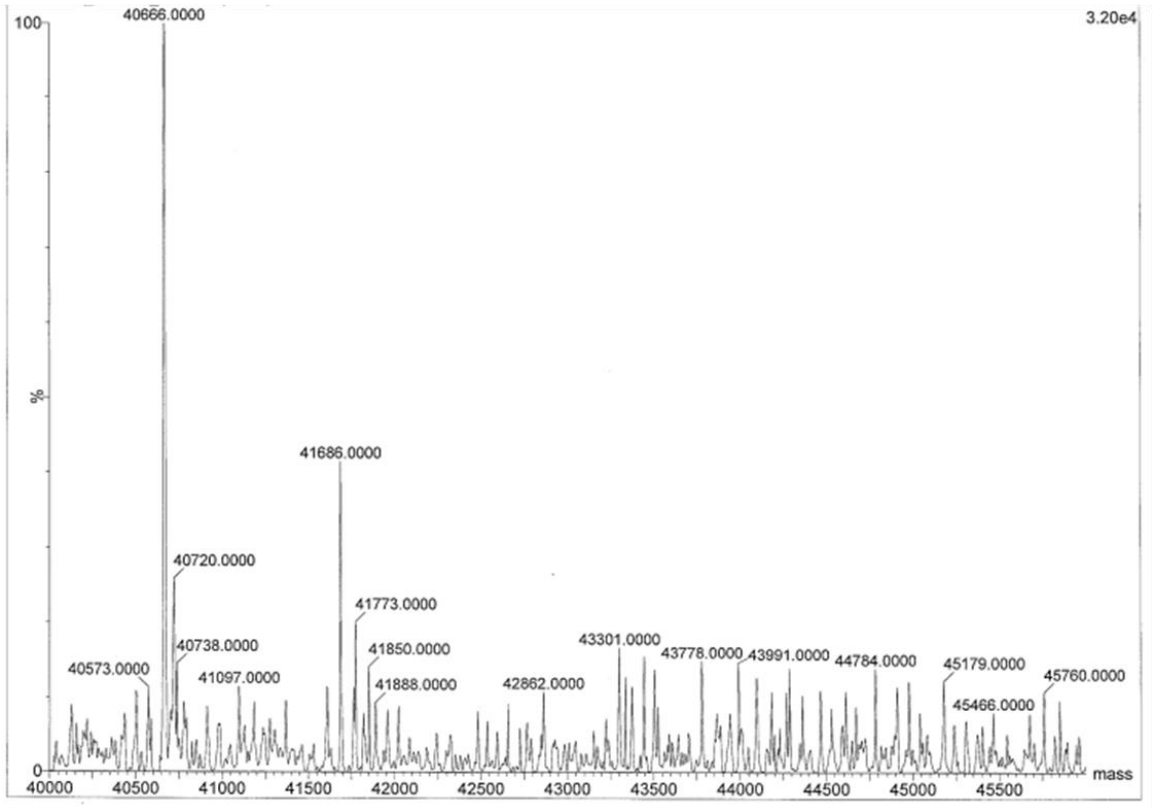

Figure 4: COL protein ESI trace
The ESI of protein PEFEP (COL) is presented above, with the primary peak showing a mass of 40666. This mass is within 0.1% of the expected mass of 40,700 Da. The prominent peak at 41686 Da is likely the result of adduct formation with Triton X-144.

Protein rheology

Both materials were characterized rheologically, to see if COL and RGD had mechanical properties similar to the control condition of methylcellulose-Matrigel. We wanted to ensure that any differences observed between cultures in methylcellulose-Matrigel and in protein could be primarily attributed to chemical rather than mechanical differences. We also needed to ensure that the moduli of the proteins were high enough to keep individual cells from either aggregating (which would make it difficult to conclude how observed colonies originated), or from settling to the bottom of the well, where the cells might

adhere, and where the results of culture might be affected by this adhesion. The rheology of these materials can be seen in Figure 5. methylcellulose-Matrigel plating material is quite soft, and displays an elastic modulus G' of approximately 20 Pa: this methylcellulose-Matrigel material consisted of 1% methylcellulose and 1% Matrigel, which was a concentration previously used by our laboratory [cite]. This elastic modulus is consistent across a broad range of frequencies, from 0.1 to 100 rad/sec. RGD and COL are slightly stiffer, with elastic moduli of approximately 80 and 120 Pa, when measured at a concentration of 2% w/v. While they are stiffer, RGD and COL have a rheological profile similar to methylcellulose-Matrigel as the elastic modulus is not dependent on frequency. We decided that 2% w/v of protein was a concentration that gave comparable elastic modulus, and this concentration was therefore used in all future experiments. It is important to establish that the culture materials have broadly similar physical properties, as physical effects such as matrix stiffness are well-known to change the differentiation behavior of a number of different cell types (33-35).

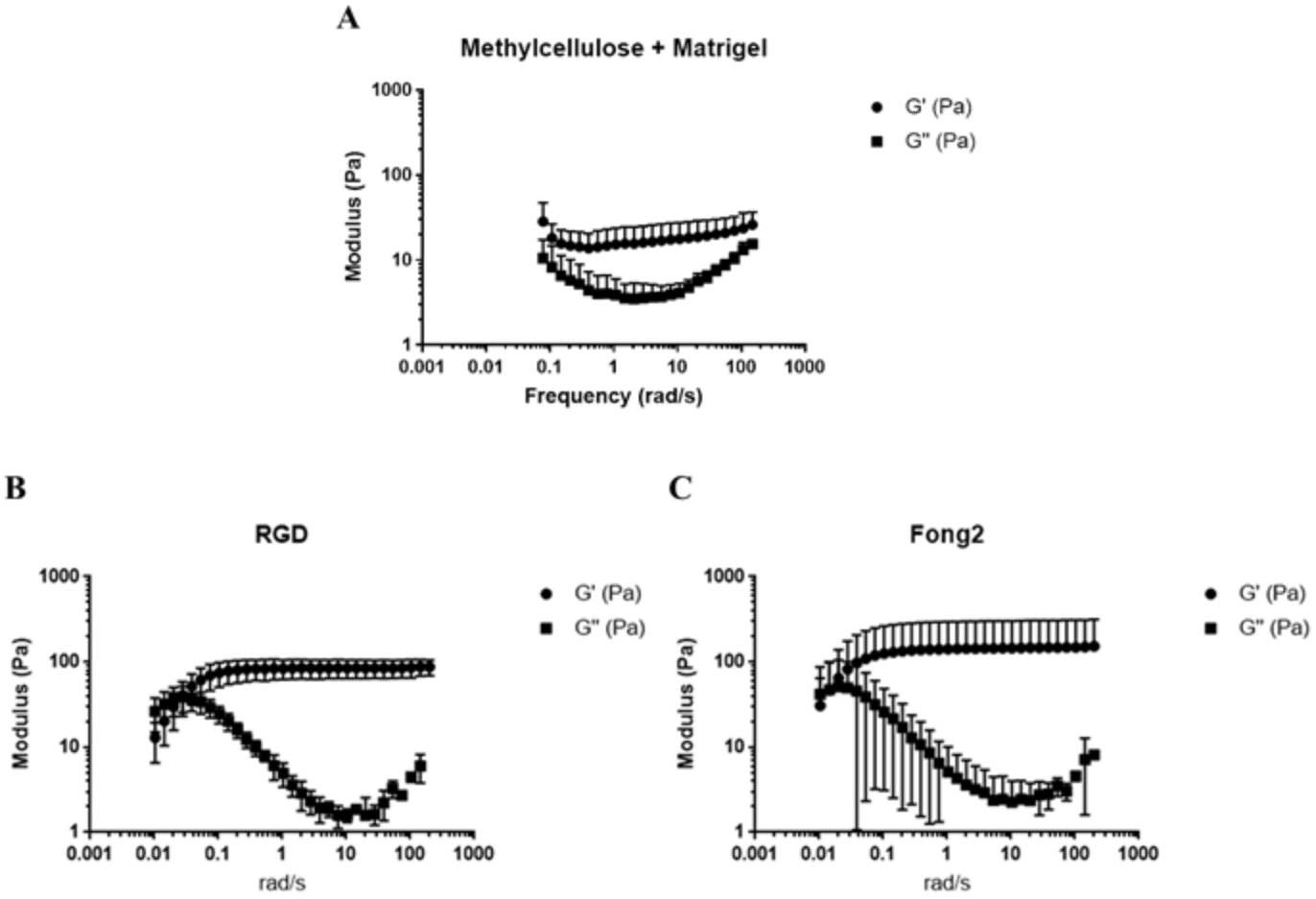

Figure 5: Rheology of methylcellulose-Matrigel, and protein-based culture medium

Shown above are the average elastic moduli G' (circles) and loss moduli G" (squares). Data represent the average of two replicates in RGD and COL, and average of 4 replicates in methylcellulose-Matrigel, and error bars represent standard deviation.

Protein-based materials prevent cellular aggregation

As our materials were quite soft, we were concerned that the cells plated in these materials might aggregate together, for the reasons previously explained. To preclude this possibility, we grew pancreatic cells in either RGD or COL materials (Figures 6 D-F and 5 G-I respectively), or in DMEM-F12 which did not contain either RGD, COL, or

methylcellulose-Matrigel (Figures 6 A-C). We monitored these cells cells under a wide-field light microscope, taking images every 10 min over 17 H. We found that growing the pancreatic cells in a 2% solution (w/v) of protein matrices RGD and COL prevented aggregation or movement of the cells (see Figures 6 D-F, 5 G-I, and supporting movies 2 and 3), whereas in DMEM-F12 the cells readily aggregated (see Figures 6 A-C and supporting movie 1). There was also some evidence of cell division in the RGD and COL media, meaning that cells are able to grow and proliferate. This suggests that observed colony formation is driven by differentiation and proliferation, rather than aggregation.

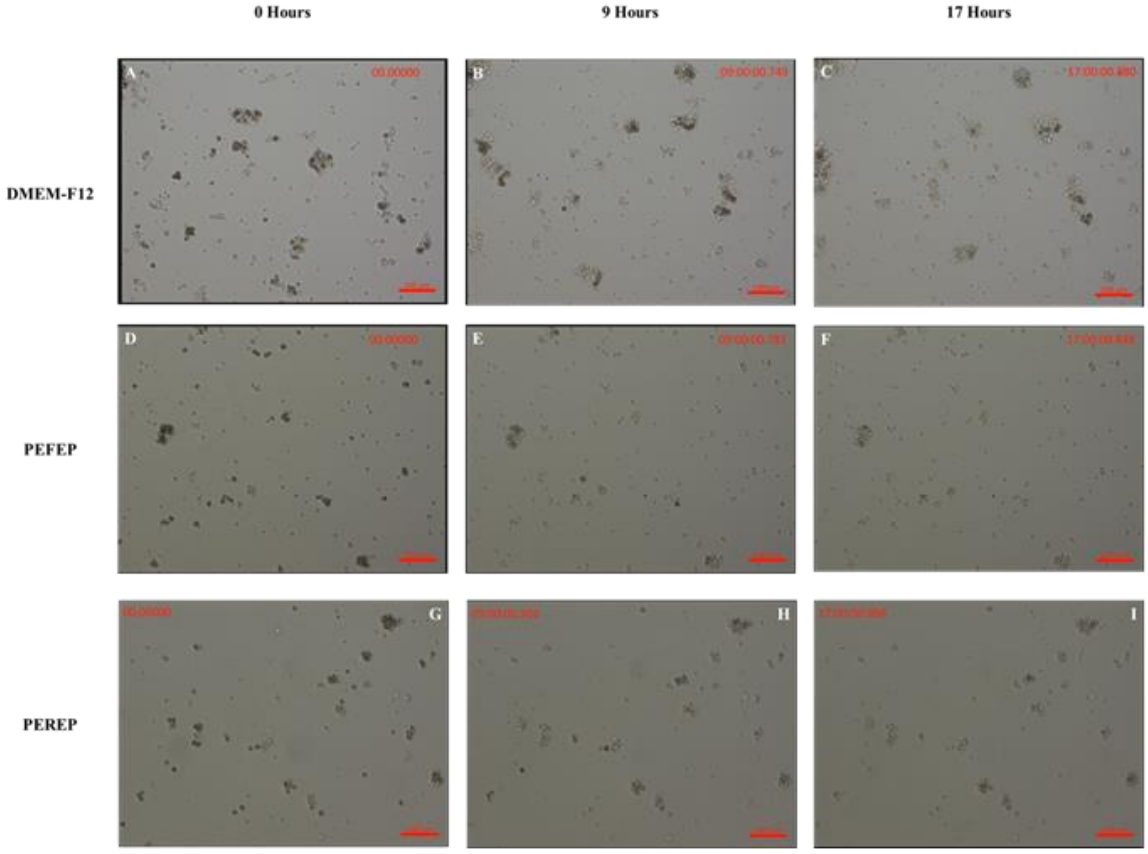

Figure 6: Protein-based materials prevent cellular aggregation

The above images show cells grown for 17 hours in our materials Fong2 (PEFEP, micrographs D-F), RGD (PEREP, micrographs G-I), and in DMEM-F12 without the addition of matrix material (micrographs A-C). Micrographs A, D, and G show an

initial timepoint in all three materials, micrographs B, E, and H show a 9H timepoint, approximately halfway through the experiment. Micrographs C, F, and I show the cultures after 17 hours of growth. In micrographs A-C, cells can clearly be seen forming larger clusters, and the extant clusters move considerably within each frame. In micrographs D-F and G-I, however, no such clustering is observed, and the clusters which have formed remain in the same part of the frame. Movies of all three of these conditions can be found in Supporting Movies 1-3.

Cells form five major colony types in Methylcellulose-Matrigel and protein-based cultures

After 2 or 3 days of culture, individual colonies could be observed. We classified the types of colonies observed into five major types: ring, budding ring, stuffed ring, beebee, and grapelike colonies. Examples of each of these colony types are shown in Figure 7: ring colonies consist of large, bright cysts that are not granular. Budding rings are ring colonies that appear to have a number of cells attached to, and perhaps emerging from, the ring. Stuffed rings are cysts that are highly granular, and dark. Small, individual, very bright and reflective cells in a cluster are referred to as beebee colonies. Grapelike colonies are similar to beebee colonies in shape and structure, but the cells composing them are slightly larger, and not as bright. Using a hand counter, we found the colony distributions of each colony type in the three types of medium we used. The results of this count are shown in Figure 8 and are averages of three biologically-independent replicates, with between 3 and 6 technical replicates conducted in each biological replicate. As shown in Figure 8, methylcellulose-Matrigel strongly favors the growth of ringlike colonies, whereas COL and RGD favor the growth of more grapelike colonies. Comparing COL to RGD, it appears that the COL material appears to favor the growth of ring colonies, whereas RGD favors the growth of grapelike colonies. A two-tailed Student's t-test shows that the difference between the percentage of colonies is statistically significant at the $P<0.05$ level for ring, beebee, and grapelike colonies.

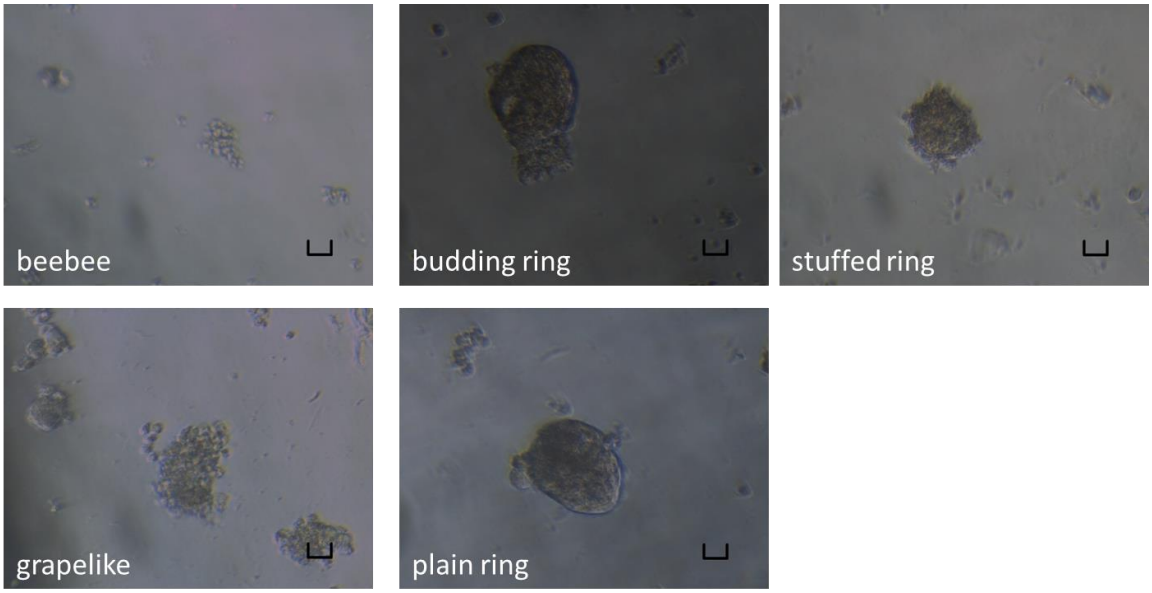

Figure7: Colony types observed in RGD, Fong, and Methylcellulose-Matrigel

The images above show the five major colony types observed in COL, RGD, or methylcellulose-Matrigel culture. The beebee colony consists of a loose agglomeration of small, bright cells. The grape or grapelike colony consists of a loose agglomeration of cells which are slightly larger, and not as bright. The ring colony consists of a large cyst which is relatively transparent. The budding ring is a ringlike colony which has a number of cells coming off of one or multiple sides. The stuffed ring is a ringlike colony that is highly granular, and dark. Scale bars are all 100 μm..

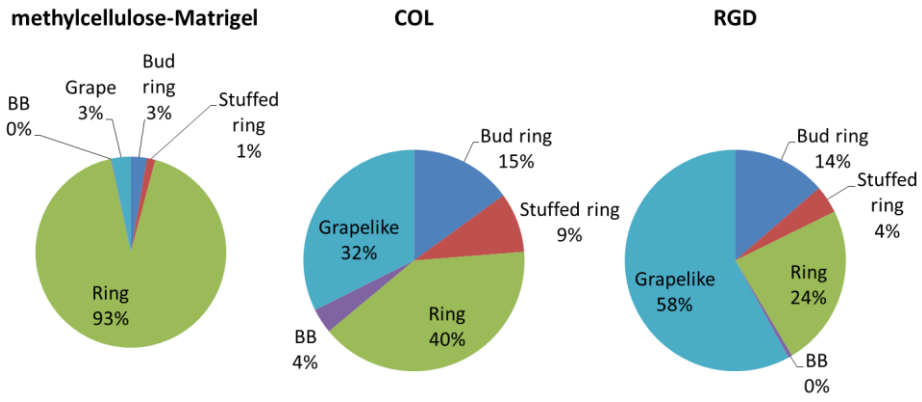

Figure 8: Colony type counts in unsorted populations after 4 days of culture in different media

Colonies were counted and classified by hand based on the colony types shown in Figure 7. Based on these counts, Methylcellulose-Matrigel favors the growth of ringlike (putative ductal) colonies, COL favors the growth of a mix of ringlike and grapelike (putative endocrine) colonies, and RGD favors the growth of grapelike colonies. Data come from the average of 2 biological replicates (Methylcellulose-Matrigel) or 3 biological replicates (COL and RGD), each consisting of between 3-6 technical replicates per biological replicate. Raw cell count data is shown in supporting information Table ST2.

Immunostaining of ringlike and grapelike colonies suggest ringlike colonies are ductal, and grapelike colonies are endocrine in nature

To characterize the colony types, we used both whole-mount immunostaining and RT-qPCR. By whole-mount immunostaining (Figure 9), ringlike colonies derived from both methylcellulose-Matrigel and COL appear to be ductal; in Figures 9A and D, the epithelial cell marker EpCAM stains strongly, but Chromogranin A, a pan-endocrine cell marker, does not (Figures 9B and E). In contrast, a grapelike colony observed in COL, while staining positive for EpCAM, is also strongly stained by Chromogranin A antibody (Figures 9G-I), meaning that this colony type consists, at least in part, of endocrine cells. Therefore, based on the evidence in Figure 8, we conclude that methylcellulose-Matrigel culture promotes the growth of ductal colonies, COL promotes the growth of a mixture of ductal and endocrine colonies, and RGD most strongly promotes the growth of endocrine colonies.

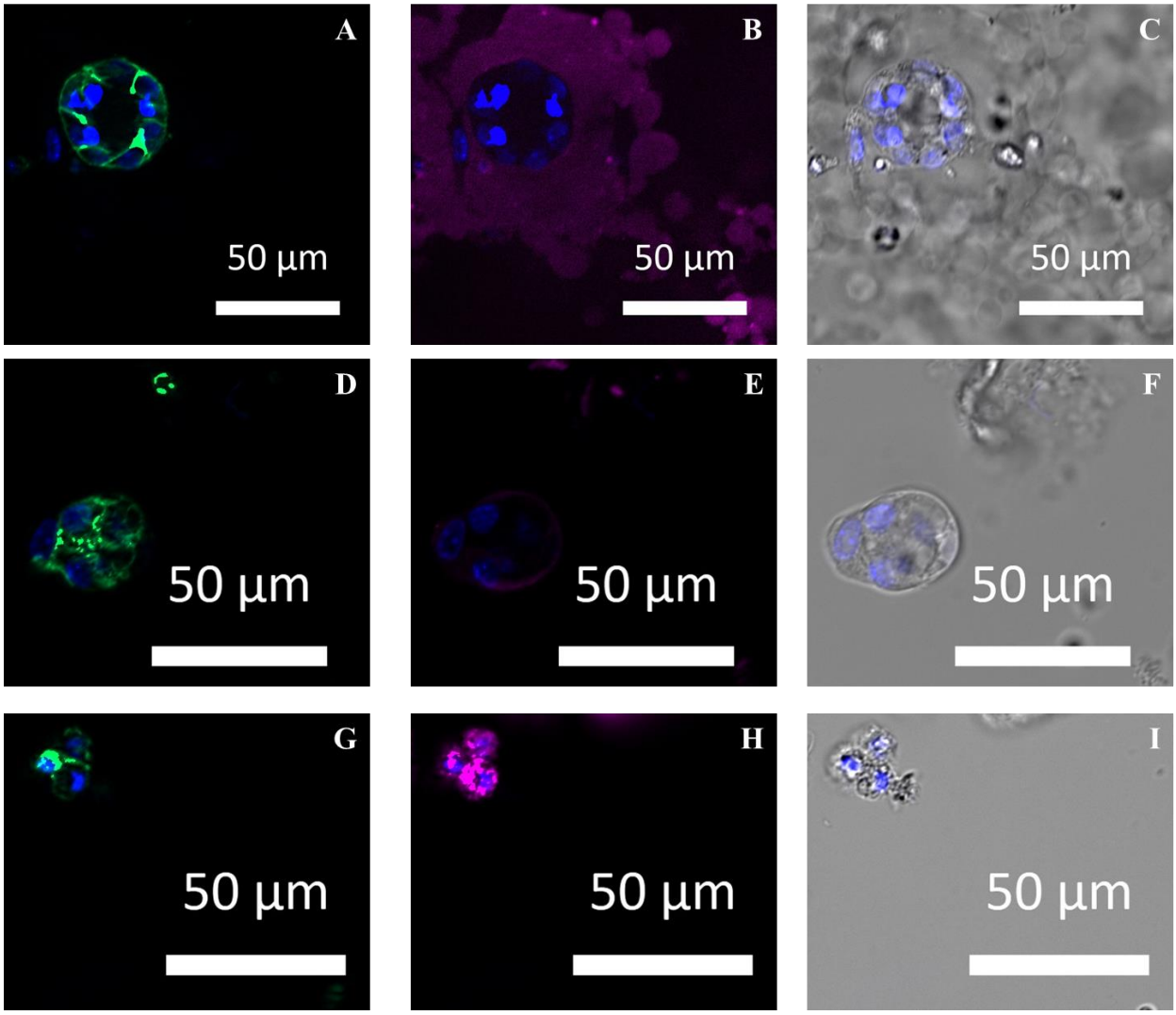

Figure 9: Ring and grapelike colonies stained for EpCAM and Chromogranin A

The above micrographs present the staining of colonies originating from methylcellulose-Matrigel (micrographs A-C), and COL (micrographs D-I). In all images, DAPI is presented in blue, the ductal marker EpCAM is in green, and the endocrine marker Chromogranin A is in pink. Brightfield images with DAPI superimposed are shown in micrographs C, F, and I. The colony derived from methylcellulose-Matrigel displays a clear ringlike morphology (micrographs A and C). This colony is positively stained for the ductal marker EpCAM (micrograph A), but does not stain for Chromogranin A: the pink color surrounding the colony is due to methylcellulose-Matrigel material which was not washed out, and appears at background levels. Similarly, one colony derived from COL also shows a ringlike morphology (micrograph F) and is stained by EpCAM, but not by Chromogranin A (micrographs D and E). In contrast, a grapelike colony derived from COL stains very strongly for Chromogranin A (micrograph H), suggesting that this colony morphology is associated with an endocrine lineage

Characterization of grape, ring, and budding ring colonies by RT-qPCR reveals a population of endocrine progenitor cells

In order to collect further evidence that links the morphology of observed colonies with specific cell types, we selected individual colonies of three major types, grapelike, budding ring, and ring colonies, and subjected them to RT-qPCR analysis. The results of this analysis are shown in Figures 10 and 11. All genes were normalized against the housekeeping gene B2MG, and the numerical value of the expression, presented on the Y-axes, is given by:

$$Expression = 2^{(-\Delta C_t)} * 1000$$

Where ΔC_t is defined as:

$$\Delta C_t = C_{t\,B2MG} - C_{t\,gene\,of\,interest}$$

and C_t is the number of PCR cycles required for the fluorescent signal in RT-qPCR to exceed a defined threshold. The expression levels characteristic of grapelike, budding ring, and ring colonies are shown in red, black, and blue vertical bars, respectively. These data are shown below in figures 10 and 11.

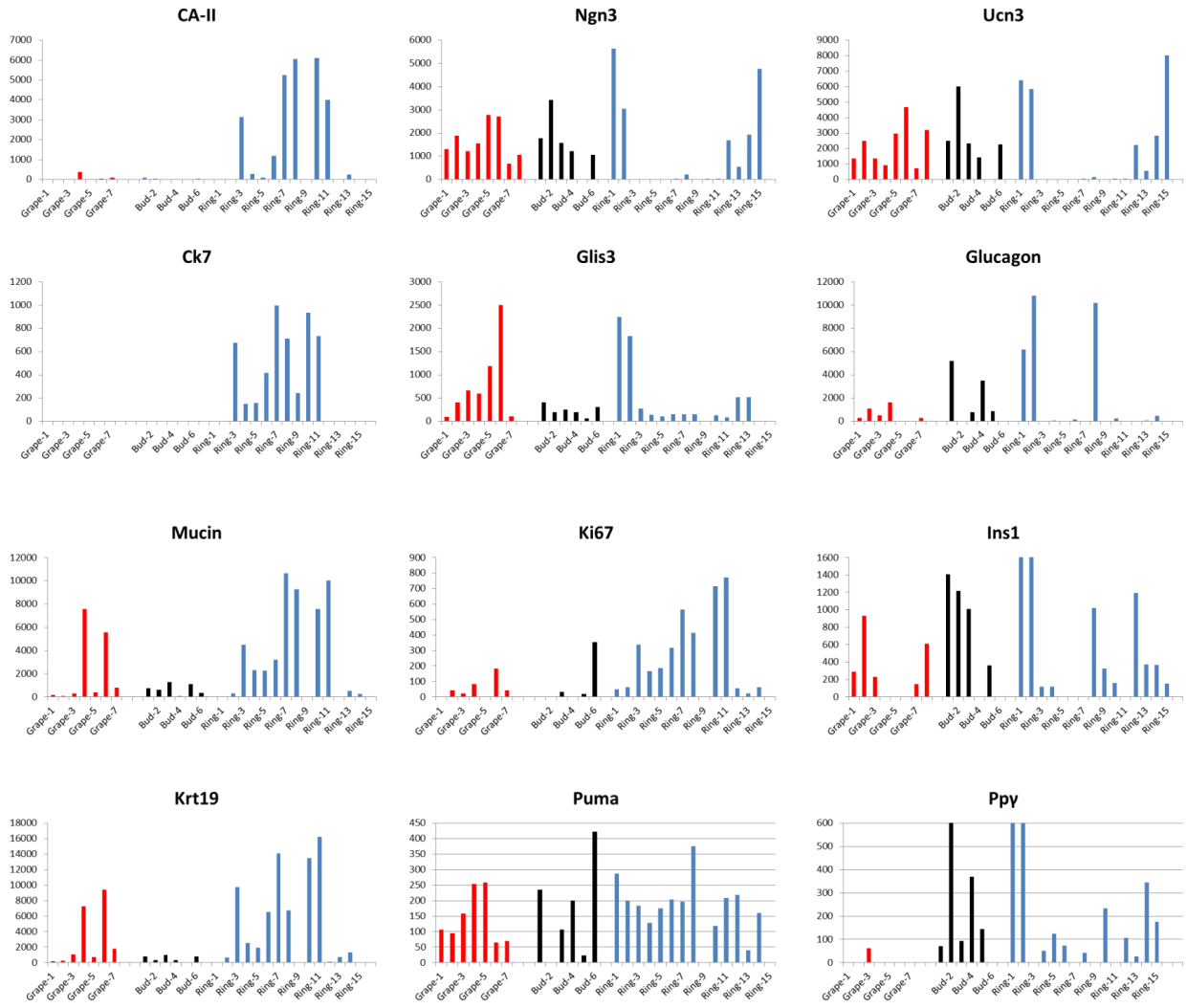

Figure 10: Gene expression by colony type

This figure presents the gene expression level of colonies selected 4 days after the start of culture, organized by observed colony morphology. On all charts, a red bar represents data collected from a single grapelike colony, a black bar, data collected from a single budding ring colony, and a blue bar, data collected from a single ring colony. The data presented were derived from 7 grapes, 6 budding rings, and 15 ringlike colonies. The Y-axis of all charts represents the normalization of gene expression against the housekeeping gene B2MG, where expression is calculated as described in the main text. The analyzed genes consist of ductal markers (left column, CA-II, Ck7, Mucin, Krt19), endocrine progenitor markers (center column, Ngn3 and Glis3), a proliferation marker (center column, Ki67),

an apoptosis marker (center column, Puma), and endocrine markers (right column, Ucn3, Glucagon, Ins1, Ppγ). These data show ringlike colonies as principally ductal, and grapelike or budding ring colonies as primarily endocrine or endocrine progenitor cells.

In these data, we note that the mature ductal markers carbonic anhydrase-2 (CA-II) (36) and cytokeratin-7 (Ck-7) (37) are strongly upregulated in ringlike colonies, relative to grapelike or budding rings. The ductal markers Mucin and keratin 19 (Krt19) are present in most of the colonies, but are more strongly expressed in ringlike colonies. In contrast, the endocrine progenitor marker Neurogenin3 (Ngn3), and Glis3, which also drives differentiation to endocrine cells (38), appear most strongly in grapelike colonies, or in budding rings, and are not as strongly expressed in ringlike colonies. The proliferation marker Ki67 is more highly expressed in ringlike colonies, though there is not much difference in the expression of the apoptosis marker Puma between colony types. The endocrine marker urocortin-3 (Ucn3) (39) is observed in grapelike and budding-ring colonies (seen in all except one of these colonies), whereas only 6 of the 15 observed ring colonies have this marker expressed. Glucagon is expressed in 5 of 7 grapelike colonies, 4 of 6 budding rings, and only 6 of 15 rings. The markers Ins1 and Ppγ do not show as sharp a distinction between colony types.

From this analysis, we conclude that the ringlike colonies are composed primarily of ductal cells, though some endocrine cells are probably also present. In contrast, budding ring and grapelike colonies contain endocrine cells, and no mature ductal cells. This is further supported by the fact that the proliferation marker Ki67 is most prominent in the ringlike compared to the grapelike colonies: while ductal cells are proliferative, endocrine and endocrine progenitor cells are usually not proliferative in normoglycemic, non-disease-state conditions (40-43). It is also encouraging to note that the apoptosis marker Puma is not expressed more strongly in RGD and COL than in methylcellulose-Matrigel.

Of particular interest is the expression level of Ngn3, a marker for endocrine progenitor cells (44-46). The Ngn3 signal is particularly strong in grapelike and budding ring colonies, suggesting these colonies are enriched for this type of cell. This means our culture method

may be useful as a source of progenitor cells, enabling further study into how to direct their differentiation into islet cells of a specific lineage.

However, there is reason for caution in interpreting these results. Of the ringlike colonies presented in Figure 10, rings 1, 2, and 12-15 are derived from COL or RGD, whereas rings 3-11 are derived from methylcellulose-Matrigel. It is precisely those rings derived from COL or RGD which show low levels of expression of ductal markers, and high levels of expression of endocrine and endocrine progenitor markers. This may be the result of gathering not only the target colony, but also surrounding cells in COL and RGD by mistake. It may also be the case that colony morphologies do not correlate well with the cells found within each colony, though this interpretation is hard to reconcile with the observations of Figure 9. We speculate that ring colonies in COL and RGD may have populations of immature ductal cells, which would not necessarily display expression of CA-II or Ck7, but which do show low levels of Mucin and Krt19 expression. Clearly, more work is needed to understand what types of cells are found within each colony type.

Single-colony RT-qPCR shows that gene expression patterns are altered by changing the material of origin

We considered the same dataset presented in Figure 10 from the perspective of the origin of each individual colony, gathering the results in Figure 11. The expression levels shown are calculated as previously described. The gene expression levels of colonies originating in COL are colored in red bars, those originating in methylcellulose-Matrigel are in black bars, and those originating in RGD are in blue bars. We find that colonies originating in COL or RGD have higher levels of endocrine and endocrine progenitor expression, and lower levels of ductal gene expression, than colonies originating in Methylcellulose-Matrigel. The mature ductal markers CA-II (36) and Ck-7 are present in Methylcellulose-Matrigel culture, but absent in RGD or Fong. In contrast, the endocrine markers urocortin-3 (Ucn3) (39) and neurogenin-3 (Ngn3) are more upregulated in COL and RGD cultures.

This suggests RGD and COL promote the growth of endocrine and endocrine progenitor cells, whereas methylcellulose-Matrigel favors the growth of mature ductal cells.

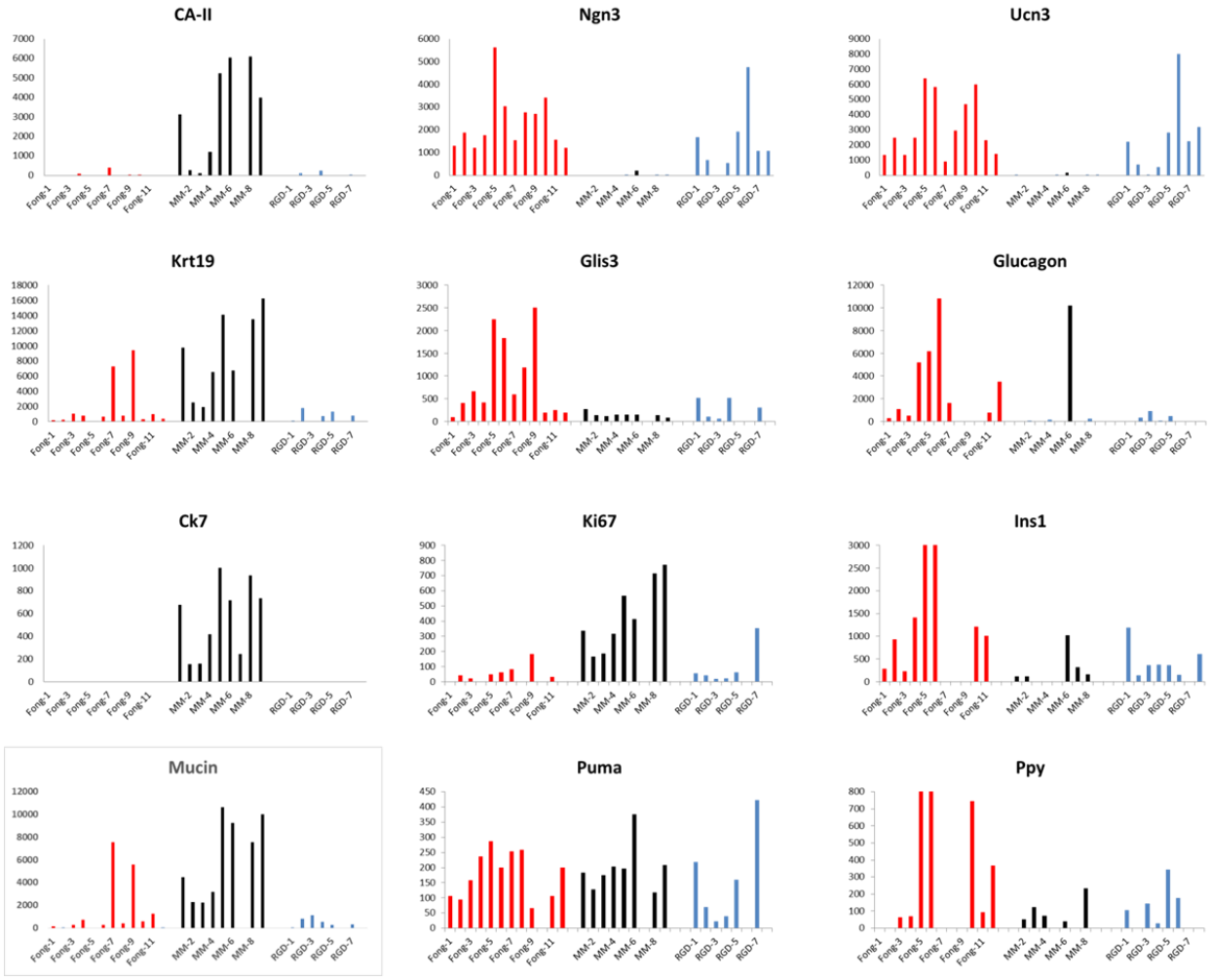

Figure 11: Gene expression by growth medium

This figure presents the same data shown in Figure 10, organized by the medium of origin for the individual colonies. Red bars represent colonies picked out of COL, black bars represent colonies selected from methylcellulose-Matrigel, and blue bars represent colonies selected from RGD. Expression (Y-axis) is calculated as

previously described, normalized on the housekeeping gene B2MG. Generally, methylcellulose-Matrigel promotes growth of ductal cells, COL and RGD promote growth of endocrine or endocrine progenitor cells.

Neurogenin 3 expression can also be observed by immunostaining

Based on the results of RT-qPCR, we wanted to confirm the presence of expressed Neurogenin3 in COL or RGD colonies, and its absence in methylcellulose-Matrigel. For this purpose, we conducted whole-mount immunostaining (Figure 12), and found that some colonies in COL contain cells that stain positive for Neurogenin 3. In one COL-derived colony, a bright red patch is observed co-localized to a nucleus (Figure 12B), but no such staining is observed in another colony derived from COL which was handled and washed in the same way (Figure 12E), meaning that the red signal observed in Figure 12B is specific, rather than being caused by nonspecific interactions of the antibodies with the cell. A methylcellulose-Matrigel colony, however, displays a red ring surrounding the entirety of the ductal cyst, and this signal is poorly colocalized to the nuclei. This suggests Neurogenin staining was non-specific in this case, which may be the result of insufficient washing, the nature of the tissue surrounding the ductal cyst, or the addition of too high a concentration of antibody.

It also appears to be the case that the colony derived from COL which is positive for Neurogenin3 was damaged by centrifugation, as its shape in the brightfield image is irregular (Figure 12C). Grapelike colonies in particular are somewhat fragile; we have observed that such colonies can fall apart when pipetted too vigorously. In order to improve the imaging and handle the cells delicately, we will next attempt to stain and wash the colonies of interest in a 2-micron mesh strainer, and remove wash and stain solutions by gravity.

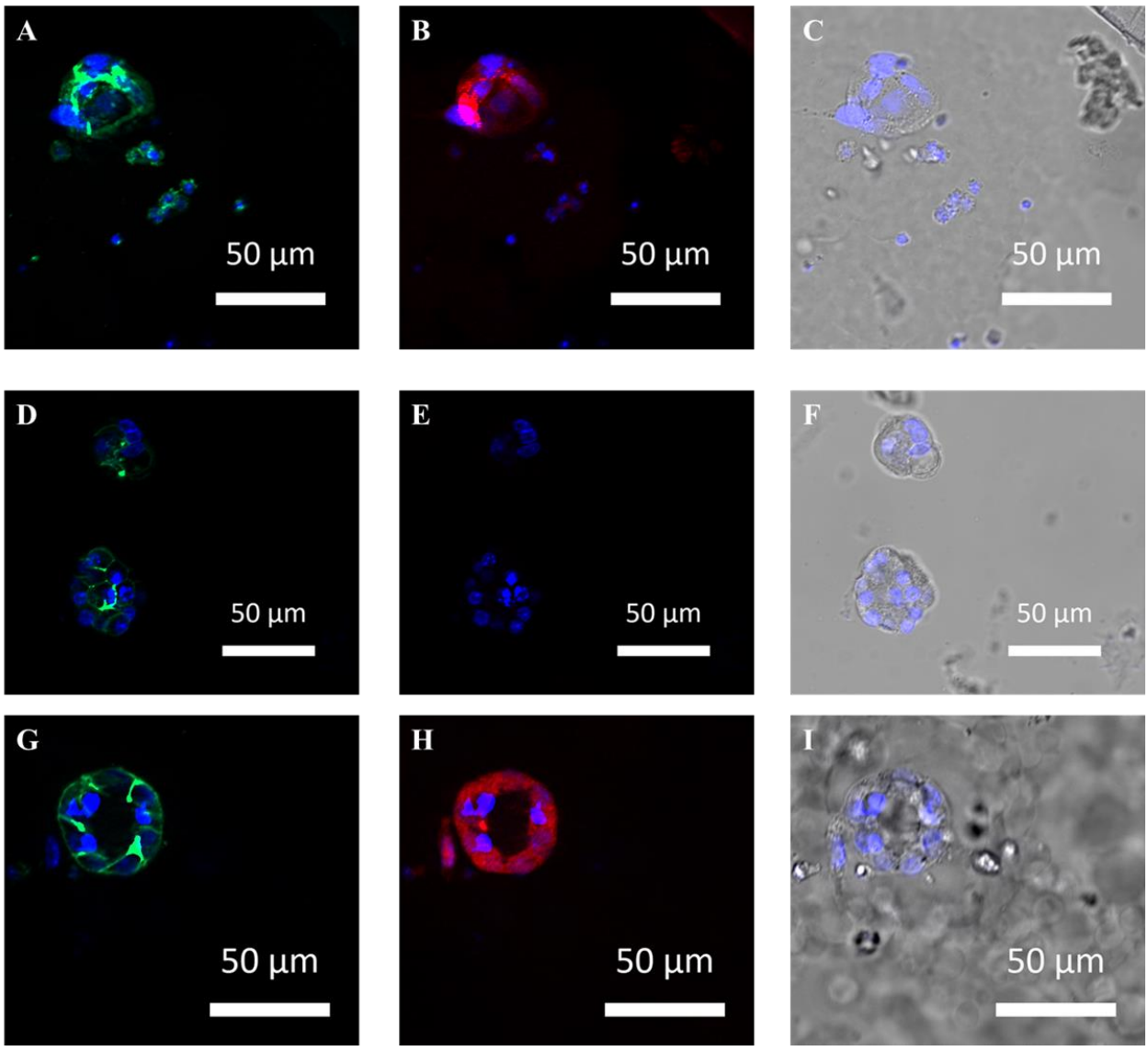

Figure 12: Immunostaining shows Ngn3 positive cells in COL

Whole-mount immunostaining micrographs are presented above for colonies grown in COL medium (A-F) and Methylcellulose-Matrigel (G-I). In all images, DAPI stains the nuclei in blue,
EpCAM is represented in green, and Ngn3 is in red. The positive EpCAM staining in micrographs A, D, and G reveal epithelial tissue characteristic of ductal cells, which appear in all colonies surveyed (image 12G is identical to image 9A and is provided for comparison). In the Ngn3 channel (micrographs B, E, and H), there is strong colocalization of staining with a cell nucleus only in one of the COL colonies, in micrograph B. We believe this staining to be specific as no staining is observed in micrograph E, which comes from another colony subjected to the exact same staining and wash

conditions and imaged at the same time. In micrograph H, the staining is non-specific as the red signal does not colocalize to the nuclei, but rather appears as a general smudge around the entirety of the ring. Bright-field images of the colonies are shown in micrographs C, F, and I. The putative Ngn3+ cell occurs within a collapsed colony in micrograph C, suggesting that these colonies are fragile when centrifuged. In contrast, the ductal cells are found within intact ringlike colonies, as seen in micrographs F and I.

Colony formation is dependent on a paracrine effect in defined, protein-based culture, but not in Methylcellulose-Matrigel culture

To determine which cell types produced particular colony types, we conducted a culture experiment with populations of sorted cells. We used a transgenic strain of mice which had one copy of Ngn3 replaced by GFP, meaning that GFP expression was driven by an endogenous Ngn3 promoter. We used CD133 as a ductal and bipotent progenitor cell marker (47), and accordingly stained cells with an anti-CD133-biotin antibody and APC-streptavidin secondary stain. DAPI was used as a stain to assess viability as it is mostly impermeant to live cells. Therefore, cells showing a high DAPI signal are assumed non-viable and excluded from the sorted population (48, 49). Approximately 45% of the cells were found to be viable. From this viable population, we sorted into four populations: P5 (representing cells that were CD133+ Ngn3+), P6 (CD133+ Ngn3-), P7 (CD133 low, Ngn3-) and P8 (CD133- Ngn3-) as shown in Figure 13. These populations were then plated separately in RGD and COL at densities of 2500 cells/100 μL and 10,000 cells/100 μL, and in methylcellulose-Matrigel at a density of 2000 cells/100 μL. It is important to note that these populations were grown in separate wells, and were therefore isolated from each other.

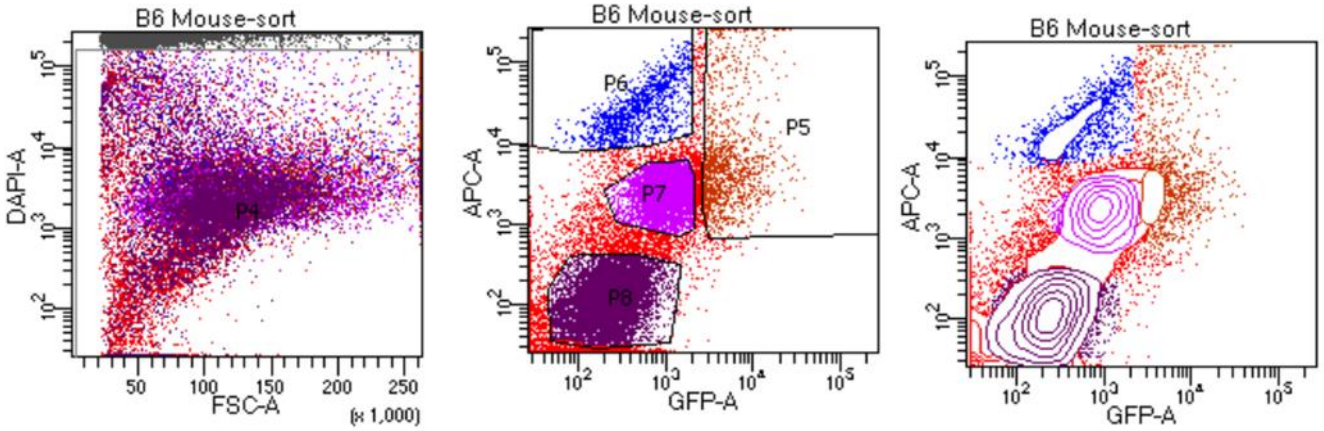

Figure 13: Sorting of cells based on Ngn3 and CD133

The above traces were collected on an Aria III flow cytometer during cell sorting. The cells used were derived from strain B6.129S-Neurog3tm1(EGFP)Khk/Mmucd (Ngn-GFP), which substituted GFP for one copy of Neurogenin3 (Ngn3) in the mouse. Staining with DAPI was used to establish cell viability, and only those cells with low DAPI staining were accepted for further sorting as population P4 (leftmost panel). This population represented approximately 45% of all recorded events. Population P4 is further sorted into four populations based on APC and GFP signal intensity (center and right boxes). We interpret the GFP signal on the horizontal axis as showing which cells are Ngn3+. APC-streptavidin was used as a secondary stain for a primary anti-CD133-biotin antibody, meaning that the vertical axis represents staining for CD133. The cells were divided into 4 populations, P5 (CD133+, Ngn3+), P6 (CD133+, Ngn3-), P7 (CD133 low, Ngn3-) and P8 (CD133- Ngn3-), representing approximately 3%, 3%, 9% and 18% of all observed events respectively. The complete flow cytometry data is presented in supporting information Figure S1.

Each of these populations was initially put into COL and RGD culture at a plating density of 2500 cells/100 μL. We found that this density was insufficient to support colony formation, in either sorted or unsorted cultures (data not shown). When the number of cells was increased to 10,000 cells/100 μL, colonies could be observed after 2 or 3 days; however no colonies were observed in population P8 in either material, and no colonies were observed in RGD in population P6. After 4 days the observed colonies were manually counted; the results are shown in Figure 14. Notably, the colonies that are observed for CD133+/Ngn3+ and CD133 low/Ngn3- cells are strongly biased towards ringlike colonies

in RGD and COL, unlike in an unsorted population where more grapelike colonies are observed (compare Figure 8). The exception to this observation is population P6 in COL, where the majority of colonies are grapelike. It is important to note, however, that the grapelike colonies in this population were very small, sometimes consisting of only a few cells, in contrast to the larger grapelike colonies observed in unsorted populations. This suggests that the colonies in population P6 in COL are not healthy or particularly long-lived, which is consistent with this population not surviving in RGD.

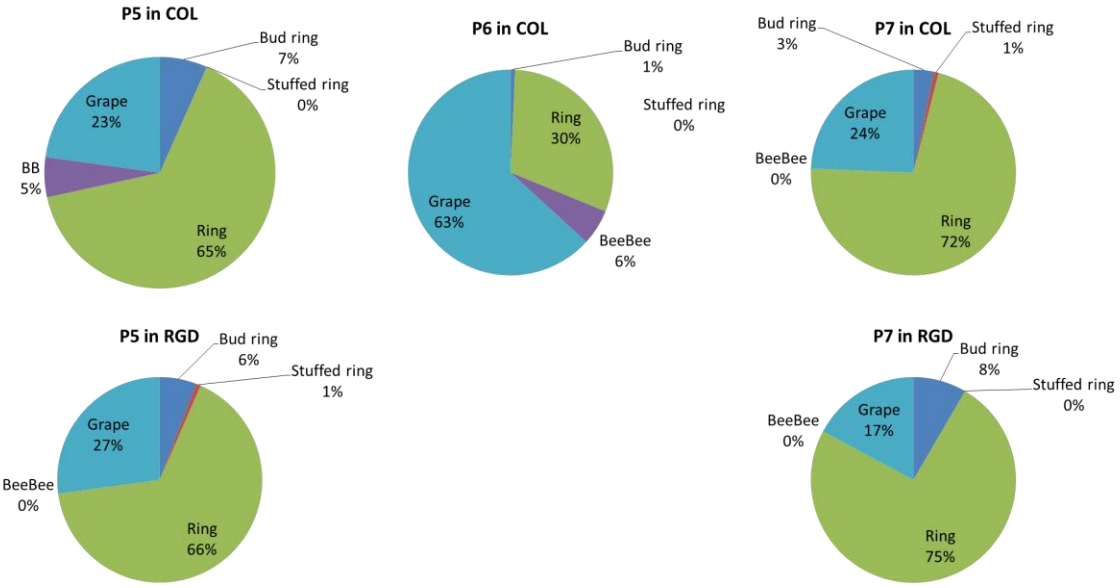

Figure 14: Colony distributions in sorted populations

A count of colonies by morphology is shown for colonies derived from populations P5-P7, and grown in materials RGD and COL. Population P8 is omitted as only single cells were observed in both materials, and population P6 in RGD is omitted as only single cells were observed in this condition. The colony distribution for unsorted populations is shown in Figure 8. Populations P5 and P7 give rise to a higher percentage of ringlike colonies in comparison to unsorted populations, and there is no significant difference observed between RGD and COL culture. Ringlike colonies do appear to be more strongly favored when using population P7 as opposed to population P5, but this difference is less than 10%.

The growth of sorted populations in RGD and COL was also notable for the large number of single cells that were still observed after 4 days of culture. Indeed, fewer colonies overall were observed when using sorted populations as opposed to unsorted populations. We present these data in terms of the colony-forming efficiency, defined as:

$$colony\ forming\ efficiency = \frac{Total\ number\ of\ colonies}{Total\ number\ of\ cells\ plated} \times 100\%$$

The colony-forming efficiency of each population in a given material is presented in Table 1. In RGD and COL, the sorted populations P5 and P7 have colony-forming efficiencies between one-third and one-half of that characteristic of the unsorted population. This is particularly remarkable considering that unsorted populations consist of up to 55% non-viable cells that should not form colonies. Also notable is that no similarly large decrease in colony-forming efficiency can be seen in methylcellulose-Matrigel culture, and in fact, sorting appears to slightly enhance colony-forming efficiency. This slight increase in the colony-forming efficiency of sorted populations is consistent with the removal of non-viable cells.

There are other important differences observed between methylcellulose-Matrigel culture and protein-based culture. First, methylcellulose-Matrigel does support the growth of colonies at a plating cell density of 2500 cells/100 μL, in contrast to protein-based materials RGD and COL. Second, all four sorted populations, P5-P8, are capable of forming colonies in Methylcellulose-Matrigel. All four of these populations resulted in the same, ring colony type in methylcellulose-Matrigel.

	methylcellulose-Matrigel	COL	RGD
P5 (CD133+/Ngn3+)	0.84%	0.39%	0.34%
P6 (CD133+/Ngn3-)	0.65%	0.43%	0.00%
P7 (CD133 low/Ngn3-)	1.03%	0.53%	0.31%
P8 (CD133-/Ngn3-)	0.74%	0.00%	0.00%
Unsorted	0.69%	0.99%	0.63%

Table 1: Colony-forming efficiencies in sorted and unsorted populations, in methylcellulose-Matrigel, RGD, and COL

These data provide an approximation as to how many seeded cells formed colonies in each material, with colony forming efficiency derived as (total number of colonies observed)/(total number of cells seeded). Of note, population P8 does not grow in COL or RGD, but has a slightly higher colony-forming efficiency than the unsorted population in methylcellulose-Matrigel. Similarly, population P6 does not form colonies in RGD, forms colonies at approximately half the rate of an unsorted population in COL, and forms colonies at the same rate as an unsorted population in methylcellulose-Matrigel. Colony-forming efficiency is slightly higher in the sorted populations in methylcellulose-Matrigel compared to the unsorted populations (except for population P6), which is consistent with the removal of non-viable cells via cell sorting.

From these observations we can draw several conclusions. First, we suggest that a paracrine effect exists between populations P5, P6, P7, and P8, and that depriving the cells of this paracrine effect promotes the growth of ringlike colonies, and suppresses the growth of grapelike colonies. Second, this paracrine effect increases the colony forming efficiency in RGD and COL. Third, as colony-forming efficiency is not hampered in methylcellulose-Matrigel, and the identities of the colonies do not change from population to population, if our observations are consistent with a paracrine effect, then the relevant paracrine factor or factors must either already be present in Matrigel, or the effects of these paracrine factors are overshadowed by other molecules also present in Matrigel. The presence of relevant paracrine factors also explains why sorted and unsorted populations of cells do not grow in COL or RGD at a plating density of 2500 cells/100 μL: at lower densities, there might not be a high-enough concentration of the relevant paracrine factors to allow for colony formation.

CONCLUSIONS AND FUTURE WORK

We have demonstrated the culture of murine pancreatic cells in defined, protein-based media, and shown that colony morphology and cell type depend on which chemical cues are present in the matrix. We have further demonstrated the presence of a population of Neurogenin3 positive, putative endocrine progenitor cells, which could be used to further elucidate the process by which these cells differentiate to mature endocrine cells.

We also have evidence which suggests that a paracrine effect may be occurring between populations of CD133+/Ngn3+, CD133+/Ngn3-, CD133low/Ngn3-, and CD133-/Ngn3- cells. This paracrine effect, which is not observed in undefined methylcellulose-Matrigel culture, appears to promote the formation of colonies by individual cells, and to favor the growth of grapelike colonies, which we currently believe to be endocrine. These conclusions demonstrate the advantages of using a defined, protein-based medium.

Future work

To further explore the putative paracrine effect, we will conduct single-cell RNAseq and proteomic analysis on cells from each population, in order to determine which secreted proteins may explain the observed effect. We will also introduce cell populations into the protein culture pair-wise, to determine which populations need to interact in order to give rise to grapelike colonies, or to promote growth. Finally, if putative growth or signaling factors can be identified, we will supplement protein-based cultures with recombinant versions of those factors, in order to duplicate the paracrine effect, and confirm which factors are most relevant.

While we have made a convincing case that the grapelike and budding ring colonies are likely endocrine in nature, the ringlike colonies derived from COL and RGD are still enigmatic, as while they are morphologically similar to ductal colonies found in methylcellulose-Matrigel, and while the immunostaining evidence presented in Figure 9 suggests that they are endocrine rather than ductal, the RNA profiles obtained by RT-qPCR suggest that ringlike colonies derived from COL and RGD are more endocrine than ductal.

We will need to further evaluate these types of colonies in order to more conclusively determine what they are.

While RT-qPCR appears to indicate that endocrine-like cells are favored in RGD and COL, it is imperative that we have better population-level statistics, in order to draw firmer conclusions about how the medium biases cell growth and differentiation. We would also like to be able to show if there is a clear difference in the population of cells grown in RGD, which has a fibronectin-like cue, compared with the population of cells grown in COL, which has a collagen IV cue. While the colony counts presented in Figure 8 do appear to show a difference in colony morphology when comparing RGD and COL, as previously stated, it is not clear what each of those colony types represent. The best experiment to obtain population-level statistics and thereby disambiguate this situation is single-cell RNAseq. To that end, we have been developing methods to extricate the colonies from the surrounding medium, and to digest them to single cells. Digestion with a combination of TryplE and Liberase results in single cells, however, the viability of these cells, as determined by Trypan Blue staining, is only about 30%, whereas single-cell RNAseq requires a viability closer to 70% in order to be effective. To solve this problem, we may need to begin our culture with a population of cells that has been sorted to remove the 55% of cells which are non-viable. We also still need to optimize the digestion time, and we are also considering the use of a dead-cell removal kit after digestion.

If we cannot get sufficient viability for single-cell RNAseq, we may instead consider conducting analytical flow cytometry on populations extracted from the culture conditions. One potential difficulty with using flow cytometry is that antibodies to detect relevant marker proteins such as insulin have to penetrate the cell in order to be effective, meaning the cells have to be permeabilized before analysis. This, in turn, would make it difficult to use DAPI as a marker for whether the cells were alive or dead, as when cells are permeabilized, DAPI is able to enter all of them, regardless of whether the cells are alive or dead. If we do eventually use this route for characterization of the entire populations, we will have to determine which surface markers are most appropriate to target.

Finally, we will continue to optimize the immunostaining of COL and RGD, with gentler handling via use of a cell strainer, and changing the amount of time that the antibodies are allowed to be in contact with the cells of interest. This will allow us to isolate more grapelike colonies, and perhaps take more conclusive images.

SUPPORTING INFORMATION FOR CHAPTER 2

Protein	Sequence	Molecular Weight
RGD	MRGSSHHHHHHENLYFQGDL APQMLRELQETNAALQDVRE LLRQQVKEATFLKNTVMESD ASGGGSVDVPGAGVPGAGVP GEGVPGAGVPGAGVPGAGVP GAGVPGEGVPGAGVPGAGVP GAGVPGAGVPGEGVPGAGVP GAGLDVPGAGVPGAGVPGEG VPGAGVPGAGVPGAGVPGAG VPGEGVPGAGVPGAGVPGAG VPGAGVPGEGVPGAGVPGAG LDDRPELYAVTGRGDSPASS APIATSLDVPGAGVPGAGVP GEGVPGAGVPGAGVPGAGVP GAGVPGEGVPGAGVPGAGVP GAGVPGAGVPGEGVPGAGVP GAGLDVPGAGVPGAGVPGEG VPGAGVPGAGVPGAGVPGAG VPGEGVPGAGVPGAGVPGAG VPGAGVPGEGVPGAGVPGAG LDENLYFQGDLAPQMLRELQ ETNAALQDVRELLRQQVKEA TFLKNTVMESDASGGKLAS	41,202 Da
COL	MRGSSHHHHHHENLYFQGDL APQMLRELQETNAALQDVRE LLRQQVKEATFLKNTVMESD ASGGGSVDVPGAGVPGAGVP GEGVPGAGVPGAGVPGAGVP GAGVPGEGVPGAGVPGAGVP GAGVPGAGVPGEGVPGAGVP GAGLDVPGAGVPGAGVPGEG VPGAGVPGAGVPGAGVPGAG VPGEGVPGAGVPGAGVPGAG VPGAGVPGEGVPGAGVPGAG LDDRPPPFLMLLKGSTRTSL DVPGAGVPGAGVPGEGVPGA GVPGAGVPGAGVPGAGVPGE GVPGAGVPGAGVPGAGVPGA GVPGEGVPGAGVPGAGLDVP GAGVPGAGVPGEGVPGAGVP GAGVPGAGVPGAGVPGEGVP GAGVPGAGVPGAGVPGAGVP GEGVPGAGVPGAGLDENLYF QGDLAPQMLRELQETNAALQ DVRELLRQQVKEATFLKNTV MESDASGGKLAS	40,700 Da

Supporting Table ST1: protein sequences and molecular weights are shown above

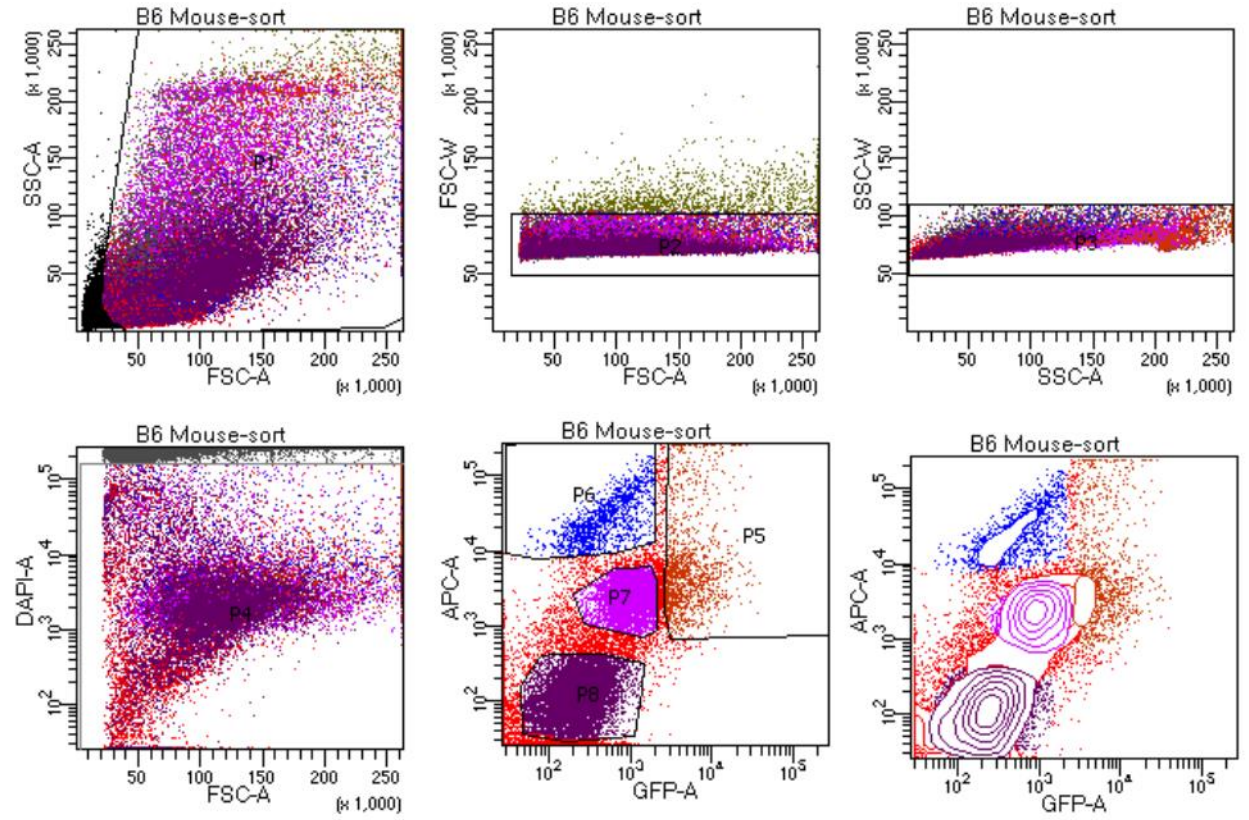

Supporting Figure S1: Complete flow cytometry gating for sorting experiments.

The above figure presents the gating, and populations, of cells derived from mouse strain B6.129S-Neurog3tm1(EGFP)Khk/Mmucd (Ngn-GFP). The top-left panel shows sorting based on side-scatter area vs. forward-scatter area (SSC-A vs FSC-A). Events that have low amounts of both types of scattering are likely debris, and are excluded from the sorted population. The remaining population P1 is further sorted by comparing forward-scatter

width with forward-scatter area (FSC-W vs FSC-A) and side-scatter width with side-scatter area (SSC-W vs SSC-A). This is done for the purpose of doublet exclusion as events that display a large peak width in relation to peak area do so because these events represent two cells that have passed through the laser while adjacent to each other. Gates P2 and P3 are drawn in order to further sort only singlet events. After population P3 is accepted for further sorting, we gate for DAPI signal: as DAPI is impermeant to viable cells, we exclude those cells that display a high DAPI signal, and retain cells with a low DAPI signal as population P4. Population P4 is then sorted based on APC signal (related to staining with an anti-CD133 antibody) and EGFP signal, which relates to Ngn3 expression. We divide these cells into populations P5, P6, P7 and P8 as shown. The final image is a contour map of the sorted population. Statistics gathered for each population are shown below the charts.

COL

	Bud ring	Stuffed ring	Ring	BeeBee	Grapelike	total
Rep1-1	18	26	50	1	46	141
Rep1-2	29	34	39	0	21	123
Rep1-3	17	30	27	6	29	109
Rep2-1	13	9	54	0	57	133
Rep2-2	15	8	56	4	28	111
Rep2-3	6	6	57	0	39	108
Rep3-1	9	0	23	2	18	52
Rep3-2	11	0	30	5	30	76
Rep3-3	17	2	45	4	33	101
Rep3-4	17	1	35	5	32	90
Rep3-5	8	0	19	5	16	48

RGD

	Bud ring	Stuffed ring	Ring	BeeBee	Grapelike	total
Rep1-1	2	5	15	0	34	56
Rep1-2	3	9	20	0	39	71
Rep1-3	9	5	15	0	48	77
Rep2-1	1	1	13	0	29	44
Rep2-2	3	3	18	0	29	53
Rep2-3	0	1	14	0	24	39
Rep3-1	23	2	25	4	55	109
Rep3-2	16	2	11	0	43	72
Rep3-3	14	0	15	1	30	60
Rep3-4	13	1	14	1	48	77
Rep3-5	11	0	8	0	30	49
Rep3-6	14	2	6	0	24	46

	Bud ring	stuffed ring	ring	beebee	grape
Rep1-1	13%	18%	35%	1%	33%
Rep1-2	24%	28%	32%	0%	17%
Rep1-3	16%	28%	25%	6%	27%
Rep2-1	10%	7%	41%	0%	43%
Rep2-2	14%	7%	50%	4%	25%
Rep2-3	6%	6%	53%	0%	36%
Rep3-1	17%	0%	44%	4%	35%
Rep3-2	14%	0%	39%	7%	39%
Rep3-3	17%	2%	45%	4%	33%
Rep3-4	19%	1%	39%	6%	36%
Rep3-5	17%	0%	40%	10%	33%
Average	15%	9%	40%	4%	32%

	Bud ring	stuffed ring	ring	beebee	grape
Rep1-1	4%	9%	27%	0%	61%
Rep1-2	4%	13%	28%	0%	55%
Rep1-3	12%	6%	19%	0%	62%
Rep2-1	2%	2%	30%	0%	66%
Rep2-2	6%	6%	34%	0%	55%
Rep2-3	0%	3%	36%	0%	62%
Rep3-1	21%	2%	23%	4%	50%
Rep3-2	22%	3%	15%	0%	60%
Rep3-3	23%	0%	25%	2%	50%
Rep3-4	17%	1%	18%	1%	62%
Rep3-5	22%	0%	16%	0%	61%
Rep3-6	30%	4%	13%	0%	52%
Average	14%	4%	24%	1%	58%

methylcellulose-Matrigel

well no.	Bud ring	Stuffed ring	Ring	BeeBee	Grapelike	total
Rep1-1	6	4	101	0	6	117
Rep1-2	9	1	142	0	6	158
Rep1-3	4	0	114	0	11	129
Rep2-1	3	3	170	0	0	176
Rep2-2	1	2	135	1	3	142
Rep2-3	0	2	147	0	0	149
By Percentage						
	Bud ring	Stuffed ring	Ring	BeeBee	Grapelike	total
Rep1-1	5.13%	3.42%	86.32%	0.00%	5.13%	100.00%
Rep1-2	5.70%	0.63%	89.87%	0.00%	3.80%	100.00%
Rep1-3	3.10%	0.00%	88.37%	0.00%	8.53%	100.00%
Rep2-1	1.70%	1.70%	96.59%	0.00%	0.00%	100.00%
Rep2-2	0.70%	1.41%	95.07%	0.70%	2.11%	100.00%
Rep2-3	0.00%	1.34%	98.66%	0.00%	0.00%	100.00%
Average	2.72%	1.42%	92.48%	0.12%	3.26%	100.00%

Supporting Table ST2: raw colony counts used to construct pie charts in Figure 8.

Primer number	Function	Gene	Cat #
1	house keeping	Actin-B (house keeping)	Mm 00607939_s1
2		B2 MG(house keeping)	Mm 00437762_m1
3		Ppig (Cyclophilin G) (house keeping)	Mm01328875_m1
4		18S rRNA	Mm04277571
5		RPLPO	Mm00725448
6	acinar	Amylase 2A (Tao) fluidigm	Mm02342487_g1
7		Carboxypeptidase A1	Mm 00465942_m1
8		Elastase 1	Mm00712898_m1
9		Ptf1a	Mm 00479622_m1
10	duct	carbonic anhydrase 2(CA-II)	Mm00501572_m1
11		HNF1B	Mm00447459_m1
12		HNF6	Mm00839394_m1
13		Keratin 19 (ck19, krt19)	Mm00492980_m1
14		Keratin 7(mCK7)	Mm00466676_m1
15		Mucin 1	Mm00449604_m1
16		Sox9	Mm 00448840_m1
17		Neurod1	Mm0180117_m1
18	Endocrine precursor	Neurod2	Mm00440465_g1
19		NgN3	Mm00437606_s1
20		Nkx2.2	Mm 00839794_m1
21		Nkx6.1	Mm 00454962_m1
22		Pax4	Mm 01159036_m1
23		Pdx1	Mm 00435565_m1
24		ARX	Mm00545903
25		new ARX	Mm01237524_m1
26		Pax6	Mm00493081_m1
27	endocrine	GHRL (Ghrelin)	Mm 00445450_m1
28		Glucagon	Mm 00801712_m1
29		Insulin 1 (Tao) fluidigm	Mm01259683_g1
30		Insulin 2	Mm 00731595_gH
31		PPY	Mm 00435889_m1
32		SST	Mm 00436671_m1
33		Urocortin 3 (Ucn3)	Mm00453206_s1*
34		Glis3	Mm01195845_m1
35	proliferation	Lgr5	Mm00438890_m1
35		Myt1	Mm00456190_m1

37		Ki67	Mm01278617_m1
38		cyclin D1	Mm00432359_m1
39		CD133	Mm00477115_m1
40		PUMA BBC3	Mm00519268

Supporting Table ST3: TaqMan Probe List

The table above reports the catalog numbers of all Applied Biosystems TaqMan probes obtained from ThermoFisher, and used in RT-qPCR.

REFERENCES FOR CHAPTER 2

1. Xu G, *et al.* (2018) Prevalence of diagnosed type 1 and type 2 diabetes among US adults in 2016 and 2017: population based study. *BMJ (Clinical research ed.)* 362:k1497-k1497.
2. Bjornstad P, Snell-Bergeon JK, Nadeau KJ, & Maahs DM (2015) Insulin sensitivity and complications in type 1 diabetes: New insights. *World journal of diabetes* 6(1):8-16.
3. Nalysnyk L, Hernandez-Medina M, & Krishnarajah G (2010) Glycaemic variability and complications in patients with diabetes mellitus: evidence from a systematic review of the literature. *Diabetes Obes. Metab.* 12(4):288-298.
4. Shapiro AMJ, Pokrywczynska M, & Ricordi C (2017) Clinical pancreatic islet transplantation. *Nat. Rev. Endocrinol.* 13(5):268-277.
5. Shapiro AMJ, *et al.* (2000) Islet transplantation in seven patients with type 1 diabetes mellitus using a glucocorticoid-free immunosuppressive regimen. *N. Engl. J. Med.* 343(4):230-238.
6. Shapiro AMJ (2011) Strategies toward single-donor islets of Langerhans transplantation. *Curr. Opin. Organ Transpl.* 16(6):627-631.
7. Moore SJ, Gala-Lopez BL, Pepper AR, Pawlick RL, & Shapiro AJ (2015) Bioengineered stem cells as an alternative for islet cell transplantation. *World journal of transplantation* 5(1):1-10.
8. Pan FC & Wright C (2011) Pancreas Organogenesis: From Bud to Plexus to Gland. *Dev. Dyn.* 240(3):530-565.
9. Rezania A, *et al.* (2014) Reversal of diabetes with insulin-producing cells derived *in vitro* from human pluripotent stem cells. *Nat. Biotechnol.* 32(11):1121-1133.
10. Pagliuca Felicia W, *et al.* (2014) Generation of Functional Human Pancreatic Beta Cells *In Vitro*. *Cell* 159(2):428-439.
11. Ma H, Wert KJ, Shvartsman D, Melton DA, & Jaenisch R (2018) Establishment of human pluripotent stem cell-derived pancreatic β-like cells in the mouse pancreas. *Proceedings of the National Academy of Sciences* 115(15):3924-3929.
12. Hughes CS, Postovit LM, & Lajoie GA (2010) Matrigel: A complex protein mixture required for optimal growth of cell culture. *Proteomics* 10(9):1886-1890.
13. Goldstein AS, *et al.* (2011) Purification and direct transformation of epithelial progenitor cells from primary human prostate. *Nat. Protoc.* 6(5):656-667.
14. Vukicevic S, *et al.* (1992) IDENTIFICATION OF MULTIPLE ACTIVE GROWTH-FACTORS IN BASEMENT-MEMBRANE MATRIGEL SUGGESTS CAUTION IN INTERPRETATION OF CELLULAR-ACTIVITY RELATED TO EXTRACELLULAR-MATRIX COMPONENTS. *Exp. Cell Res.* 202(1):1-8.
15. Unger C, Skottman H, Blomberg P, Dilber MS, & Hovatta O (2008) Good manufacturing practice and clinical-grade human embryonic stem cell lines. *Hum. Mol. Genet.* 17:R48-R53.
16. Ludwig TE, *et al.* (2006) Derivation of human embryonic stem cells in defined conditions. *Nat. Biotechnol.* 24(2):185-187.
17. Prokhorova TA, *et al.* (2009) Teratoma Formation by Human Embryonic Stem Cells Is Site Dependent and Enhanced by the Presence of Matrigel. *Stem Cells Dev.* 18(1):47-54.
18. Hentze H, *et al.* (2009) Teratoma formation by human embryonic stem cells: Evaluation of essential parameters for future safety studies. *Stem Cell Res.* 2(3):198-210.

19. Vaillant F, Lindeman GJ, & Visvader JE (2011) Jekyll or Hyde: does Matrigel provide a more or less physiological environment in mammary repopulating assays? *Breast Cancer Res.* 13(3):4.
20. Petka WA, Harden JL, McGrath KP, Wirtz D, & Tirrell DA (1998) Reversible hydrogels from self-assembling artificial proteins. *Science* 281(5375):389-392.
21. Olsen BD, Kornfield JA, & Tirrell DA (2010) Yielding Behavior in Injectable Hydrogels from Telechelic Proteins. *Macromolecules* 43(21):9094-9099.
22. Shen W, Zhang KC, Kornfield JA, & Tirrell DA (2006) Tuning the erosion rate of artificial protein hydrogels through control of network topology. *Nature materials* 5(2):153-158.
23. Rapp PB, *et al.* (2017) Analysis and Control of Chain Mobility in Protein Hydrogels. *J. Am. Chem. Soc.* 139(10):3796-3804.
24. Rapp PB, Omar AK, Silverman BR, Wang Z-G, & Tirrell DA (2018) Mechanisms of Diffusion in Associative Polymer Networks: Evidence for Chain Hopping. *J. Am. Chem. Soc.* 140(43):14185-14194.
25. Dooling LJ & Tirrell DA (2016) Engineering the Dynamic Properties of Protein Networks through Sequence Variation. *ACS Central Sci.* 2(11):812-819.
26. Dooling LJ (2016) Programming Molecular Association and Viscoelastic Behavior in Protein Hydrogels. Doctor of Philosophy (California Institute of Technology).
27. Jin L, *et al.* (2013) Colony-forming cells in the adult mouse pancreas are expandable in Matrigel and form endocrine/acinar colonies in laminin hydrogel. *Proc. Natl. Acad. Sci. U. S. A.* 110(10):3907-3912.
28. Ghazalli N, *et al.* (2015) Postnatal Pancreas of Mice Contains Tripotent Progenitors Capable of Giving Rise to Duct, Acinar, and Endocrine Cells *In Vitro*. *Stem Cells Dev.* 24(17):1995-2008.
29. Tjin MS, Chua AWC, Ma DR, Lee ST, & Fong E (2014) Human Epidermal Keratinocyte Cell Response on Integrin-Specific Artificial Extracellular Matrix Proteins. *Macromol. Biosci.* 14(8):1125-1134.
30. Lee CS, Perreault N, Brestelli JE, & Kaestner KH (2002) Neurogenin 3 is essential for the proper specification of gastric enteroendocrine cells and the maintenance of gastric epithelial cell identity. *Genes Dev* 16(12):1488-1497.
31. Wedeken L, *et al.* (2017) Adult Murine Pancreatic Progenitors Require Epidermal Growth Factor and Nicotinamide for Self-Renewal and Differentiation in a Serum-and Conditioned Medium-Free Culture. *Stem Cells Dev.* 26(8):599-607.
32. Henseleit KD, *et al.* (2005) NKX6 transcription factor activity is required for alpha- and beta-cell development in the pancreas. *Development* 132(13):3139-3149.
33. Engler AJ, Sen S, Sweeney HL, & Discher DE (2006) Matrix elasticity directs stem cell lineage specification. *Cell* 126(4):677-689.
34. Murphy WL, McDevitt TC, & Engler AJ (2014) Materials as stem cell regulators. *Nature materials* 13(6):547-557.
35. Lv H, *et al.* (2015) Mechanism of regulation of stem cell differentiation by matrix stiffness. *Stem Cell Res. Ther.* 6(1):103-103.
36. Inada A, Nienaber C, Fonseca S, & Bonner-Weir S (2006) Timing and expression pattern of carbonic anhydrase II in pancreas. *Developmental dynamics : an official publication of the American Association of Anatomists* 235(6):1571-1577.
37. Pujal J, *et al.* (2009) Keratin 7 promoter selectively targets transgene expression to normal and neoplastic pancreatic ductal cells *in vitro* and *in vivo*. *FASEB journal : official publication of the Federation of American Societies for Experimental Biology* 23(5):1366-1375.

38. Kang HS, *et al.* (2009) Transcription factor Glis3, a novel critical player in the regulation of pancreatic beta-cell development and insulin gene expression. *Mol. Cell. Biol.* 29(24):6366-6379.
39. Pechhold K, *et al.* (2009) Blood Glucose Levels Regulate Pancreatic β-Cell Proliferation during Experimentally-Induced and Spontaneous Autoimmune Diabetes in Mice. *PLoS One* 4(3):e4827.
40. Klochendler A, *et al.* (2016) The Genetic Program of Pancreatic beta-Cell Replication *In Vivo*. *Diabetes* 65(7):2081-2093.
41. Puri S, *et al.* (2018) Replication confers beta cell immaturity. *Nat. Commun.* 9:12.
42. Miyatsuka T, Kosaka Y, Kim H, & German MS (2011) Neurogenin3 inhibits proliferation in endocrine progenitors by inducing Cdkn1a. *Proc. Natl. Acad. Sci. U. S. A.* 108(1):185-190.
43. Schonhoff SE, Giel-Moloney M, & Leiter AB (2004) Neurogenin 3-expressing progenitor cells in the gastrointestinal tract differentiate into both endocrine and non-endocrine cell types. *Developmental Biology* 270(2):443-454.
44. Schwitzgebel VM, *et al.* (2000) Expression of neurogenin3 reveals an islet cell precursor population in the pancreas. *Development* 127(16):3533-3542.
45. Jensen J, *et al.* (2000) Independent development of pancreatic alpha- and beta-cells from neurogenin3-expressing precursors: a role for the notch pathway in repression of premature differentiation. *Diabetes* 49(2):163-176.
46. Li C, Chen P, Vaughan J, Lee K-F, & Vale W (2007) Urocortin 3 regulates glucose-stimulated insulin secretion and energy homeostasis. *Proceedings of the National Academy of Sciences* 104(10):4206.
47. Oshima Y, *et al.* (2007) Isolation of mouse pancreatic ductal progenitor cells expressing CD133 and c-Met by flow cytornetric cell sorting. *Gastroenterology* 132(2):720-732.
48. Darzynkiewicz Z, *et al.* (1992) FEATURES OF APOPTOTIC CELLS MEASURED BY FLOW-CYTOMETRY. *Cytometry* 13(8):795-808.
49. Hotz MA, Gong JP, Traganos F, & Darzynkiewicz Z (1994) FLOW CYTOMETRIC DETECTION OF APOPTOSIS - COMPARISON OF THE ASSAYS OF IN-SITU DNA-DEGRADATION AND CHROMATIN CHANGES. *Cytometry* 15(3):237-244.

Chapter III

GENETICALLY PROGRAMMABLE BACTERIAL ASSEMBLY

Authorship Note: This chapter is the result of a collaboration with Bradley R. Silverman, who will share first authorship on the forthcoming paper. BRS is responsible for Figure 1, and quantitative image analysis. MTK and BRS also wrote this chapter jointly.

INTRODUCTION

Bacteria and other microorganisms are often found living in complex, multispecies consortia in a wide variety of environments such as marine sediments (1), soils (2), biofilms (3), and the human gut (4). Living in a consortium affords important advantages for the member species, such as protection from toxins and antibiotics (5), cross-feeding relationships allowing more flexible utilization of nutrients (6, 7), and efficient division of labor (8). Recently, there has been a great deal of interest in the development of artificial consortia for the purposes of environmental remediation (9, 10), biofuel production (11), and construction of microbial fuel cells (12). By dividing metabolic tasks across multiple organisms, the genetic and metabolic stress placed on individual organisms can be minimized, leading to overall improved yields (13).

Imposing spatial organization on a consortium, which minimizes the transport distance of relevant intermediates, is a method that could further increase yields. Spatial organization can also be used to protect sensitive members of the consortium from environmental insult. For example, pentachlorophenol (PCP) is commonly found in sites that also contain significant concentrations of mercury (14, 15). The concentration of mercury is often high enough to kill microorganisms tasked with remediation of PCP. To remedy this, Ismagilov and co-workers used extrusion to construct a consortium of *Sphingobium chlorophenolicum* to oxidize PCP, surrounded by a protective shell of *Ralstonia metallidurans* that reduces mercury ions and enables *S. chlorophenolicum* to remain viable (16). Other techniques for organization of bacterial consortia include inkjet

printing (17) and 3D printing (18). However, all of these methods require external apparatus rather than relying entirely on genetic controls, and are more difficult to scale. Genetic control of aggregation may be preferable, as expression of proteins that mediate aggregation can be triggered *in situ* using biochemical or optogenetic stimuli (19, 20), increasing the number of environments in which such aggregates could be used.

One system for genetically-controlled bacterial assembly was reported by Fernandez and co-workers, whereby the expression of the Junβ and Fosβ leucine zippers fused to the C-terminal region of the adhesin protein EhaA of *Escherichia coli* was shown to lead to bacterial aggregation (21). Recently, our group demonstrated the selective, orthogonal, and controlled assembly of micro-particles functionalized by covalently-attached self-associating proteins (22). Here we combine the earlier work of Fernandez and co-workers with our own observations on particle assembly to direct assembly of *Escherichia coli* into aggregates of controlled size and morphology. Further, we demonstrate that genetically-controlled aggregation of bacterial cells can lead to the triggering of a quorum-sensing circuit at a population density that does not ordinarily support quorum sensing.

RESULTS AND DISCUSSION

Design of the bacterial aggregation system

To prepare bacterial aggregates, we expressed two sets of self-associating proteins on the *E. coli* cell surface, building on the autodisplay system first reported by Maurer, Jose, and Mayer (23). Since its introduction, the autodisplay system has been used to display a wide variety of proteins, including hydrolases, esterases, enzyme inhibitors, and epitopes for vaccine development (24, 25). Here we used the autotransporter system to display two pairs of cross-associating proteins, SynZip17/18, and SpyTag/SpyCatcher (sequences supplied in the supporting information). The SynZip proteins were adapted from a library of leucine zipper proteins reported by the Keating laboratory (26). SynZip17 and 18 are reported to form anti-parallel coiled-coil dimers with high (< 10 nM) affinity and cross-

association specificity. SpyTag and SpyCatcher were derived from the fibronectin-binding protein FbaB of *Staphylococcus pyogenes*, as first reported by Howarth and coworkers (27, 28). After splitting the full-length protein into two polypeptide chains, Howarth and coworkers showed that the resulting SpyTag and SpyCatcher fragments undergo spontaneous coupling via formation of an isopeptide bond between lysine residue K31 in SpyCatcher and aspartic acid residue D117 in SpyTag. These proteins have been used to control protein topology (29), crosslink protein hydrogels (30), engineer novel protein vaccines (31), and cyclize enzymes for enhanced thermal stability (32).

The expression constructs are shown in supporting information Figure S1. In each construct, the target associative domain is fused to a 6xHis tag (for immunostaining) and inserted between a PelB secretion sequence and the autotransporter. The entire construct is placed under control of a T5-Lac or araBAD promoter, to enable induction by isopropyl- β-D-1-thiogalactopyranoside (IPTG) or L-arabinose, respectively. Plasmids bearing SynZip17, SynZip18, SpyTag, or SpyCatcher, and under control of the T5-Lac promoter on a pQE80 backbone, are referred to as pAT-17, pAT-18, pAT-ST. and pAT-SC, respectively. The same protein constructs under control of an arabinose promoter on a pBAD33 backbone are referred to as pBAD-17, pBAD-18, pBAD-ST. and pBAD-SC. Expression plasmids were introduced into *E. coli* strain DH10B for aggregation experiments. Cells were co-transformed with plasmids encoding mWasabi or mCherry to allow the aggregation process to be monitored by fluorescence confocal microscopy.

Procedures for forming bacterial aggregates

Individual colonies chosen from LB plates were grown in LB medium supplemented with 100 mg/L ampicillin or 35 mg/L of chloramphenicol overnight, then used to inoculate fresh cultures at a 100:1 ratio. When the optical density (OD_{600}) reached 0.6-0.8, cultures were induced with 0.1 mM IPTG and allowed to express for 90 min. The induced cells were then mixed at 300 rpm in a shaking incubator at 37^{o}C for an additional 90 min. Aliquots were spotted on glass cover-slips for confocal imaging. Depending on the

degree of protein surface expression and nature of the associative protein, we observed aggregates ranging from 10^3 to 10^5 μm^3 in volume (see below). In some cases, aggregates were visible to the naked eye.

Control of aggregate size by control of expression levels

For many applications of bacterial clusters, the average size of the clusters is an important design parameter, and thus genetic control of the size of clusters is desirable. We hypothesized that the size of clusters is determined in part by the surface expression levels of the associative proteins expressed. To test this hypothesis, we chose to lower the expression of the associative proteins by weakening the ribosome-binding site (RBS), thereby maintaining inducible control of the aggregation, while enabling separate control of the expression levels of each associative protein.

Starting from the arabinose-inducible constructs pBAD-ST and pBAD-SC, we engineered an RBS predicted to be significantly weaker than the wild-type (33). Expression levels were quantified by immunostaining and subsequent flow cytometry (Figure 1A). We found that use of the weaker RBS led to an approximately 4-fold decrease in the surface expression of both SpyTag and SpyCatcher. All combinations of the wild-type and lower-expressing RBS constructs were then expressed in aggregation experiments and imaged (Figure 1C-F). Automated image analysis found that aggregate size was well-correlated with the measured expression levels of the associative proteins (Figure 1B).

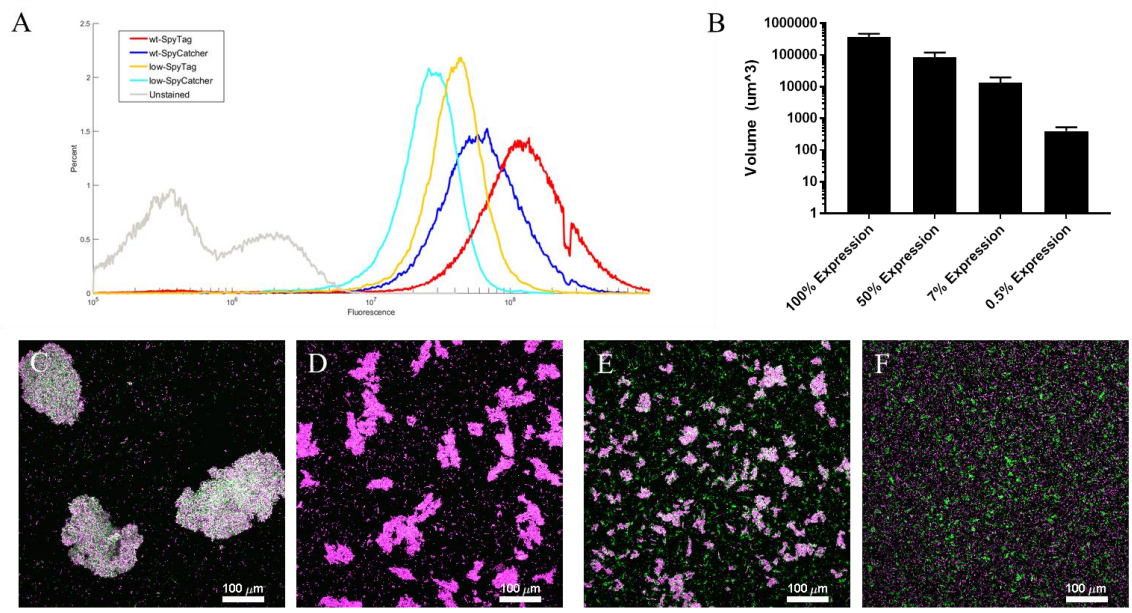

Figure 1: Expression levels control size of bacterial aggregates.

A) Flow cytometry analysis enables quantification of protein expression levels; mutant RBS's lead to an approximate 4-fold decrease in expression levels. By constructing a family of mutant ribosomal binding sites with weaker surface expression, it is possible to precisely control the size of the resulting aggregates, as quantified in panel B and as shown in micrographs C-F. Bacteria which surface-display SpyCatcher are shown in magenta, and bacteria which surface-express SpyTag are shown in green

Dissociation of bacterial aggregates

Two different principles, the physical association of SynZip leucine zippers, and the formation of covalent isopeptide bonds between SpyTag and SpyCatcher, drive cellular aggregation in the systems introduced here. We expected SynZip-mediated aggregation to be reversible in the presence of excess (soluble) competing protein, and the SpyTag/SpyCatcher aggregation to be irreversible. To test this hypothesis, SynZip 17 and SpyCatcher proteins were expressed recombinantly in *E. coli* and purified via Ni-NTA affinity chromatography using methods described in previous work (22). Aggregates mediated by the SynZip system were formed using the method described above, and then recombinant SynZip 17 was added to a final concentration of 0, 0.001, or 0.1 mg/mL in LB

medium. Three biological replicates were examined for each disaggregation condition. Representative micrographs and aggregate sizes (reported as volume-weighted averages) are shown in Figure 2. Titration of soluble SynZip17 into SynZip17/18 cultures decreased the size of the aggregates in a dose-dependent manner, consistent with the hypothesis that aggregated cells are bridged by specific biomolecular interactions.

By contrast, when soluble SpyCatcher was added to aggregates mediated by SpyTag/SpyCatcher interactions, no significant changes in aggregate size were observed, even when 1 mg/mL of protein was added. This result suggests that the clusters mediated by SpyTag and SpyCatcher are held together by covalent bonds that cannot be disrupted by introduction of a competing protein. Clusters mediated by SpyTag and SpyCatcher are also substantially larger than those mediated by reversible SynZip interactions, as these clusters are more stable to shear-induced disruption (34).

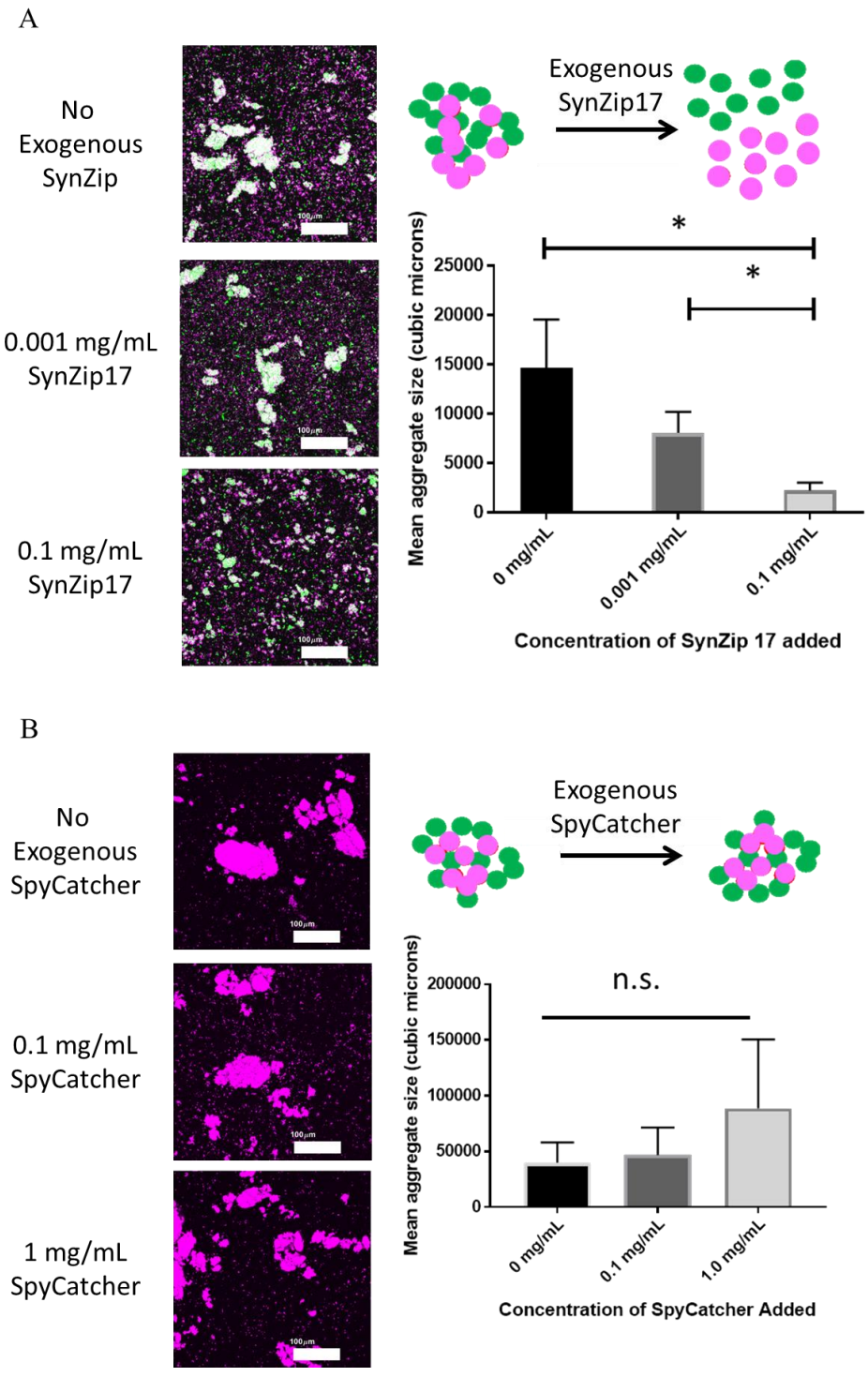

Figure 2: Dissociation and non-dissociation of bacterial aggregates by the addition of competing recombinant protein

In panel (A), various concentrations of recombinantly-expressed SynZip17 were added to aggregates formed by expression of pAT-17 and pAT-18 as-labelled. Cells expressing pAT-17 are shown in green and cells expressing pAT-18 are shown in magenta. When no soluble protein is added, the average aggregate (volume-weighted) volume is approximately 15000 μm^2. With 0.1 mg/mL of SynZip17 added, this size drops be-low 5000 cubic microns. Braces in the graph in (A) denote that the changes in aggregate size are statistically significant at the $p<0.05$ confidence interval by a one-tail Student's t-test. In contrast, in panel (B), where cells expressing pAT-ST and pAT-SC are both shown in magenta, the addition of recombinant SpyCatcher does not result in a statistically-significant change in aggregate size. All scale bars are 100 μm in length.

Formation of core-shell architectures.

Many potential applications of bacterial aggregates require protection of a member of the consortium from environmental insult. We assembled mCherry-labeled cellular "cores" by SpyTag/SpyCatcher interaction. We then added mWasabi-labeled cells that either expressed SpyCatcher or contained an empty pQE80 plasmid. After 30 min incubation, we found that cells carrying the SpyCatcher plasmid formed distinct green shells around magenta cores. No core-shell structures were observed for control cultures (Figures 3A and 3C). These structures were characterized by line profiles drawn through the centroid of aggregates. Core-shell aggregates increase in mWasabi fluorescence from the centroid to the exterior of the aggregate, while control samples exhibited no correlation between radial location and fluorescence (Figures 3B and 3D). Line profiles for individual core-shell clusters, and a 63x image of a core-shell structure, are shown in the supporting information (Figure S3).

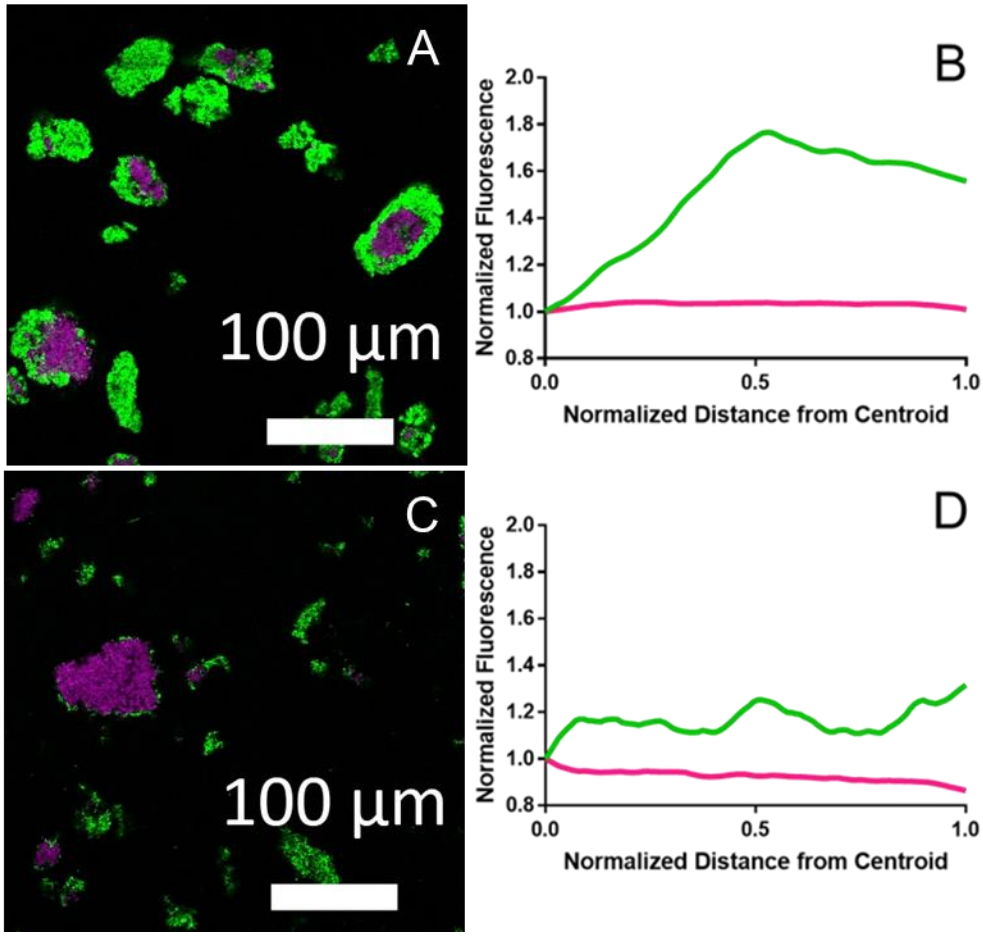

Figure 3: Formation of aggregates with a core-shell architecture

Cores of SpyTag and SpyCatcher surface-expressing bacteria, along with mCherry fluorescent marker, were made using our standard methods. Next, we added cells either expressing Spy-Catcher and mWasabi (micrograph A), or only mWasabi (micrograph C). When the DH-Green cells express pAT-SC, a green shell can be observed around the red core, as shown in micrograph A. However, DH-Green cells that have a control pQE80 plasmid rather than pAT-SC do not form this green shell. This can be quantified by constructing a line profile from the center of the core out-ward, and averaging over all aggregates in the image. If a core-shell structure is observed, we expect points further away from the centroid to be less red, and more green, as shown in graph B. If there is no core-shell structure, there should be no correlation between distance from the centroid and pixel color, as seen in graph D.

Triggering quorum-sensing in clusters

In order to demonstrate that aggregation may have physiological consequences, we investigated whether aggregation could be used to activate a quorum-sensing circuit. In particular, we chose to use the LuxI-LuxR quorum-sensing circuit derived from *Vibrio harveyi*, which has been extensively studied (35-37). The LuxR-LuxI system expresses a gene of interest when an activator protein, LuxR, binds to a small molecule signal, N-(3-oxohexanoyl)-homoserine lactone (AHL), the concentration of which is correlated to the density of bacterial cells. We anticipated that by aggregating bacteria, we would artificially increase the local concentration of AHL, and so trigger a quorum sensing response.

To allow co-transformation of quorum-sensing and aggregation plasmids, we chromosomally integrated mCherry under control of a T5 promoter in DH10B *E. coli* using the "Clonetegration" system described by Shearwin and coworkers (39). Our quorum-sensing system was a modification of pLuxRI2, which was a generous gift of the laboratory of Frances Arnold (40). The quorum sensing circuit is shown in Figure 4. Briefly, the acyl-homoserine-lactone synthetase LuxI along with LuxR were expressed under constitutive control. In order to obtain positive feedback, LuxI was also expressed under a pLuxI promoter, along with an mWasabi reporter gene. This circuit was co-transformed with the aggregation system. Initially, no difference could be observed in quorum-sensing response when comparing cells that were aggregated with cells that were grown without aggregation (data not shown). We attributed this to over-sensitivity of the quorum-sensing circuit. By introducing a mutation into the P_{luxI} promoter, and using a weaker constitutive promoter to drive expression of the LuxI synthetase, we were able to tune the quorum sensing circuit such that cells in stationary phase did not demonstrate a quorum-sensing response unless additional exogenous AHL was added (see Supporting Information Figures S4 and S5).

Cells containing the modified quorum-sensing circuit were grown to mid-log phase (OD≈0.2), and this culture was then split into three. One of these cultures was induced with 0.2% arabinose, the other was left uninduced, and the third had 2 mM AHL added as a positive control: this experimental scheme is outlined in Figure 4. After 1 H, aggregates formed in the induced culture, but not in the uninduced culture. Aliquots were taken of the induced and uninduced cultures 75 min after induction, and the results are shown in Figure 5.

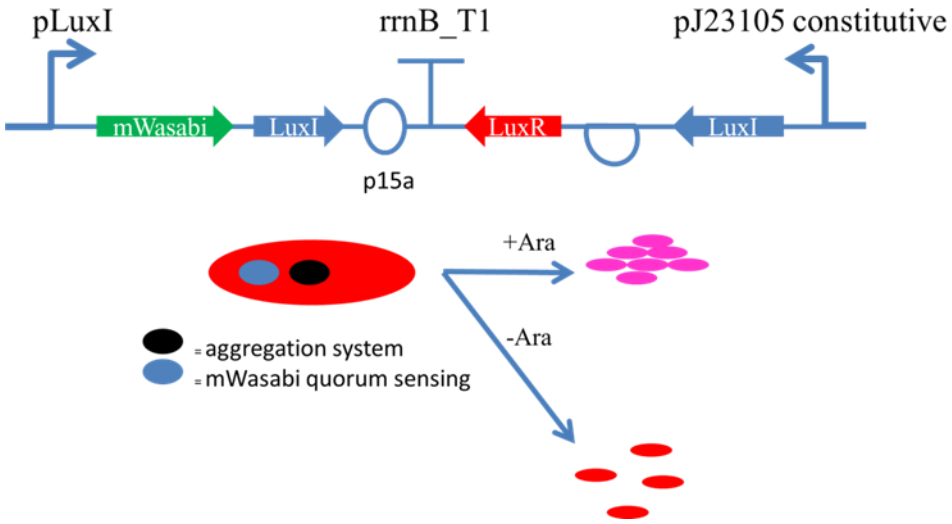

Figure 4: Illustration of quorum-sensing circuit, and our experimental scheme

In the quorum-sensing circuit (top), the activator protein LuxR and acyl homoserine lactone (AHL) synthetase LuxI are driven by a constitutive promoter. When a sufficient concentration of AHL is present, LuxR is activated, binds to the pLuxI promoter, and recruits RNA polymerase, leading to expression of mWasabi as well as additional copies of LuxI, thus generating a positive-feedback loop). The *E. coli* strain has an integrated, constitutively-expressing mCherry cassette for confocal imaging. In our scheme, upon aggregation, quorum sensing is activated, leading to the joint expression of mWasabi and mCherry (represented by pink cells). However, without induction of aggregation, the cells do not express mWasabi and express only mCherry.

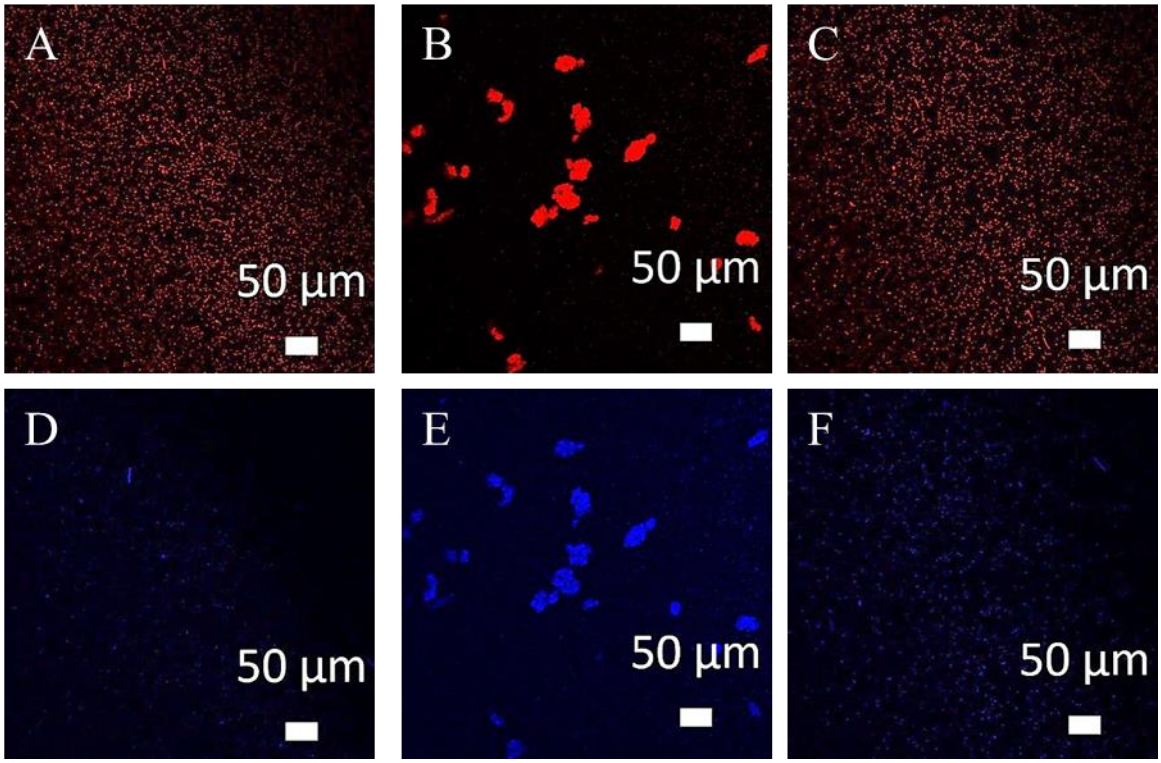

Figure 5: Aggregation leads to more-rapid activation of a quorum-sensing circuit

In this figure we demonstrate the activation of a quorum-sensing circuit by aggregation. Micrographs A-C show a red signal indicative of the presence of a cell which is constitutively expressing mCherry (the DHred strain). Micrographs D-F show a signal indicative of the expression of mWasabi, whose expression is dependent upon the activation of a quorum-sensing circuit. The mWasabi signal has been false-colored blue for clarity. DHred cells containing either pBAD-ST or pBAD-SC were grown for 2 hours, then the culture was split into 3 different conditions. One condition remained uninduced and was imaged 75 min later, which resulted in very little mWasabi signal (micrographs A and D). A second condition was induced with L-arabinose, which led to aggregation and observable quorum sensing (micrographs B and E). The third condition consisted of adding 2mM AHL to the cells as a positive control. Some quorum-sensing signal was observed after 75 minutes (micrographs C and F). All presented images represent a single section of a 3D confocal Z-stack at 20x magnification.

In this experiment, the mCherry signal from the cassette integrated in KY36 serves as a cell marker, and the mWasabi signal serves as a marker for the activation of a quorum sensing circuit. The mWasabi signal is false-colored blue for clarity. As shown in Figure 5, the aggregated sample appears to have more cells that are expressing mWasabi. To quantify this observation, we determined the Manders overlap coefficients (MOC) between red and blue signals, which represents the percentage of cells that have activated their quorum-sensing circuits. At 75 min after induction, we find the MOC of the induced, aggregated sample is 0.244, while the uninduced sample MOC is 0.022, as shown in Figure 6. We interpret this to mean that in the aggregated case, approximately 24% of cells display quorum-sensing behavior, whereas in the uninduced case, only 2% of the cells are quorum-sensing. This suggests a substantial increase in quorum sensing can be observed by aggregating cells. Interestingly, the addition of exogenous AHL resulted in a MOC of 0.065, suggesting that aggregation resulted in a greater enhancement of quorum sensing than the addition of a large amount of exogenous inducer.

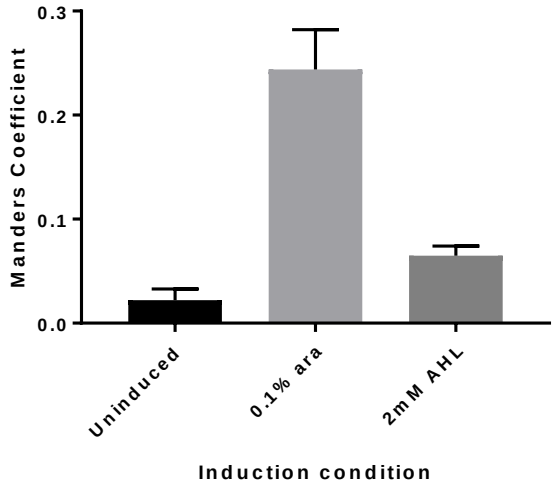

Figure 6: Aggregation leads to more-rapid activation of a quorum-sensing circuit

Approximately 2% of uninduced cells show a quorum-sensing response, whereas 24% of cells that have aggregated show a quorum-sensing response, a 12-fold difference that is statistically-significant ($p=0.003$, using a one-tailed Student's t-test). Notably, in these experiments only 6.5% of cells induced with 2mM AHL show a quorum-sensing response.

CONCLUSIONS

We have successfully demonstrated methods by which the size and architecture of bacterial aggregates can be controlled in a genetically-programmable manner. By choosing the appropriate associative protein, we can control the reversibility of aggregation; while by controlling the surface expression levels of the associative proteins we can control the resulting size of aggregates. We have further demonstrated the construction of a core-shell architecture which may be useful in protecting sensitive bacteria from environmental insult or for creating complex biocatalysts. This work therefore represents an important step towards recapitulating the complex structures exhibited by natural microbial consortia, as well as a method by which cellular behavior can be made dependent on aggregation state through the use of a quorum sensing circuit (41).

Methods developed in this work may enable the production of structured whole-cell biocatalysts, whereby multi-step reactions may be performed in series in bacterial aggregates, enabling enhanced intermediate channeling between cells in a manner complementary to previous work for substrate channeling within cells (42, 43). Particularly where biosynthetic steps may be difficult or impossible to place in the same cell, performing these steps in aggregates will enable channeling between metabolic steps without dilution into the bulk solution phase. Triggering of quorum sensing may play an important role here, as in order to minimize off-target reactivity, enzyme expression can be efficiently linked to aggregation.

We believe that the methods developed in this work are broadly applicable to other species of microbes and extendible to other types of protein-association domains. All that is required is an effective method of cell-surface display of the appropriate associative domain in the bacterial species of interest. In this manner, multi-species consortia of

microbes may be established. Finally, similar techniques have recently been used for programmable surface binding (19) and may similarly be used for immobilization into protein hydrogels to form artificial biofilms..

METHODS

Bacterial strains

All experiments were conducted in *E. coli* strain DH10B, obtained from Invitrogen (Carlsbad, CA). Aggregation experiments were initially conducted in DH10B. Aggregation for quorum sensing was conducted in *E. coli* strain KY36 which contained a chromosomally-integrated mCherry under control of a leaky LacI promoter.

Other experimental details of cloning and protein expression are supplied in the supporting information.

Image Acquisition and Analysis

Microscopy images were taken on a Zeiss 800 LSM inverted confocal microscope (Carl Zeiss AG, Oberkochen, Germany).

All image analysis was performed using custom Matlab scripts.

Aggregate size analysis was performed similarly to what we described previously.(22) Briefly, confocal z-stacks were manually thresholded based on the intensity in each fluorescent channel. Pixels above the threshold were described as “bright.” Contiguous “bright” pixels (in 3D) were identified, and the observed volume of each aggregate was determined. The volume-weighted average volume of each aggregate was determined using the following equation:

$$\bar{V} = \frac{\sum V_i^2}{\sum V_i}$$

where sums are taken over all of the aggregate volumes. This average represents the volume of the aggregate that the average bacterium would be found in, and is more appropriate than the number-weighted average, which is dominated by disassociated bacteria.

Core-shell fluorescence profiles were created as described previously (22). Maximum intensity projections of the images were taken, and large aggregates were identified using thresholding. For each large aggregate, z-stacks with high levels of fluorescence were combined into a mean intensity projection. Then, starting at the centroid of the mean intensity projection, 100 radii representing equally spaced direction vectors were drawn to the edge of the aggregate, extracting the fluorescence intensities of each channel. Fluorescence intensities were scaled in each channel (with the maximum intensity in the aggregate being 1), and plotted along a radial axis where 0 represents the centroid and 1 represents the edge of the aggregate.

Manders overlap coefficients (MOCs) were calculated via the equations:

$$M_{red} = \frac{\sum R_i G_i}{\sum R_i}$$

$$M_{blue} = \frac{\sum B_i G_i}{\sum B_i}$$

where sums are taken over all pixels and R_i,G_i, and B_i are equal to 1 if the red, green, or blue channel respectively is "bright." Thus M_{red} represents the proportion of red pixels that are also green, and M_{blue} represents the proportion of blue pixels that are also green. Thresholds were determined initially manually, but due to the strong dependence of MOCs on threshold values, were confirmed to be robust to changes (+/- 20%) in value.

All image analysis code can be downloaded at https://tirrell-lab.caltech.edu/code

Flow cytometry

Measurement of surface expression levels was done using direct immunocytochemistry and flow cytometry. Overnight cultures of autotransporters were diluted 100x, and were grown to an optical density of approximately 0.6 prior to induction with 0.1% L-Arabinose. Expression was allowed to proceed for 90 min, after which the culture was centrifuged and blocked for 30 min with agitation (3% BSA in PBS). Cells were then centrifuged and resuspended in staining solution (5 µg/mL Anti-His conjugated Alexa-Fluor 488 Antibody (HIS.H8 Thermofisher), 1% BSA in PBS). This solution was then agitated for 1 H, after which the cells were washed three times in PBS. Cells were strained through a 40 µm filter to remove aggregates and run on a MoFlo XDP cell sorter equipped with a 488 nm laser. Flow cytometry data were analyzed using EasyFlow (44).

Quorum sensing

N-(β-ketocaproyl)-DL-homoserine lactone (synonymous with N-(3-oxohexanoyl)-homoserine lactone) was purchased from MilliporeSigma (Milwaukee, WI) and used as received.

Characterization of quorum sensing in bulk samples was done on a VarioSkan LUX instrument (ThermoFisher, San Diego CA). Overnight cultures of pMTK1, pMTK2, and pMTK3 were grown in LB medium supplemented with 35 mg/L chloramphenicol. The overnight cultures were then used to inoculate 150 µL cultures at a ratio of 100:1 in flat-bottomed, clear 96 well plates with a lid (BD Falcon, Corning Inc, Corning, NY). The cultures then had varying amounts of AHL added (0-2 mM), and the plate was incubated, with shaking, at 37 degrees for 18 H. OD600 as well as mWasabi fluorescence (ex. 485 em. 515) was measured every 10 min. The results of this characterization are presented in the supporting information.

SUPPORTING INFORMATION FOR CHAPTER 3

General

Restriction enzymes, ligase, and Q5 DNA polymerase were purchased from New England Biolabs (Beverly, NJ). Nickel NTA was purchased from Qiagen (Hilden, Germany). DNA oligos and G-blocks were purchased from Integrated DNA Technologies (Coralville, IA).

Cloning of plasmids for recombinant protein expression, protein surface display, and quorum sensing.

Recombinant fusion proteins were produced by standard recombinant DNA technology. DH10b or Mach1 Escherichia coli were used for all cloning steps.

Genes encoding soluble Z17 and SpyCatcher proteins along with elastin solubility/stability tags have been previously cloned by our group into modified pQE-80L plasmids (1).

Plasmids kPY680 and kPY681, which constitutively express mWasabi and mCherry, respectively, were constructed using mWasabi-N1/pmCherry-N1 as the template. Primers were ordered to amplify mWasabi/mCherry as well as add NsiI-J23100 promoter-SpeI-RBS-MRGS-6xHis to the 5’ end of mWasabi/mCherry, and to add HindIII to the 3’ end. This fragment was inserted into pBAD33 using endogenous NsiI and HindII sites.

To make the surface-expression construct, the autotransporter domain downstream of the pelB leader sequence was removed from pHEA by PCR using a PhusionII polymerase (NEB) and the primers listed below. The primers added a XhoI and HindIII site to the autotransporter construct, which was then digested and inserted into a modified pQE-80L plasmid. Another G-block was ordered with EcoRI and XhoI sites that contained the T5 promoter, pelB, a 6xHis tag, and the protein of interest (SpyTag, SpyCatcher, SynZip17, SynZip18). No restriction sites were ablated, and a schematic of the autotransporter cloning is shown below.

The autotransporter constructs were also placed under the araBAD promoter to enable orthogonal control of different aggregation systems. The autotransporter-associative domain fusions were shuttled into the MCS of pBAD33 using Gibson isothermal assembly.

The RBS mutant constructs were obtained from the pBAD33-based aggregation constructs by site-directed mutagenesis.

Plasmid pLuxRI2 was a generous gift from the lab of Prof. Frances Arnold. To make plasmid construct pMTK1, we first replaced the pLac/Ara1 promoter in that plasmid with a constitutive pJ23105 promoter, which is listed in the Registry of Standard Biological Parts. A DNA duplex containing the reverse complement of the pJ23105 promoter, and EcoRI and XhoI sites on the 5' and 3' ends respectively, was ordered from IDT and inserted into pLuxRI2 following digestion with EcoRI and XhoI. The second modification required was the insertion of the quorum sensing cassette consisting of mWasabi and an additional copy of LuxI synthetase under the control of the PluxI promoter, as well as a p15a origin. This cassette was supplied by a gBlock gene fragment ordered from IDT, and contained restriction sites for SacI and AvrII on the 5' and 3' ends respectively. Plasmid pLuxRI2 was then digested with SacI and AvrII, allowing for the insertion of the gBlock fragment.

Fluorescent proteins were chromosomally integrated using the pOSIP clonetegration system (2). Genes encoding mWasabi and mCherry under the control of the T5 promoter were PCR amplified and assembled into pOSIP-KO (Addgene). Z-competent *E. coli* MegaX DH10B T1R cells were mixed with the unpurified assembly reaction and spread on 2xYT agar plates supplemented with 35 mg/L kanamycin sulfate.

Expression of soluble SynZip and SpyCatcher proteins

Constructs were transformed into BL21 *E. coli* for expression. Expression was performed in Terrific Broth (12 g/L casein, 24 g/L yeast extract, 0.4% w/v glycerol, 0.017 M monobasic potassium phosphate, 0.072 M dibasic potassium phosphate). Cultures were induced at an optical density of 0.6-0.9 to a final concentration of 1 mM isopropyl β-D-1-

thiogalactopyranoside (IPTG). Expression was allowed to proceed for 5 H, after which cells were harvested by centrifugation. For Z17 purification, cultures were resuspended in lysis buffer in denaturing lysis buffer (8 M urea, 0.1 M Na_2HPO_4, 10 mM imidazole; pH 8.0), and lysed by sonication. Lysates were cleared by centrifugation, and incubated with NiNTA. The resin was washed with lysis buffer, wash buffer (8 M urea, 0.1 M Na2HPO4, 25 mM imidazole; pH 6.3). Protein was eluted with elution buffer (8 M urea, 0.1 M Na_2HPO_4, 250 mM imidazole; pH 3.5). Purity was confirmed with SDS-PAGE. Proteins were then extensively dialyzed against water and lyophilized for storage.

SpyCatcher was purified under native conditions. Cultures were resuspended in native lysis buffer (50 mM NaH2PO4, 300 mM NaCl, 10 mM imidazole, 1 mg/mL lysozyme; pH 8.0). Cells were lysed by sonication, and cleared lysates were incubated with NiNTA. The resin was washed with native wash buffer (50 mM NaH_2PO_4, 300 mM NaCl, 25 mM imidazole; pH 8.0), and eluted with native elution buffer (50 mM NaH_2PO_4, 300 mM NaCl, 250 mM imidazole; pH 8.0). Purity was confirmed with SDS-PAGE, and purified SpyCatcher was dialyzed against water, and lyophilized.

Plasmid maps and protein sequences

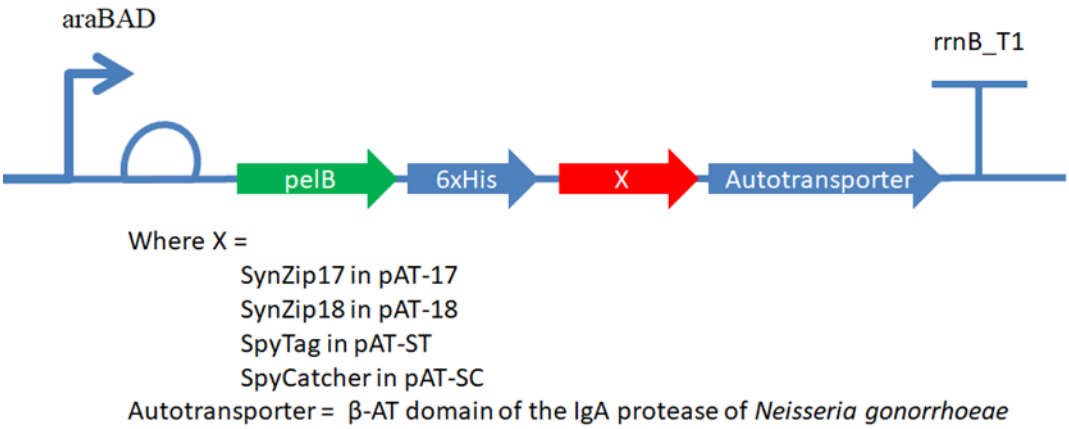

Figure S1: Schematic of aggregation plasmids

Under the control of an araBAD promoter on a ColE1 plasmid, there is a signalling sequence pelB and a 6xHistidine tag upstream of protein of interest X, where X represents a self-associating protein domain. On the C-terminal end is the C-terminal domain of the adhesin protein EhaA of *Escherichia coli*. The entire ensemble is expressed as a translational fusion, and leads to the surface expression of the protein of interest.

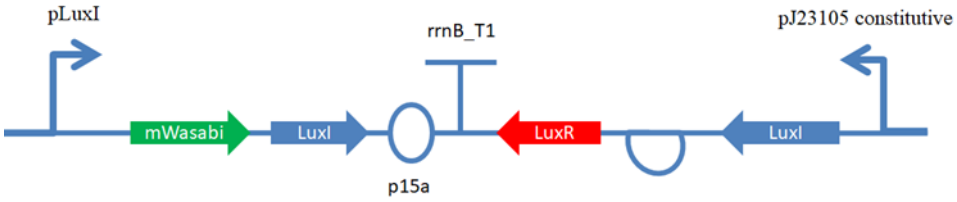

Figure S2: Schematic of quorum-sensing plasmid

On a plasmid with a p15a origin (to ensure compatibility with the aggregation plasmid on a ColE1 backbone), we have a LuxR activator protein and LuxI AHL synthetase under the control of a pJ23105 constitutive promoter. The LuxR protein, in the presence of a sufficient concentration of AHL, binds to the pLuxI promoter driving expression of mWasabi and an additional copy of LuxI AHL synthetase.

Table S1: Plasmids used in this study

Name	Backbone/origin/promoter	Purpose
kPY680	pBAD33/p15a/pJ23100	Constitutive expression of mWasabi
kPY681	pBAD33/p15a/pJ23100	Constitutive expression of mCherry
pAT-17	pQE80/colE1/T5	IPTG-inducible expression of SynZip 17
pAT-18	pQE80/colE1/T5	IPTG-inducible expression of SynZip 18
pAT-ST	pQE80/colE1/T5	IPTG-inducible expression of SpyTag
pAT-SC	pQE80/colE1/T5	IPTG-inducible expression of SpyCatcher
pBAT-17	pQE60/colE1/araBAD	Arabinose-inducible expression of SynZip 17 and compatibility with pMTK1-3
pBAT-18	pQE60/colE1/araBAD	Arabinose-inducible expression of SynZip 18 and compatibility with pMTK1-3
pBAT-ST	pQE60/colE1/araBAD	Arabinose-inducible expression of SpyTag and compatibility with pMTK1-3
pBAT-SC	pQE60/colE1/araBAD	Arabinose-inducible expression of SpyCatcher and compatibility with pMTK1-3
pBAD-ST	pBAD33/p15a/araBAD	Arabinose-inducible expression of SpyTag
pBAD-SC	pBAD33/p15a/araBAD	Arabinose-inducible

		expression of SpyCatcher
pMTK1	pHTSUB-105/p15a/luxI	"wild-type" quorum sensing
pMTK2	pHTSUB-105/p15a/luxI	Less-sensitive quorum sensing plasmid.
pMTK3	pHTSUB-105/p15a/luxI	Less-sensitive quorum sensing plasmid.

Table S2: Protein Sequences

Protein:	Sequence
Z17 (soluble)	MRGSHHHHHHGSVDGSGSGSGSGSGANEKEELKSKK AELRNRIEQLKQKREQLKQKIANLRKEIEAYKGSGSG SGSGSGALDVPGAGVPGAGVPGEGVPGAGVPGAGVP GAGVPGAGVPGEGVPGAGVPGAGVPGAGVPGAGVP GEGVPGAGVPGAGLDVPGAGVPGAGVPGEGVPGAG VPGAGVPGAGVPGAGVPGEGVPGAGVPGAGVPGAG VPGAGVPGEGVPGAGVPGAGLEHHHHHHKLC
SpyCatcher (soluble)	MRGSHHHHHHGSVDGSGSGSGSGSGAAMVDTLSGLS SEQGQSGDMTIEEDSATHIKFSKRDEDGKELAGATME LRDSSGKTISTWISDGQVKDFYLYPGKYTFVETAAPD GYEVATAITFTVNEQGQVTVNGKATKGDAHIDGSGS GSGSGSGALDVPGAGVPGAGVPGEGVPGAGVPGAGV PGAGVPGAGVPGEGVPGAGVPGAGVPGAGVPGAGV PGEGVPGAGVPGAGLDVPGAGVPGAGVPGEGVPGAG VPGAGVPGAGVPGAGVPGEGVPGAGVPGAGVPGAG VPGAGVPGEGVPGAGVPGAGLEHHHHHHKLC
SpyCatcher-Autotransporter	MKYLLPTAAAGLLLLAAQPAMAMRGSHHHHHHGSV DGAMVDTLSGLSSEQGQSGDMTIEEDSATHIKFSKRD EDGKELAGATMELRDSSGKTISTWISDGQVKDFYLYP GKYTFVETAAPDGYEVATAITFTVNEQGQVTVNGKA TKGDAHIDLETPTPGPDLNVDNDLRPEAGSYIANLAA ANTMFTTRLHERLGNTYYTDMVTGEQKQTTMWMRH EGGHNKWRDGSGQLKTQSNRYVLQLGGDVAQWSQ NGSDRWHVGVMAGYGNSDSKTISSRTGYRAKASVN

	GYSTGLYATWYADDESRNGAYLDSWAQYSWFDNTV KGDDLQSESYKSKGFTASLEAGYKHKLAEFNGSQGT RNEWYVQPQAQVTWMGVKADKHRESNGTLVHSNG DGNVQTRLGVKTWLKSHHKMDDGKSREFQPFVEVN WLHNSKDFSTSMDGVSVTQDGARNIAEIKTGVEGQL NANLNVWGNVGVQVADRGYNDTSAMVGIKWQF
SpyTag-Autotransporter	MKYLLPTAAAGLLLLAAQPAMAMRGSHHHHHHGSV DAHIVMVDAYKPTKLDVPGAGVPGAGVPGEGVPGA GVPGAGVPGAGVPGAGVPGEGVPGAGVPGAGVPGA GVPGAGVPGEGVPGAGVPGAGLDVPGAGVPGAGVP GEGVPGAGVPGAGVPGAGVPGAGVPGEGVPGAGVP GAGVPGAGVPGAGVPGEGVPGAGVPGAGLETPTPGP DLNVDNDLRPEAGSYIANLAAANTMFTTRLHERLGN TYYTDMVTGEQKQTTMWMRHEGGHNKWRDGSGQL KTQSNRYVLQLGGDVAQWSQNGSDRWHVGVMAGY GNSDSKTISSRTGYRAKASVNGYSTGLYATWYADDE SRNGAYLDSWAQYSWFDNTVKGDDLQSESYKSKGFT ASLEAGYKHKLAEFNGSQGTRNEWYVQPQAQVTWM GVKADKHRESNGTLVHSNGDGNVQTRLGVKTWLKS HHKMDDGKSREFQPFVEVNWLHNSKDFSTSMDGVS VTQDGARNIAEIKTGVEGQLNANLNVWGNVGVQVA DRGYNDTSAMVGIKWQF
Z17-Autotransporter	MKYLLPTAAAGLLLLAAQPAMAMRGSHHHHHHGSV DGSGSGSGSGSGSNEKEELKSKKAELRNRIEQLKQKR EQLKQKIANLRKEIEAYKGSGSGSGSGSGSLETPTPGP DLNVDNDLRPEAGSYIANLAAANTMFTTRLHERLGN TYYTDMVTGEQKQTTMWMRHEGGHNKWRDGSGQL KTQSNRYVLQLGGDVAQWSQNGSDRWHVGVMAGY GNSDSKTISSRTGYRAKASVNGYSTGLYATWYADDE SRNGAYLDSWAQYSWFDNTVKGDDLQSESYKSKGFT ASLEAGYKHKLAEFNGSQGTRNEWYVQPQAQVTWM GVKADKHRESNGTLVHSNGDGNVQTRLGVKTWLKS HHKMDDGKSREFQPFVEVNWLHNSKDFSTSMDGVS VTQDGARNIAEIKTGVEGQLNANLNVWGNVGVQVA DRGYNDTSAMVGIKWQF
Z18-Autotransporter	MKYLLPTAAAGLLLLAAQPAMAMRGSHHHHHHGSV DGSGSGSGSGSGSSIAATLENDLARLENENARLEKDIA NLERDLAKLEREEAYFGSGSGSGSGSGSLETPTPGPDL NVDNDLRPEAGSYIANLAAANTMFTTRLHERLGNTY YTDMVTGEQKQTTMWMRHEGGHNKWRDGSGQLKT QSNRYVLQLGGDVAQWSQNGSDRWHVGVMAGYGN SDSKTISSRTGYRAKASVNGYSTGLYATWYADDESR NGAYLDSWAQYSWFDNTVKGDDLQSESYKSKGFTA SLEAGYKHKLAEFNGSQGTRNEWYVQPQAQVTWMG

	VKADKHRESNGTLVHSNGDGNVQTRLGVKTWLKSH HKMDDGKSREFQPFVEVNWLHNSKDFSTSMDGVSVT QDGARNIAEIKTGVEGQLNANLNVWGNVGVQVADR GYNDTSAMVGIKWQF

Individual core-shell images

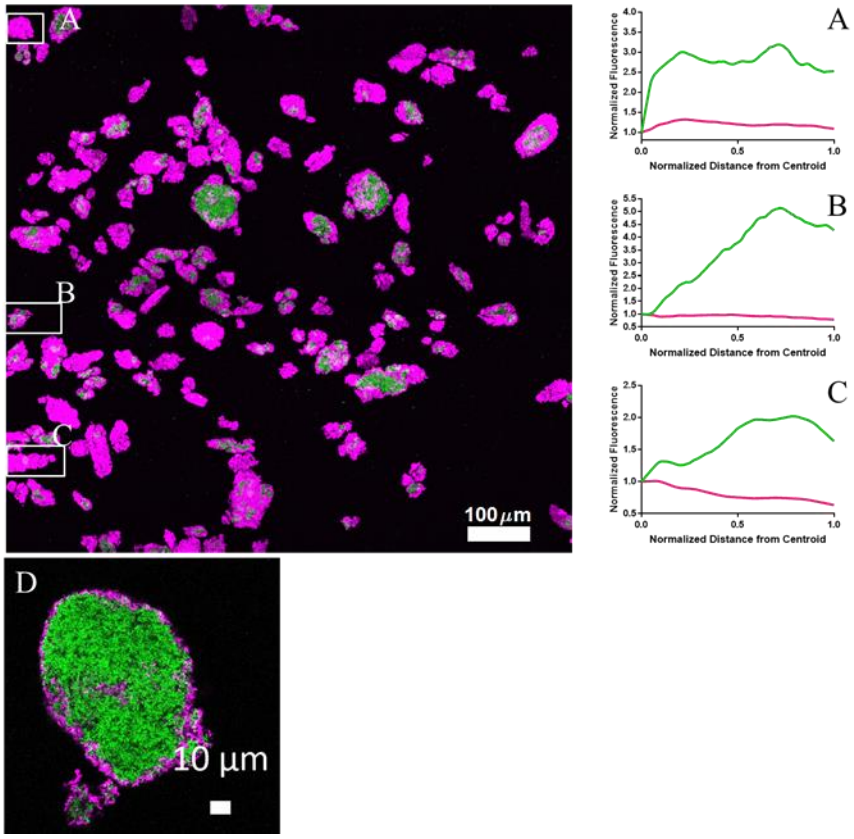

Figure S3: Individual line plots of core-shell structure

In this figure we illustrate the line profiles generated for individual clusters A, B, and C (as outlined in boxes in main image, and line profiles in the right-hand panel). In micrograph D, we also show an individual core-shell structure taken at 63x magnification.

Confirmation of quorum sensing activity of pMTK1

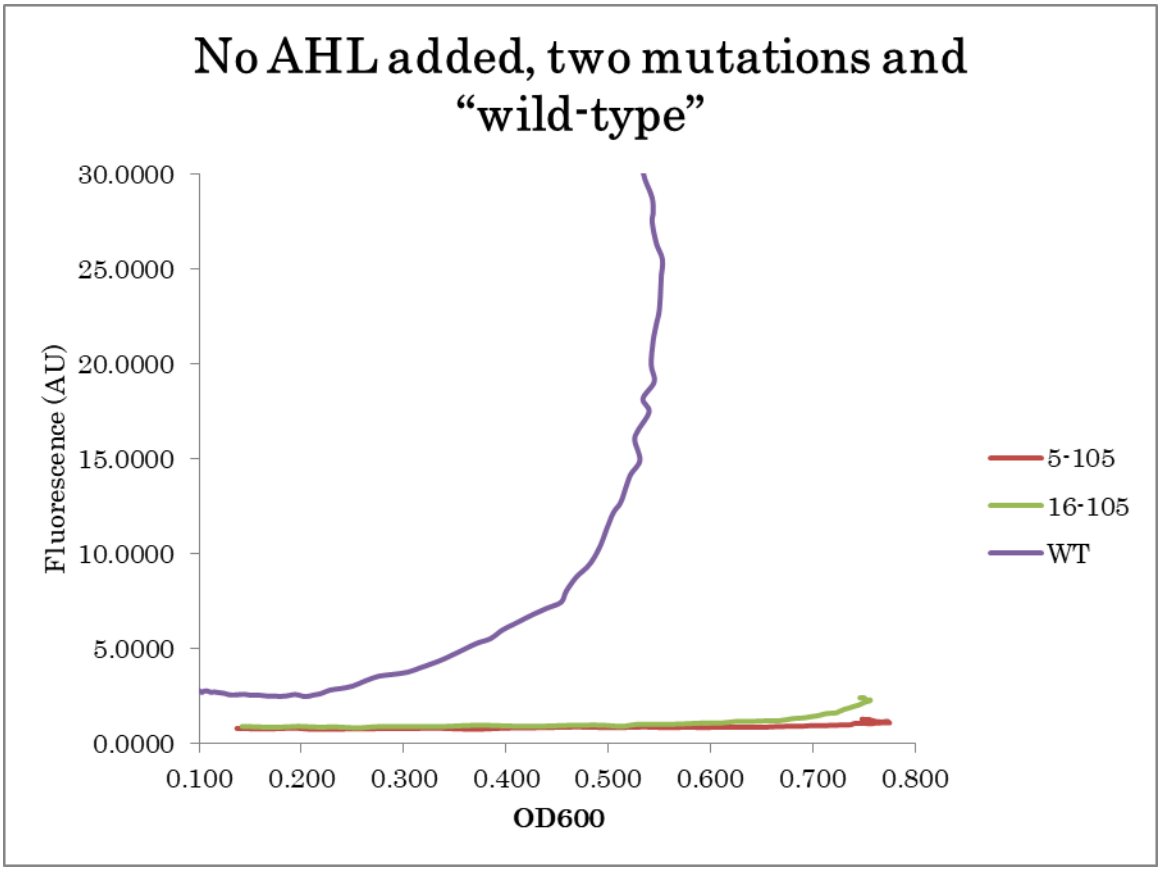

Figure S4: Characterization of "wild-type" and mutant quorum-sensing constructs.

We determined that the wild-type quorum-sensing construct gave a strong fluorescent signal at an OD of approximately 0.4. As the quorum sensing circuit was already quite sensitive to a low population of cells, we were concerned that aggregation would not make a significant difference in the speed of its activation. We decided to systematically reduce the sensitivity of the quorum-sensing circuit to AHL, using point mutations identified in Antunes et al. In particular, mutations to the quorum-sensing promoter (Lux box) C5A and C16A were made, measured, and noted to effectively abolish quorum-sensing response even at high ODs (see Red and Green traces). Fluorescence and OD600 were measured on a plate reader, with readings taken every 10 min.

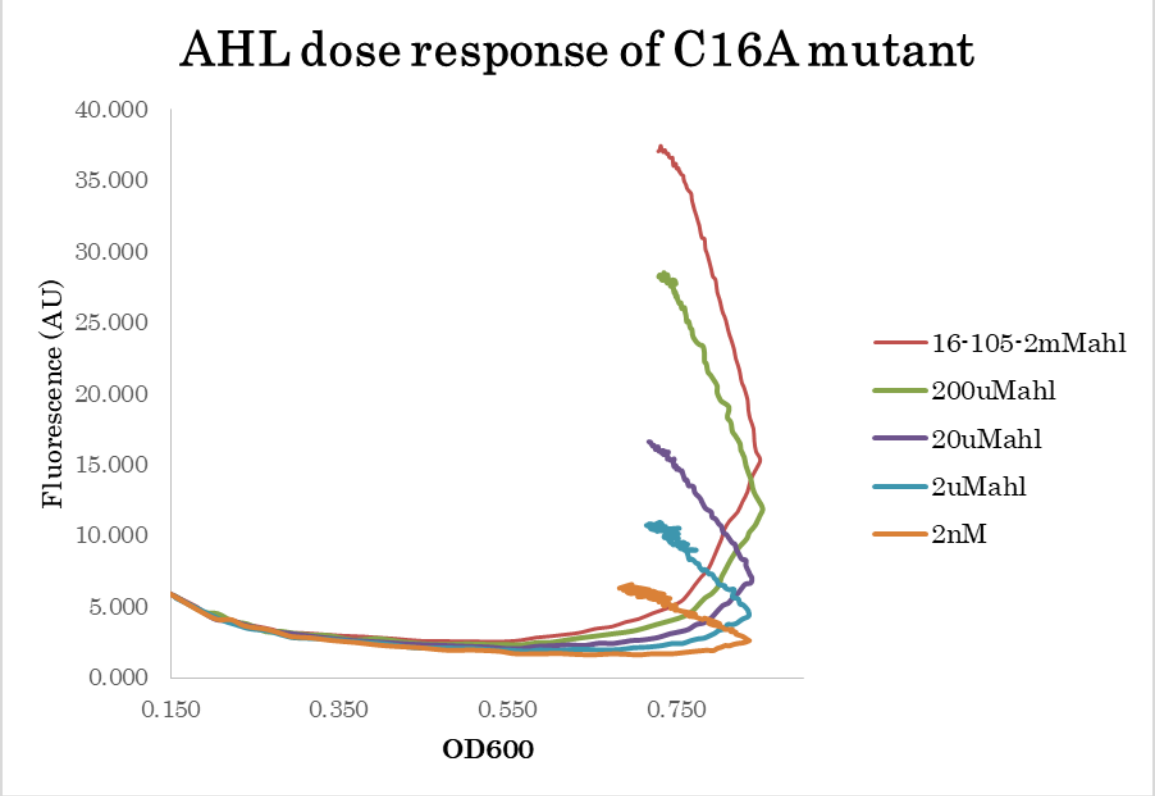

Figure S5: Acyl homoserine lactone (AHL) response of the Mut16 variety of the quorum-sensing construct

Having established in Figure S3 that quorum sensing is nearly abolished in the Mut16 variety of our quorum-sensing circuit, we wanted to confirm that the addition of a large concentration of AHL would lead to a fluorescent response. Adding 2mM AHL leads to a 10-fold increase in fluorescence, and therefore the system is still responsive to large quantities of AHL.

REFERENCES FOR SUPPORTING INFORMATION TO CH. 3

1. Obana M, Silverman BR, & Tirrell DA (2017) Protein-Mediated Colloidal Assembly. *J. Am. Chem. Soc.* 139(40):14251-14256.
2. St-Pierre F, *et al.* (2013) One-Step Cloning and Chromosomal Integration of DNA. *ACS Synth. Biol.* 2(9):537-541.
3. Deen WM (2011) *Analysis of Transport Phenomena* (Oxford University Press) p 688.
4. Suel GM, Garcia-Ojalvo J, Liberman LM, & Elowitz MB (2006) An excitable gene regulatory circuit induces transient cellular differentiation. *Nature* 440(7083):545-550.
5. Rai N, *et al.* (2012) Prediction by Promoter Logic in Bacterial Quorum Sensing. *PLoS Comput. Biol.* 8(1):14.
6. Thiele EW (1939) Relation between catalytic activity and size of particle. *Industrial and Engineering Chemistry* 31:916-920.

REFERENCES FOR CHAPTER 3

1. Boetius A, *et al.* (2000) A marine microbial consortium apparently mediating anaerobic oxidation of methane. *Nature* 407(6804):623-626.
2. van der Heijden MGA, Bardgett RD, & van Straalen NM (2008) The unseen majority: soil microbes as drivers of plant diversity and productivity in terrestrial ecosystems. *Ecol. Lett.* 11(3):296-310.
3. Burmolle M, *et al.* (2006) Enhanced biofilm formation and increased resistance to antimicrobial agents and bacterial invasion are caused by synergistic interactions in multispecies biofilms. *Appl. Environ. Microbiol.* 72(6):3916-3923.
4. Wiles TJ, *et al.* (2016) Host Gut Motility Promotes Competitive Exclusion within a Model Intestinal Microbiota. *PLoS. Biol.* 14(7):24.
5. Perez AC, *et al.* (2014) Residence of Streptococcus pneumoniae and Moraxella catarrhalis within polymicrobial biofilm promotes antibiotic resistance and bacterial persistence. *Pathog. Dis.* 70(3):280-288.
6. Liu ZF, *et al.* (2013) Genomic analysis reveals key aspects of prokaryotic symbiosis in the phototrophic consortium "Chlorochromatium aggregatum". *Genome Biol.* 14(11):16.
7. Cerqueda-Garcia D, Martinez-Castilla LP, Falcon LI, & Delaye L (2014) Metabolic analysis of Chlorobium chlorochromatii CaD3 reveals clues of the symbiosis in 'Chlorochromatium aggregatum'. *Isme J.* 8(5):991-998.
8. Hays SG, Patrick WG, Ziesack M, Oxman N, & Silver PA (2015) Better together: engineering and application of microbial symbioses. *Curr. Opin. Biotechnol.* 36:40-49.
9. Gieg LM, Fowler SJ, & Berdugo-Clavijo C (2014) Syntrophic biodegradation of hydrocarbon contaminants. *Curr. Opin. Biotechnol.* 27:21-29.
10. Antoniou E, Fodelianakis S, Korkakaki E, & Kalogerakis N (2015) Biosurfactant production from marine hydrocarbon-degrading consortia and pure bacterial strains using crude oil as carbon source. *Front. Microbiol.* 6:14.
11. Du R, *et al.* (2015) Cellulosic ethanol production by natural bacterial consortia is enhanced by Pseudoxanthomonas taiwanensis. *Biotechnol. Biofuels* 8:10.
12. Bourdakos N, Marsili E, & Mahadevan R (2014) A Defined Co-Culture of Geobacter Sulfurreducens and Escherichia Coli in a Membrane-Less Microbial Fuel Cell. *Biotechnology and Bioengineering* 111(4):709-718.
13. Brenner K, You LC, & Arnold FH (2008) Engineering microbial consortia: a new frontier in synthetic biology. *Trends Biotechnol.* 26(9):483-489.
14. Liao PY, Liu CW, & Liu WY (2016) Bioaccumulation of mercury and polychlorinated dibenzo-p-dioxins and dibenzofurans in salty water organisms. *Environ. Monit. Assess.* 188(1):15.
15. Chang JW, *et al.* (2011) Simultaneous exposure of non-diabetics to high levels of dioxins and mercury increases their risk of insulin resistance. *J. Hazard. Mater.* 185(2-3):749-755.

16. Kim HJ, Du WB, & Ismagilov RF (2011) Complex function by design using spatially pre-structured synthetic microbial communities: degradation of pentachlorophenol in the presence of Hg(II). *Integr. Biol.* 3(2):126-133.
17. Drachuk I, *et al.* (2015) Printed Dual Cell Arrays for Multiplexed Sensing. *ACS Biomater. Sci. Eng.* 1(5):287-294.
18. Murray JL, Connell JL, Stacy A, Turner KH, & Whiteley M (2014) Mechanisms of Synergy in Polymicrobial Infections. *J. Microbiol.* 52(3):188-199.
19. Jin X & Riedel-Kruse IH (2018) Biofilm Lithography enables high-resolution cell patterning via optogenetic adhesin expression. *Proc Natl Acad Sci U S A* 115(14):3698-3703.
20. Glass DS & Riedel-Kruse IH (2018) A Synthetic Bacterial Cell-Cell Adhesion Toolbox for Programming Multicellular Morphologies and Patterns. *Cell* 174(3):649-658 e616.
21. Marin E, Bodelon G, & Fernandez LA (2010) Comparative Analysis of the Biochemical and Functional Properties of C-Terminal Domains of Autotransporters. *J. Bacteriol.* 192(21):5588-5602.
22. Obana M, Silverman BR, & Tirrell DA (2017) Protein-Mediated Colloidal Assembly. *J. Am. Chem. Soc.* 139(40):14251-14256.
23. Maurer J, Jose J, & Meyer TF (1997) Autodisplay: One-component system for efficient surface display and release of soluble recombinant proteins from Escherichia coli. *J. Bacteriol.* 179(3):794-804.
24. Jose J & Meyer TF (2007) The autodisplay story, from discovery to biotechnical and biomedical applications. *Microbiol. Mol. Biol. Rev.* 71(4):600-+.
25. Schuurmann J, Quehl P, Festel G, & Jose J (2014) Bacterial whole-cell biocatalysts by surface display of enzymes: toward industrial application. *Appl. Microbiol. Biotechnol.* 98(19):8031-8046.
26. Thompson KE, Bashor CJ, Lim WA, & Keating AE (2012) SYNZIP Protein Interaction Toolbox: *in Vitro* and *in Vivo* Specifications of Heterospecific Coiled-Coil Interaction Domains. *ACS Synth. Biol.* 1(4):118-129.
27. Zakeri B & Howarth M (2010) Spontaneous Intermolecular Amide Bond Formation between Side Chains for Irreversible Peptide Targeting. *J. Am. Chem. Soc.* 132(13):4526-+.
28. Zakeri B, *et al.* (2012) Peptide tag forming a rapid covalent bond to a protein, through engineering a bacterial adhesin. *Proc. Natl. Acad. Sci. U. S. A.* 109(12):E690-E697.
29. Zhang WB, Sun F, Tirrell DA, & Arnold FH (2013) Controlling Macromolecular Topology with Genetically Encoded SpyTag-SpyCatcher Chemistry. *J. Am. Chem. Soc.* 135(37):13988-13997.
30. Sun F, Zhang WB, Mahdavi A, Arnold FH, & Tirrell DA (2014) Synthesis of bioactive protein hydrogels by genetically encoded SpyTag-SpyCatcher chemistry. *Proc. Natl. Acad. Sci. U. S. A.* 111(31):11269-11274.
31. Liu ZD, *et al.* (2014) A novel method for synthetic vaccine construction based on protein assembly. *Sci Rep* 4:8.

32. Schoene C, Fierer JO, Bennett SP, & Howarth M (2014) SpyTag/SpyCatcher Cyclization Confers Resilience to Boiling on a Mesophilic Enzyme. *Angew. Chem.-Int. Edit.* 53(24):6101-6104.
33. Na D, Lee S, & Lee D (2010) Mathematical modeling of translation initiation for the estimation of its efficiency to computationally design mRNA sequences with desired expression levels in prokaryotes. *BMC Syst. Biol.* 4:16.
34. Serra T, Colomer J, & Casamitjana X (1997) Aggregation and breakup of particles in a shear flow. *J. Colloid Interface Sci.* 187(2):466-473.
35. Fuqua WC, Winans SC, & Greenberg EP (1994) QUORUM SENSING IN BACTERIA - THE LUXR-LUXI FAMILY OF CELL DENSITY-RESPONSIVE TRANSCRIPTIONAL REGULATORS. *J. Bacteriol.* 176(2):269-275.
36. Whitehead NA, Barnard AML, Slater H, Simpson NJL, & Salmond GPC (2001) Quorum-sensing in gram-negative bacteria. *Fems Microbiol. Rev.* 25(4):365-404.
37. Langebrake JB, Dilanji GE, Hagen SJ, & De Leenheer P (2014) Traveling waves in response to a diffusing quorum sensing signal in spatially-extended bacterial colonies. *J. Theor. Biol.* 363:53-61.
38. Thiele EW (1939) Relation between catalytic activity and size of particle. *Industrial and Engineering Chemistry* 31:916-920.
39. St-Pierre F, *et al.* (2013) One-Step Cloning and Chromosomal Integration of DNA. *ACS Synth. Biol.* 2(9):537-541.
40. You LC, Cox RS, Weiss R, & Arnold FH (2004) Programmed population control by cell-cell communication and regulated killing. *Nature* 428(6985):868-871.
41. Elias S & Banin E (2012) Multi-species biofilms: living with friendly neighbors. *Fems Microbiol. Rev.* 36(5):990-1004.
42. Conrado RJ, *et al.* (2012) DNA-guided assembly of biosynthetic pathways promotes improved catalytic efficiency. *Nucleic acids research* 40(4):1879-1889.
43. Conrado RJ, Varner JD, & DeLisa MP (2008) Engineering the spatial organization of metabolic enzymes: mimicking nature's synergy. *Curr Opin Biotechnol* 19(5):492-499.
44. Bintu L, *et al.* (2016) Dynamics of epigenetic regulation at the single-cell level. *Science* 351(6274):720-724.

If you can keep your head when all about you
  Are losing theirs and blaming it on you,
If you can trust yourself when all men doubt you,
  But make allowance for their doubting too;
If you can wait and not be tired by waiting,
  Or being lied about, don't deal in lies,
Or being hated, don't give way to hating,
  And yet don't look too good, nor talk too wise:

If you can dream—and not make dreams your master;
  If you can think—and not make thoughts your aim;
If you can meet with Triumph and Disaster
  And treat those two impostors just the same;
If you can bear to hear the truth you've spoken
  Twisted by knaves to make a trap for fools,
Or watch the things you gave your life to, broken,
  And stoop and build 'em up with worn-out tools:

If you can make one heap of all your winnings
  And risk it on one turn of pitch-and-toss,
And lose, and start again at your beginnings
  And never breathe a word about your loss;
If you can force your heart and nerve and sinew
  To serve your turn long after they are gone,
And so hold on when there is nothing in you
  Except the Will which says to them: 'Hold on!'

If you can talk with crowds and keep your virtue,
  Or walk with Kings—nor lose the common touch,
If neither foes nor loving friends can hurt you,
  If all men count with you, but none too much;
If you can fill the unforgiving minute
  With sixty seconds' worth of distance run,
Yours is the Earth and everything that's in it,
  And—which is more—you'll be a Man, my son!

— Rudyard Kipling, "If" (1910)

In loving memory of:
Maria Kozłowska, Teobald Kozłowski, Radzisław Sadżak,
George H. Pavach, and Helen J. Pavach.

Alles hat ein Ende. Nur die Wurst hat zwei.
Trzymajmy się, nie dajmy się